Dissertation

Mariugenia Salas Ramirez

Wireless Sensors and Actuators for Structural Health Monitoring of Fiber Composite Materials

UNIVERSITÄT BREMEN
INSTITUT FÜR MIKROSENSOREN, -AKTOREN UND –SYSTEME
NOVEMBER 2016

Wireless Sensors and Actuators for Structural Health Monitoring of Fiber Composite Materials

zur Erlangung des akademischen Grades eines

Doktor- Ingenieur (Dr.-Ing.)

Genehmigte Dissertation

von

M.Sc. Mariugenia Salas Ramirez

aus Venezuela

Referent:	Prof. Dr.-Ing. Walter Lang
Korreferent:	Prof. Dr.-Ing. Axel Herrmann
Eingereicht am:	23. November 2016
Tag des Promotionskolloquiums:	12. April 2017

Abstract

This work evaluates and investigates the wireless generation and detection of Lamb-waves on fiber-reinforced materials using surface applied or embedded piezo elements. The general target is to achieve wireless systems or sensor networks for Structural Health Monitoring (SHM), a type of Non-Destructive-Evaluation (NDE). In this sense, a fully wireless measurement system that achieves power transmission implementing inductive coils is reported. This system allows a reduction of total system weight as well as better integration in the structure.

A great concern is the characteristics of the material, in which the system is integrated, because the properties can have a direct impact on the strength of the magnetic field. Carbon-Fiber-Reinforced-Polymer (CFRP) is known to behave as an electrical conductor, shielding radio waves with increasing worse effects at higher frequencies. Due to the need of high power and voltage, interest is raised to evaluate the operation of piezo as actuators at the lower frequency ranges. To this end, actuating occurs at the International Scientific and Medical (ISM) band of 125 kHz or low-frequency (LF) range. The feasibility of such system is evaluated extensively in this work.

Direct excitation, is done by combining the actuator bonded to the surface or embedded in the material with an inductive LF coil and setting the circuit in resonance. A more controlled possibility, also explored, is the use of electronics to generate a Hanning-windowed-sine to excite the PWAS in a narrow spectrum. In this case, only wireless power is transmitted to the actuator node, and this lastly implements a Piezo-driver to independently excite Lamb-waves.

Sensing and data transfer, on the other hand, is done using the high-frequency (HF) 13.56 MHz. The HF range covers the requirements of faster sampling rate and lower energy content. A re-tuning of the antenna coils is performed to obtain better transmission qualities when the system is implemented in CFRP. Several quasi-isotropic (QI) CFRP plates with sensor and actuator nodes were made to measure the quality of transmission and the necessary energy to stimulate the actuator-sensor system.

In order to produce baselines, measurements are prepared from a healthy plate under specific temperature and humidity conditions. The signals are evaluated to verify the functionality in the presence of defects. The measurements demonstrate that it is possible to wirelessly generate Lamb-waves while early results show the feasibility to determine the presence of structural failure. For instance, progress has been achieved detecting the presence of a failure in the form of drilled holes introduced to the structure. This work shows a complete set of experimental results of different sensor/-actuator nodes.

Kurzfassung

Ziel dieser Arbeit ist die Untersuchung und Evaluierung der drahtlosen Erzeugung und Detektion von Lamb-Wellen auf Faserverbundwerkstoffen mittels auf der Oberfläche applizierten oder im Material eingebetteten Piezoelementen. Das allgemeine Zweck ist es, drahtlose Systeme bzw. Sensornetzwerke für Structural-Health-Monitoring (SHM), eine Art Non-Destructive-Evaluation (NDE), zu erzeugen. In diesem Sinne wird ein vollständig kabelloses Messsystem entwickelt, das eine Leistungsübertragung mit Hilfe von induktiven Spulen realisiert. Ein solches System zeichnet sich durch ein geringes Gesamtsystemgewichts sowie eine einfache Integration in die Struktur aus.

Eine große Herauforderung sind die Eigenschaften des Faserverbundmaterials, in dem das System integriert ist, da diese einen direkten Einfluss auf die Stärke des Magnetfeldes haben. Kohlenstoff-Faserverbund-Kunststoff (CFK) ist ein elektrischer Leiter, wodurch Funkwellen insbesondere bei höheren Frequenzen abgeschirmt werden. Aufgrund des Bedarfs an hoher Leistung und hoher Spannung ist es von Interesse, den Betrieb von Piezos als Aktuatoren im niedrigen Frequenzbereich zu bewerten. Zu diesem Zweck erfolgt die Anregung im International Scientific and Medical (ISM) Band von 125 kHz oder im Niederfrequenzbereich (LF). Die Machbarkeit eines solchen Systems wird in dieser Arbeit untersucht.

Zur direkten Anregung von Lamb-wellen wird ein Aktuator auf der Oberfläche oder eingebettet in das Material mit einer induktiven LF-Spule in Resonanz versetzt. Außerdem wird die Verwendung von Elektronik zur Erzeugung eines Hanning-windowes-Sinus als kontrolliertere Möglichkeit der Anregung untersucht. Dadurch wird die Piezoelement in einem engen Spektrum zu angeregt. In diesem Fall wird nur drahtlose Energie an den Aktorknoten übertragen, was letztlich einen Piezo-Treiber veranlasst, unabhängig Lamb-Wellen anzuregen.

Die Erfassung und Datenübertragung erfolgt im Hochfrequenzband (HF) um 13,56 MHz. Der HF-Bereich deckt die Anforderungen an eine schnelle Abtastrate und einen geringen Energiegehalt ab. Eine Anpassung der Antennenspulen wird durchgeführt, um bessere Übertragungsqualitäten zu erhalten, wenn das System in CFK implementiert ist. Es werden mehrere quasiisotrope (QI) CFK-Platten mit Sensor- und Aktorknoten hergestellt, um die Übertragungsqualität und die zur Stimulierung des Aktorsensorsystems notwendige Energie zu messen.

Zur Aufnahme von Basislinien werden Messungen mit einer unbeschädigten Platte unter bestimmten Temperatur- und Feuchtigkeitsbedingungen durchgeführt. Die Signale werden ausgewertet, um die Funktionalität bei Vorhandensein von Defekten zu verifizieren. Die Messungen zeigen, dass es möglich ist, drahtlos Lamb-Wellen zu erzeugen. Frühere Ergebnisse zeigen die Möglichkeit, das Vorliegen eines strukturellen Defekten zu bestimmen. Es werden etwa Fortschritte erzielt, das Vorhandensein eines Fehlers in Form von Bohrlöcher in der Struktur festzustellen. Diese Arbeit zeigt einen vollständigen Satz von experimentellen Ergebnissen verschiedener Sensor-Aktor-Knoten.

Table of Contents

Nomenclature

Symbol	Description	Units
ε_o	the permittivity of free space	8.854×10^{-12} F/m
μ_o	the permeability of free space	$4\pi \times 10^{-7}$ H/m
μ_r	relative Permeability	m
a	planar coil mean radius	m
B	magnetic flux density	Wb/m^2
c	winding thickness for planar coil	m
C	capacitance	F
C_{par}	parasitic capacitance	F
D	coil diameter	m
E	electric field	V/m
h	the height of the solenoid coil	m
J	current density in a conductor	A/m^2
J_S	conductor surface current density	A/m^2
k	coupling factor between coils	
l	square coil side length	m
L	coil self-inductance	H
M	mutual inductance	H
N	number of windings	
r	coil radius	m
s	square coil space between traces	m
S_{11}	antenna reflection coefficient	dB
W	energy density	10^{-1} J/m^3
w	square coil trace width	m
x	distance between PWAS-actuator and PWAS-sensor	m
z	the distance between coils	m
δ	skin depth	m
ε	electromotive force	Volts
ρ	the resistivity of the conductor	Ω·m
σ	electrical conductivity	S/m

Abbreviations

ADC	Analog-To-Digital-Converter
CFRP	Carbon-Fiber-Reinforced-Polymer
DAC	Digital-To-Analog Converter
DWT	Discrete Wavelet Transform
FBG	Fiber Bragg Gratings
FEM	Finite Element Method
FRP	Fiber-Reinforced-Polymer
GFRP	Glass-Fiber-Reinforced-Polymer
GMRES	Generalized Minimal Residual Method
HF	High Frequency
HFRX	High-Frequency Receiver Coil
HFTX	High-Frequency Transmitter Coil
LF	Low Frequency
LFRX	Low-Frequency Receiver Coil
LFTX	Low-Frequency Transmitter Coil
NDE	Non-Destructive-Testing
PWAS	Piezo-Wafer-Active-Sensor
QI	Quasi-Isotropic
RFID	Radio-Frequency-Identification
SHM	Structural-Health-Monitoring
SNR	Signal-To-Noise-Ratio
SSWC	Simple-Serial-Wireless-Communication
TFP	Taylor-Fiber-Placement
THD	Total Harmonic Distortion
UD	Unidirectional
WFR	WaveFormRevealer

1

Introduction

Structural Health Monitoring (SHM) consists of evaluating the status of a structure or its material. Generally, sensors and actuators are used to collect information about fatigue, material degradation, and negative environmental conditions. There is a growing interest towards wireless technologies that would enable SHM of fiber reinforced polymers (FRP) with applications in different industries, including but not limited to aeronautics, automotive and wind energy. FRP structures are interesting because of their strength and light weight even though their complex mechanical and electrical anisotropic properties are a challenge for the use of SHM systems. A typical application of FRP materials is in the construct of airplanes, as seen in Figure 1; the Boing 787 presents a majority of purely carbon composites or sandwich structures.

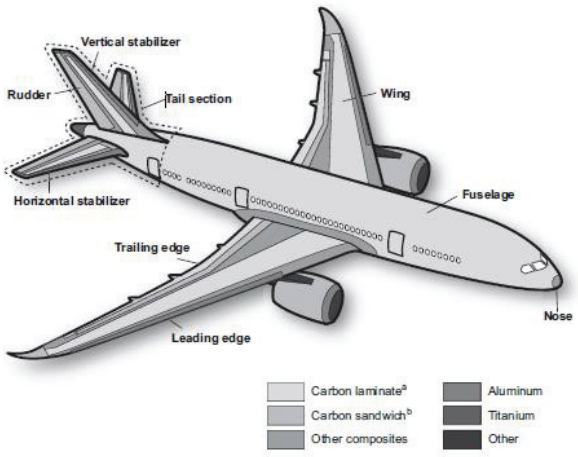

Figure 1: Representation of material composition of the Boeing 787 [1]

The focus of this work is the design and development of a wireless non-destructive SHM system integrated into fiber composite materials. The system composed of sensor and actuator nodes is capable of detecting damages, and so disasters can be prevented and the lifetime of structures is increased. This wireless system

is done by implementing inductively coupled coils. The damage detection with ultrasound is the preferred method for composite materials. Lamb-waves are acoustic vibrations arising from piezoelectric sensors when electrically stimulated [2]. The majority of the piezoelectric elements used in this research project are denoted as PWAS (Piezoelectric Wafer Active Sensor). They are able to produce and detect these oscillations. With a sensor network, structural damage in the fiber composite can be accurately detected. A significant advantage of this method in comparison to others, such as the strain measurement with the Fiber Bragg Gratings (FBG) or strain gauges is the ability of surface oriented structure monitoring.

The research presented here includes surface integrated PWAS acting both as sensors nodes as well as actuators nodes, powered directly from a quasi-stationary magnetic field. The energy source is applied externally and received at the nodes wirelessly by means of surface integrated inductive coils. The life expectancy of such SHM system increases significantly compared to battery-powered SHM systems. There is a reduction of space usage due to the material integration of the system, which in addition will be conceived during manufacture to reduce costs.

One of the main goals was the design and simulation of high (13.56 MHz) and low frequency (125 kHz) coils before integration in FRP. This was done by implementing theoretical models, simulations with software like COMSOL Multiphysics and Fasthenry; as well as inductance evaluation with coupling tests. Furthermore, it was of importance to observe the influence carbon fiber composite has on the wireless power. Experimental tests at high and low frequency were carried, where the CFRP material was be placed behind and between the coils while observing the coupling and the reflection coefficient of the antenna. In this case, the simulations at high frequency were carried in Microwave Studio CST since at this range the coil has an antenna like properties.

The system consists of the direct connection of the PWAS-actuator to the coil for generation of a signal to excite it. Later, collecting the signal from the PWAS-sensor via a wireless coil, and observing the quality of the transmission. There are different approaches for a reader i.e. Analog frequency or amplitude modulation or use of a RFID transponder or a microcontroller to achieve digital modulation. A point of attention is the integration of the nodes into the FRP. Integrating the wireless PWAS using Taylor-Fiber-Placement process in which the sensors and actuators are embroidered on a textile has benefits for application to different fiber composite materials and provides flexibility in the design of the network. The integration is done in the lamination process during the production of fiber composite of structures such as the fuselage or the rotor blades of wind power plants.

A demonstrator was achieved with a custom portable reader able to store signals for later processing using PC-software-based on Matlab. Such signal analysis is prepared to take Lamb-waves symmetric and asymmetric modes. The evaluation and experimental tests of the finished wireless nodes were done by comparing to an original wired network, proving the functionality of the system. The calibration is done by a reference measurement of the finished structure itself.

A relevant part of this work focused on the evaluation of the impact harsh environment has on the system. It is considered that anything that changes the system without affecting the performance of the structure should not be taken as damage, and should be compensated for. For instance, an aircraft can experience drastic changes in temperature from the time it is in the air, at extremely low temperatures, to the time it is parked at an airport or inside a maintenance hall. The results will be biased subject by the in-situ environmental conditions at the time when the structural test is to be run.

Likewise, it is a great concern the moisture abortion by most of the thermoset resin used for reinforced polymers in industry. The mechanical characteristics change over time in presence of humid environments, generating aging of the composite. Therefore, it is necessary to be able to distinguish between this effect and real damages like delamination or cracks. In this thesis, preliminary tests and evaluation of a humidity sensor and a temperature sensor are done. The aim is to expand the sensor node to include environmental monitoring.

The innovative contribution is a viable industrial use of the system made possible by the practical integration, which is primarily due to the miniaturization and the absence of complex electronic components on the wireless nodes. A final reader system and a real plate structure with integrated sensor network was delivered as Proof-of-Concept including evaluation of its functionality. Lastly, other sensors to be powered by the same wireless technology were investigated in order to evaluate environmental influences like temperature and humidity. This technology enables further research on material integrated sensors. With the results from this project, future concepts to power and collect data wirelessly from other kinds of material integrated sensors and actuators can be developed. Most importantly, it is shown that such system can be successfully implemented embedded in an electrically conductive material, like CFRP, by using proper tuning.

2

Background and State-of-the-Art

There is an increasing interest in integrating sensory functions in textile materials and semi-finished products. In Germany, technical universities and institutes (e.g. Fraunhofer IZM and IZFP, Leibniz IFW, TITZ Greiz) are working on the integration of sensors in textiles and fiber composite materials. The definition of intelligent materials and the applications of these technologies in structures are explained in Section 2.1. Additionally, it is mentioned the integration into the fabric without starting a delamination point; which requires better methods such as the Taylor-Fiber-Placement (TFP) and the use of suitable binders, through which bonding of the piezoelectric elements and coils can be achieved.

Structural Health Monitoring (SHM) is a novel technique for an autonomous, integrated and Non-Destructive-Evaluation (NDE) of the condition of civil, aerospace, and other structures. Especially in the last decade, there have been substantial advances in the implantation of SHM systems in the fiber composite. In section 2.2 the principles of SHM technologies using Lamb-waves are exhaustively explained. The wireless SHM system has to be successfully implemented in practice, including the data collection with a reader, which is able to selectively control and process the sensor data from multiple wireless PWAS. The signal processing is an essential component of an SHM system as explained in the end of this section, where the algorithms are introduced. Fiber composites will be introduced in more detail in this section 2.3 as well as the electrically conductive properties of some composite materials, like Carbon Fiber Reinforced Polymer. This material requires special care including additional insulation of the sensor and actuator nodes. It is necessary to study in detail the effect of CFRP on the wireless system. SHM systems must demonstrate their benefits in a cost/benefit analysis in order to gain the acceptance of the industry. For example, conventional wired systems in an aircraft must provide a significant benefit to justify their weight, their cost and increasing the complexity of the overall system. In a wireless system that operates completely independently, a considerable weight saving can be expected. In this case, the wireless signal processing of such complex SHM system is a challenge and an essential aspect in order to

establish the utility of these systems. The main emphasis of this research was the practical implementation in an industrial application with a final product solution, which is versatile.

There was a sub-project from the cluster Cool Silicon e.V. in Saxony, called CoolSensornet [3]. This project deals with sensors for structural monitoring. CoolSensornet worked in cooperation with the airplane producer Airbus to integrate sensors that monitor vibrations and detect anomalies before a problem might occur. They followed a similar approach as presented in this research. However, CoolSensornet used sensors with "Energy Harvesting" skills based on piezoelectric actuators combined with a data interface. With the help of a fully integrated energy supply and capacitive energy storage, a self-sufficient system was achieved. Such approach implied complex electronic components and therefore differs from the proposed methodology of this research. Since PWAS require a reliable energy source for both the excitation and the measurement of acoustic signals; the energy requirements are done implementing inductive coils as it will be explained in subsection 2.4. The magnetic field generated by a primary coil in resonance is used by a secondary coil to supply the connected sensors or actuators and modulate the sensor data independently, similar to Radio Frequency Identification (RFID) [4]. Previous monitoring methods realized the power and information transmission by means of cables [5]; however, this is not always possible because of the geometry and location of the structure. Energy supply by means of built-in batteries results in a reduced service life of the monitoring system. The technology here introduced will enable more effective quality management of structures in aeronautics and other industries employing reinforced materials. Moreover, it will allow other sensors [6] and electronics [7] to be embedded without putting in jeopardy the integrity of the structure.

2.1. Intelligent Materials and Structures

In technology, intelligent structures are considered the integration of actuators, sensors, and controls within a material or structure. According to [8] in science, intelligent structures are seen as material systems that have life-like features integrated into the microstructure of the material in order to reduce to total mass and energy and produce an adaptive functionality.

The goal of these structures is to learn from nature and living schemes in a way as to enable man-made things to have the adaptive features. This leads to the description of the anatomy of an intelligent material system as explained by [8]: Actuators or motors that behave like muscles; sensors that have the functionality of the five senses and communication and computational networks that represent the nerves, brain, memory, and muscular control systems. Although the analogy moves towards biological systems, it must be emphasized that intelligent structures are designed by humans in order to achieve human-related objectives. Therefore, the system boundary must necessarily be drawn to include the human end user. Seen

from a different point of view as in [9], intelligent materials are multifunctional due to their unique molecular structure and respond to external stimuli by a characteristic behavior to the outside world.

The aim is to integrate sensors in a way which does provide the information needed for monitoring but which does not downgrade the macroscopic behavior of the material. In a way, the sensor and its interconnections may be considered as a wound in the material [10].

Some studies dealt with the effect on the placement of piezoelectric sensors and actuators within the fiber composite structure and the use of different integrating techniques to minimize the effect of larger piezoelectric [11]. The main problem in the inclusion is that the sensors and actuators area used is generally too thick or large on the surface.

Figure 2 presents a polished cross section of the laminate with an embedded sensor [10]. The sensor is about 10 µm thick and the carbon fiber bundles have diameters of around 8 µm. By having the flexibility of a foil, the sensor can adapt to the geometry of the laminate material and follow elastic deformations. Although, being a foil of about 3 x 3 mm² area, the sensor is a disruption of the polymer carbon fiber matrix [10]. To achieve integration without wounding the matrix it is necessary to further miniaturize or keep the sensing out of the structure. Therefore, in this work, the integration takes place at the surface of the material and the interconnections for read out are replaced by the wireless solution.

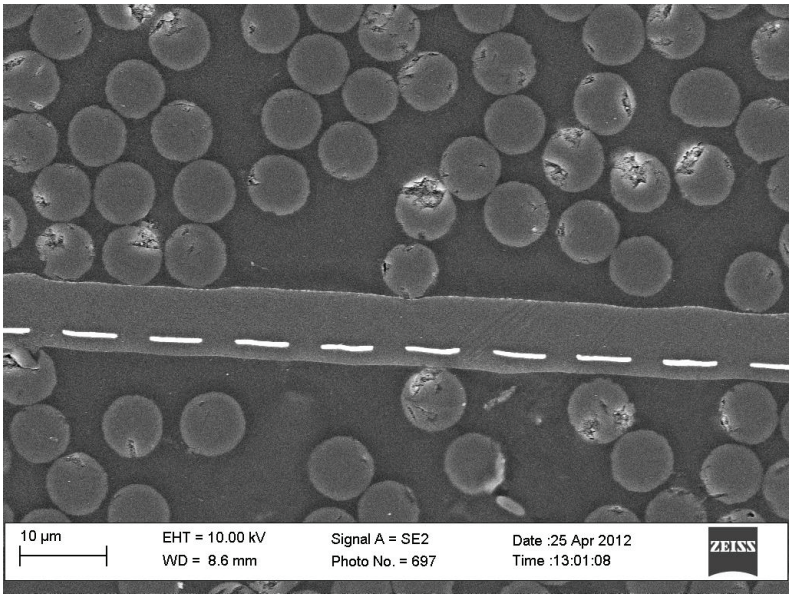

Figure 2: SEM picture of a thin sensor for the measurement of local dielectric embedded in CFRP [10]

For the production-ready integration of sensors or sensor nodes in the semi-finished textile product, various methods exist. Particularly suitable for the integration of several elements and the necessary conductor tracks is the introduction as an added layer of the textile prior to the resin infiltration. The advantages of this process are the high positional accuracy of the sensors relative to each other and their

protection during manufacture. Disadvantages are the insertion of a flat foreign in the structure; the consequences need to be investigated on the mechanical properties. Metallic inserts can be done for example, by sewing or embroidering [12]. A self-adhesive film allows also the fixation on a semi-finished product and the subsequent application to solid surfaces.

2.2. Structural Health Monitoring and Lamb-waves

One of the possible SHM methods is the use of a type of guided plate waves, called Lamb-waves. These waves propagate in two dimensions allowing for distributed sensor arrays; in this case, integrated or surface-applied piezoelectric elements. Lamb-waves are easily excited and measured and they are highly sensitive to most types of damage occurring in composites.

Lamb-waves are a type of ultrasonic waves, as explained before, they remain guided between two parallel surfaces, for example, the upper and lower surfaces of a plate or shell. Lamb-wave theory is fully documented in a number of publications and textbooks (Viktorov, 1967) [13]. Here, only the essentials are reproduced as in [13]. The analysis starts from the wave equations:

$$\frac{\partial^2 \phi}{\partial x^2} + \frac{\partial^2 \phi}{\partial y^2} + \frac{\omega^2}{c_L^2}\phi = 0 \qquad \text{Eq. 1}$$

$$\frac{\partial^2 \psi}{\partial x^2} + \frac{\partial^2 \psi}{\partial y^2} + \frac{\omega^2}{c_T^2}\psi = 0 \qquad \text{Eq. 2}$$

Here ϕ and ψ are two potential functions, and $c_L^2 = (\lambda + 2\mu)/\rho$ and $c_T^2 = \mu/\rho$ are the pressure (longitudinal) and shear (transverse) wave speeds. Here ρ is the mass density. The Lamé constants λ and μ are material dependent constants arising from the strain-stress relationship. The time dependence is assumed harmonic in the form $e^{-i\omega t}$. The general solution as explained in [13]:

$$\phi = (A_1 \sin py + A_2 \cos py)e^{i(\xi x - \omega t)} \qquad \text{Eq. 3}$$

$$\psi = (B_1 \sin qy + B_2 \cos qy)e^{i(\xi x - \omega t)} \qquad \text{Eq. 4}$$

The four integration constants, A_1, A_2, B_1, B_2, are to be found from the boundary conditions. Using the relations between the potential functions and the displacements, stresses, and strains [13]:

$$u_x = \frac{\partial \phi}{\partial x} + \frac{\partial \psi}{\partial y} \; ; \; \tau_{yx} = \mu\left(2\frac{\partial^2 \phi}{\partial x \partial y} - \frac{\partial^2 \psi}{\partial x^2} + \frac{\partial^2 \psi}{\partial y^2}\right) \qquad \text{Eq. 5}$$

$$u_y = \frac{\partial \phi}{\partial y} - \frac{\partial \psi}{\partial x} \; ; \; \tau_{yy} = \lambda \left(\frac{\partial^2 \phi}{\partial x^2} + \frac{\partial^2 \phi}{\partial y} \right) + 2\mu \left(\frac{\partial^2 \phi}{\partial x^2} - \frac{\partial^2 \psi}{\partial x \partial y} \right) \quad \text{Eq. 6}$$

$$\varepsilon_x = \frac{\partial u_x}{\partial x} \quad \text{Eq. 7}$$

By substitution it can be grouped into two parts as seen in Eq. 8 and Eq. 9 the first corresponds to symmetric motion and the second to the antisymmetric motion.

$$u_x = \left[(A_2 i\xi \cos py + B_1 q \cos qy) + (A_1 i\xi \sin py - B_2 q \sin qy) e^{i(\xi x - \omega t)} \right] \quad \text{Eq. 8}$$

$$u_y = \left[-(A_2 p \sin py + B_1 i\xi \sin qy) + (A_1 ip \cos py - B_2 i\xi \cos qy) e^{i(\xi x - \omega t)} \right] \quad \text{Eq. 9}$$

For free wave motion, the homogenous solution is derived by applying the stress-free boundary conditions at the upper and lower surfaces (y=±d where d is the plate half thickness). The characteristic equations are obtained:

$$D_S = (\xi^2 - q^2)^2 \cos pd \sin qd + 4\xi^2 pq \sin pd \cos qd = 0 \quad \text{Symmetric Motion} \quad \text{Eq. 10}$$

$$D_A = (\xi^2 - q^2)^2 \sin pd \cos qd + 4\xi^2 pq \cos pd \sin qd = 0 \quad \text{Antisymmetric Motion} \quad \text{Eq. 11}$$

These equations can be rewritten in the compact form as the Rayleigh–Lamb equation:

$$\frac{\tan pd}{\tan qd} = -\left[\frac{4\xi^2 pq}{(\xi^2 - q^2)^2} \right]^{\pm 1} \quad \text{Eq. 12}$$

Here the exponent +1 corresponds to symmetric (S) motion and -1 to antisymmetric (A) motion. These equations accept a number of eigenvalues $\xi_0^S, \xi_1^S, \xi_2^S, \ldots$, and $\xi_0^A, \xi_1^A, \xi_2^A, \ldots$, respectively. To each eigenvalue corresponds a set of Eigen coefficients: (A_2, B_1) for the symmetric case, and (A_1, B_2) for the antisymmetric case. Substitution of these coefficients into Equation yields the corresponding Lamb mode shapes. The symmetric modes are designated S_0, S_1, S_2. . . while the antisymmetric are designated A_0, A_1, A_2, …, Since the coefficients p and q depend on the angular frequency, ω the Eigenvalues ξ_i^S and ξ_i^A will change with the excitation frequency. The corresponding wave speeds, given by $c_i = \omega/\xi_i$ will also change with frequency. The change of wave speed with frequency gives the wave dispersion. Lamb-waves are very dispersive, and their speed depends on the product *f·d* between the frequency, *f*, and the plate half thickness, *d*. At a given frequency thickness product, for each solution of the Rayleigh–Lamb equation, one finds a corresponding Lamb-wave speed and a corresponding Lamb-wave mode. The plot of the Lamb-wave speeds against the *f·d* product gives the wave speed dispersion curves as seen in Figure 3.

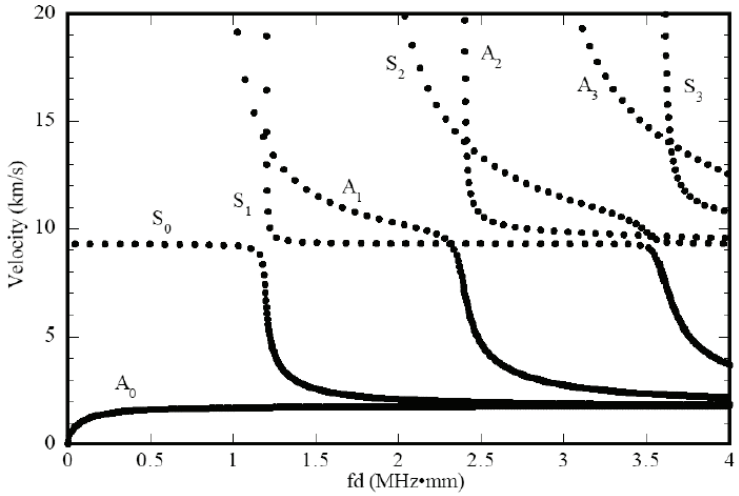

Unidirectional CFRP plate in reinforcement direction-group phase velocity [14, 15]

Figure 3: Theoretically calculated curves for the lowest Lamb-wave modes

The modes at low frequencies are S_0, A_0 and SH, the latter one, denoting the shear horizontal wave. The symmetrical modes are called, S_0, S_1 S_2…and the anti- symmetric ones A_0 A_1, A_2…, starting with the mode that has the lowest frequency for a given wave number [16].

These waves are easily excited and measured, for example by integrated or surface-applied piezoelectric elements. They have successfully been used to identify and localize both various discrete, localized damage, such as holes, notches, cracks, delamination or weak bonds [2] as well as distributed, non-localized damage such as fatigue in composites [17]. Examples of other investigations are a characterization of the influence of moisture absorption on Lamb-wave propagation [18] or the inverse measurement of mechanical properties [19]. Especially the detection of non-visible and barely visible damages such as delamination, these are typical and hard to detect from outside the structure when using classical visual inspection methods.

Lamb-wave-based SHM methods can be distinguished in a passive or an active system [20]. The first one uses the waves; which are created by damaging events, such as crack initiation and growth or an impact event (hail, bird strike). An active system, on the other hand, uses an actuator to create the Lamb-waves in a controlled fashion. For SHM purposes, where the sensing ability is integrated into or onto the structure, they are most commonly excited and measured using piezoelectric elements. Figure 5 shows a simple example of an SHM-System with piezoelectric elements bonded to the plate's surface. An excitation signal is applied to a piezoelectric element which performs as an actuator. These generated waves depend therefore on the interaction between the actuator, adhesive, and local material properties. While traveling dispersive through the structure, these waves are underlying damping due to viscoelastic material behavior and contact to surrounding fluids or materials. Reaching the sensor, the strains are transmitted through the

bonding layer to the piezoelectric element, based on the inverse piezoelectric effect an electric output signal is created which then can be displayed and subsequently can be analyzed.

SHM using Lamb-waves is based on the fact that damage represents a discrete, local change of the waveguide which interacts with the propagating Lamb-wave or, in the case of a passive system, that the damaging event generates a Lamb-wave of certain properties. The signal analysis has to take into account that these waves are reflected at edges or transmitted through interfaces, and therefore undergoing also mode changes. Lamb-waves should be excited at frequencies in the range of 0 kHz to 500 kHz. And these waves travel with different group velocities. Depending on the distance between actuator and sensor the S_0 and A_0 signal arrive at different arrival times. Therefore the modes can be identified. The Lamb-wave frequencies depend on the excitation time of the actuator, the output voltage on the sensor materials Young´s modulus, its piezoelectric constant, the sum of extensional surface strains, the sensor thickness and the sensor area [2].

This method has continuously been used to identify both various types of discrete, localized damage [2, 21] as well as distributed, non-localized damage such as fatigue in composites. The next stage for this SHM technology goes towards more practical systems; this development motivates the growing interest in wireless embedded sensors.

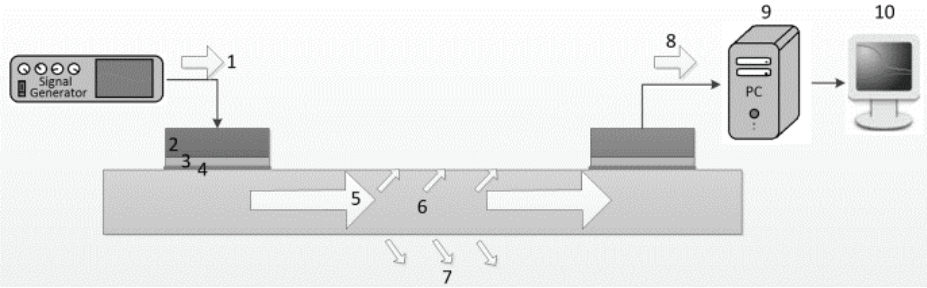

(1) Excitation signal (2) PWAS Actuator (3) Coupling layer (4) Adhesive and local material properties (5) Traveling wave disperses through the structure (6-7) Damping due to viscoelastic material behavior and contact to surrounding fluids or materials. (8) Sensor based on the inverse piezoelectric effect (9) Electric output signal (10) display and analysis

Figure 4: Principle of active Lamb-wave-based SHM [22].

Damage Detection Algorithms

If the Lamb-wave displacement is associated with a particle displacement they can be very useful to detect surface or inner flaws. As previously explained propagating Lamb modes are symmetric and antisymmetric. Each mode is associated with an infinite number of propagation orders. According to the frequency by plate thickness product $f \cdot d$ and for a given mode of given order, the Lamb-wave should be located either inside a dispersive operating area or a non-dispersive operating area. In the first case, the product f·d is met with a time spreading of the Lamb-waves during their propagation. In the other case, as the Lamb-waves propagate with a quasi-constant group velocity, its temporal form is quasi-invariant. The

wavenumbers of Lamb-waves have to satisfy the Rayleigh-Lamb equations for the two types of propagation modes: symmetrical and antisymmetric.

It is necessary to extract the arrival times of the fastest or multi-mode Lamb-wave modes. For this, the majority of methods are based on enveloping techniques, and various time-frequency methods such as Wigner-Ville distribution (WVD), short-time Fourier transform (STFT), and discrete wavelet transform (DWT). The goal of using signal processing methods is the extraction of the arrival time of the Lamb-wave modes. With such methods, the so-called Lamb-wave tomography can be obtained which is considered an effective NDE technique for plate-like structures.

To this end, in the last decade, various techniques to improve the extraction algorithms have been researched and presented. Essential components of the research were the reduction of noise effects, the time-frequency analysis of non-stationary signals, pattern recognition, and optimal localization methods. Giurgiutiu and Yu investigated the discrete wavelet transform (DWT) and a digital filter for noise reduction for Lamb-wave-based SHM techniques [2]. They introduced a compression factor by which the noise component could be reduced at the signal. The time-frequency analysis of non-stationary signals in SHM systems was successfully researched and presented with the refined fast Fourier transform (FFT), as well as the short time Fourier transforms (STFT), the Wigner-Ville distribution and the wavelet transform. Hilbert-Huang transform (HHT) is also an efficient way for analyzing and processing non-stationary signals. Other work has been done in Single Mode Tuning of Lamb-wave to use a time reversal technique with PWAS.

This work focuses on the viability of a wireless network and assumes the Lamb-wave analysis takes place after data collection using Matlab GUI. Keeping this in mind only a simplified method is used to verify the information obtained. The wavelet transform performs a time-frequency analysis of the Lamb-wave signals, with enough resolution in the frequency and time domains for practical applications. The main idea of the wavelet transform is the decomposition of the signal $s(t)$ into a sum of so called *daughter* wavelets $\psi_{a,b}(t)$. These wavelets are shifted and translated versions of the *mother* wavelet $\psi(t)$. The extraction of the signal characteristics can be done with high precision, because high and low-frequency transient components can be resolved. The information can be used to obtain remove noise from the signals and additionally, the Hilbert Transform can be further used to determine the arrival times or time of flight (TOF) and thus the velocities.

2.3. Principles of Fiber Reinforced Polymers

The use of Fiber-reinforced polymer (FRP) in aeronautics has grown due to their high specific strength and stiffness when compared to more conventional materials like aluminum. Additionally, they present

the ability to be shaped to create more efficient structural configurations. Refinements in process technology over the past years have led to improvements in tensile strength and in strain to fracture.

FRP composites can be simply described as reinforcing fibers embedded in a rigid polymer matrix. The fibers used for reinforced materials can be in the form of particles, whiskers, or filaments. Most composites used in engineering applications contain fibers made of glass, carbon, or aramid. An assorted range of polymers can be used as the matrix of the composites, and these are generally classified as a thermoset or thermoplastic resin. Conventionally, aerospace epoxy resins are designed to cure at 120–135 or 180 °C usually in an autoclave or closed cavity tool at pressures up to 8 bars, occasionally with a post cure at a higher temperature. The resins must have a room temperature life beyond the time it takes to lay-up a structure and have a temperature, and viscosity suitable for handling.

In almost all engineering applications requiring high stiffness, strength, and fatigue resistance, composites are reinforced with continuous fibers rather than small particles or whiskers [23]. Roving, the basic form in which fibers are supplied, are a number of strands or bundles of filaments wound into a package. Roving can be woven in different fabric constructs, such as plain, twills and satin weave.

The largest proportion of carbon fiber composites used on primary class-one structures is fabricated by placing layer upon layer of unidirectional (UD) material to the designer's requirement in terms of ply profile and fiber orientation. The laminate stacking sequence can significantly influence the magnitude of the shear stresses [25]. For aerospace applications, the sequences of ply stacking normally involve a combination of three angles: ±0°, ±45°, and ±90°, where the angles are relative to main loading direction of the applied load, such laminates are called Quasi- Isotropic (QI) as seen in Figure 5 the side view of such construction is presented.

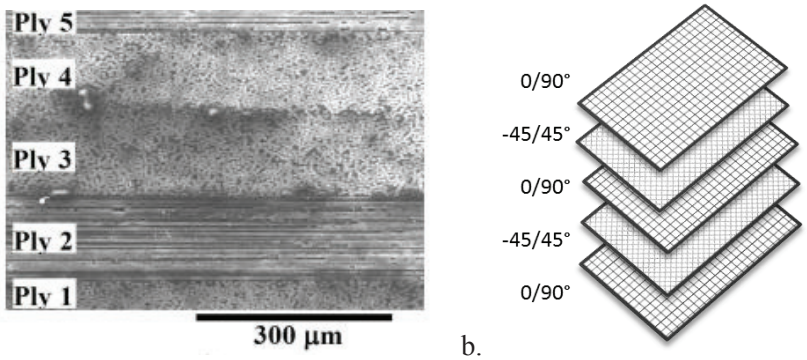

a. b.

Figure 5: Quasi-isotropic CFRP: (a) Side view [24] , (b) Lay-up representation

The manufacturing process after laid up consists on closing the mold in a flexible bag custom-made approximately to the desired shape and the assembly usually in an autoclave. A pressure vessel designed to contain a gas at pressures generally up to 1.5 MPa is used. The internal temperature is raised to that required to cure the resin. The flexible bag is first evacuated, thereby removing trapped air and organic

vapors from the composite, after which the chamber is pressurized to provide additional consolidation during cure. Resin film infusion (RFI) and resin transfer molding (RTM) are the predominant curing processes nowadays of which there are several variations. In traditional pre-preg technology, the resin is already infiltrated in the fibers and processing just removes air and volatiles, consolidates and cures. RTM in its simplest form involves a fabric preform being placed in an enclosed cavity and resin forced into the mold to fill the gaps under pressure and cure.

Electromagnetic Behavior of CFRP

Quasi-isotropic CFRP with fibers on each layer placed on a 45° rotation relative to the previous one can lead to higher electrical conductivity related to frequency similar to a metal plate [24]. A metal contains free electrons moving in all directions at high speed, when an external magnetic field is applied, the electrons move in a circular motion due to Lorentz force. Therefore, when such plate is in a changing magnetic field or moving relative to the magnetic field, induced current is generated. Because each position may form a circuit and the magnetic flux through these circuits keeps varying, there can be currents flowing through each loop, which is known as eddy currents [26]. In other words, Eddy currents are currents induced inside metal substances by a time-varying magnetic field. This gives rise to two negative effects. There will be ohmic power loss and heating inside the metal substance due to eddy currents circulating inside it [27].

The electromagnetic force exerted on an electric charge q (C) moving at velocity u (m/s) in an electric field E and a magnetic field B is known as the Lorentz force equation given by:

$$\mathbf{F} = q\mathbf{E} + q\mathbf{u} \times \mathbf{B} \qquad \text{Eq. 13}$$

The force exerted by the electric field is in the direction of the electric field and will be present whether the electric charge is stationary or moving. The force exerted by the magnetic field is perpendicular to the magnetic field, and it is absent if the electric charge is stationary. The magnetic force may change the direction of the motion of a charged particle, but it consumes no energy in moving the electric charge. The electric force alone changes the kinetic energy and velocity of the electric charge [27].

The Lorentz force defines the physical effects electric and magnetic fields. The electric field intensity E (in V/m) and magnetic flux density B (in T) are the physical quantities that produce a flow of electric currents in conductors, or movement of current carrying conductors in a magnetic field. Both magnetic field intensity H and electric flux density D are fictitious quantities defined to make the field definitions complete. Here $H = B/\mu$ and $D = \varepsilon E$ and $J = \sigma E$, where material properties μ, ε and σ are, respectively, the permeability, permittivity and electric conductivity of the material in which the fields exist. The conduction current ($J = \sigma E$) will not exist in regions of zero conductivity, namely, in dielectric medium

such as free space. However, the displacement current density, $\partial D/\partial t = \partial \varepsilon E/\partial t = J_D$, may flow in dielectric materials too. According to Lenz's law, the induced load voltage V_L (volts) in a coil cut by time-changing magnetic field will be in such a direction as to produce a current that opposes the voltage-inducing magnetic flux change. The two quantities E and B are mutually related and defined by the four Maxwell's equations given below in their integral form:

Faraday's law	$\oint_\ell E\, d\ell = -\oint_S \frac{\partial B}{\partial t} ds$	Eq.14
Ampere's law	$\oint_\ell H\, d\ell = \oint_S \left(J + \frac{\partial D}{\partial t}\right) ds$	Eq. 15
Gauss's law	$\oint_S D\, ds = Q$	Eq. 16
Gauss's law for magnetism	$\oint_S B\ ds = 0$	Eq. 17

According to Faraday's law (Eq.14) a wire loop, in this case, a planar coil, defines a surface *S*. The magnetic flux passing through the loop is given by B and *dS;* the last is a differential element of surface area. Faraday's law states that a voltage is induced around the loop when the magnetic flux changes. Changes in it can arise from a time-varying field at constant loop position.

If there is magnetic field changing near a conductive material, eddy currents will generate in the material, due to Faraday's law: the induced electromotive force is generated because of the magnetic flux through the circuit changes [27]. In other words, eddy currents are the reactions to a changing magnetic field within a conductor. The reason why the motion trajectories of electrons are circular is that only Lorenz force acts on the free electrons and the direction of Lorentz force is perpendicular to the moving direction of electrons.

Lenz law also contributes to the definition of eddy current. Lenz law explains that the current caused by external magnetic fields always generates an induced magnetic field which opposes to the magnetic field that creates it. This means that the induced voltage (ε) and the change in magnetic flux ($\partial\Phi$) have opposite signs:

$$\varepsilon = -\frac{\partial \Phi_B}{\partial t} \qquad \text{Eq.18}$$

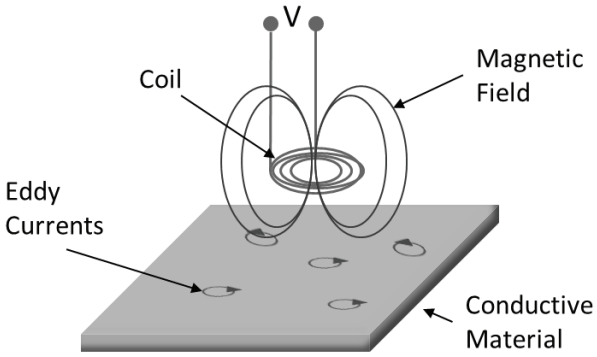

Figure 6: Eddy current caused by a coil magnetic field

So the left or right rotation of eddy currents depends on the applied magnetic field direction and the magnetic field strength. It means that the conductive material which is set near a varying magnetic field can influence the electromagnetic behavior and propagation of the external magnetic field. When the conductor has been placed farther away from the source field, the influence will become less. For example, to reduce eddy currents, in equipment, such as transformers, the iron core is laminated to reduce the path length allowed for the eddy current to flow.

A consequence of self-induced eddy currents is the skin effect. In a high-frequency circuit, the current changing rate is high, so there is an uneven distribution of current. The generated magnetic field which is caused by high frequency induces the maximum force in the central region of the wire conductor. Since the induced current is always in the opposite direction of original current direction, the total current density distributes close to the surface of the wire, which is called skin effect. The calculation of total current density caused by skin effect is:

$$J = J_D e^{-t_S/\delta} \qquad \text{Eq.19}$$

The amplitude of an electromagnetic wave B_O is exponentially reduced according to the Skin's formula as it propagates through the metal thru a distance t_S:

$$B'_O = B_O e^{-t_S/\delta} \qquad \text{Eq. 20}$$

B'_O is the amplitude of the magnetic field after having covered the distance t_S through the metal. This is the distance in which the amplitude of the magnetic field is reduced a factor e. It is also where the current density reduces to 1/e of the conductor surface current density; it is known as skin depth δ. It can be calculated as:

$$\delta = \sqrt{\frac{2\rho}{\omega\mu_0\mu_r}} \qquad \text{Eq. 21}$$

where μ is the permeability of the metal, σ its conductivity and ω the angular frequency of the electromagnetic field. Figure 7 shows the skin depth for different materials. The ferrite Mn-Zn, (3R1[1]), has a permittivity of about 800 and a resistivity of $103\,\Omega \cdot m$. Stainless steel 410 corresponds to a resistivity of about $48 \cdot 10^{-8}\Omega \cdot m$ and permittivity of 95 for hardened steel[2].

Systems that work with magnetic fields show different problems in the presence of conductive materials like CFRP. Many studies evaluate the characteristics of CFRP as a conductor. Previous research has been done in the realization of RFID antennas with carbon fiber composites [28] where the authors benefited from the material properties and investigated its radiation efficiency and gain at Ultra-High-Frequency (UHF). In the same way in [29] the feasibility of microstrip antennas on CFRP was studied by implementing an approximation model of the electrical characteristics of this material. In [30] the re-tunning of an antenna at High Frequency (HF) was done to compensate resonance shifts in the presence of CFRP.

The low frequency (LF) systems can work with metals in the surroundings as explained in [31]. These systems will only receive a fraction of the total energy without shielding. This is due to a reduction of the intensity of the magnetic field. Being the amplitude of the applied magnetic field H_0 when reaching the surface of the metal, the average power loss per unit volume in the metal due to eddy currents is as explained in [31]:

$$p = \frac{1}{24}\sigma\omega^2 t_s^2 \mu_s^2 H_0^2 \qquad \text{Eq. 22}$$

Inductive coupling-based systems can work through metals only with thicknesses bellow the skin depth. According to Figure 7, it can be concluded for example that a system at the LF band cannot work through any aluminum layer thicker than 0.25 mm approximately.

Similar to aluminum, a CFRP plate also acts as a conductor. Compared with aluminum plate, the difference between the two kinds of materials is that aluminum is an isotropic material while CFRP is an anisotropic material. For an aluminum plate, the material properties: electrical conductivity, relative permittivity and relative permeability are the same in all directions. But a CFRP plate properties need to be described not just as constants but as matrices with values for each direction as:

$$\sigma = \begin{pmatrix} \sigma_x & 0 & 0 \\ 0 & \sigma_y & 0 \\ 0 & 0 & \sigma_z \end{pmatrix} \varepsilon = \begin{pmatrix} \varepsilon_x & 0 & 0 \\ 0 & \varepsilon_y & 0 \\ 0 & 0 & \varepsilon_z \end{pmatrix} \mu = \begin{pmatrix} \mu_x & 0 & 0 \\ 0 & \mu_y & 0 \\ 0 & 0 & \mu_z \end{pmatrix}$$

[1] Ferroxcube International Holding B.V. http://www.ferroxcube.com/FerroxcubeCorporateReception/index.jsp

[2] CRS Holdings Inc. "Magnetic Properties of Stainless Steel" https://www.cartech.com/techarticles.aspx?id=1476

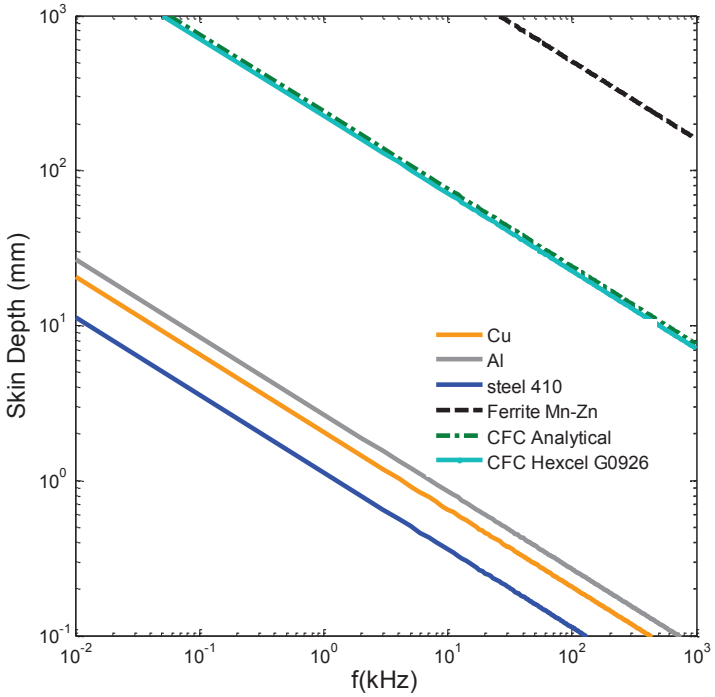

Figure 7: Calculated Skin depth versus frequency for different materials

The calculation method of electrical conductivity σ and relative permittivity ε is explained in reference [32]. It is based on the 1 layer inhomogeneous model. So, there are 3 directions (X, Y, Z) of each parameter. The model as explained in [32], according to which g is the ratio of fiber to resin or fill and it is assumed constant. This is the relative volume of space occupied by the fiber in a period cell and it is calculated as:

$$g = \frac{\pi D^2}{4PL} \qquad \text{Eq. 23}$$

D: Diameter of the fiber

P: Period

L: Layer thickness

Assume that the surface x and y directions are constant while z across the plate is different. The next formulas are inferred in [32] as follows:

$$\sigma_x = \sigma_y = g\sigma_{fiber} + (1-g)\sigma_{resin} \qquad \text{Eq. 24}$$

$$\sigma_z = g\sigma_{fiber}^{-1} + (1-g)\sigma_{resin}^{-1} \qquad \text{Eq. 25}$$

$$\varepsilon_x = \varepsilon_y = g\varepsilon_{fiber} + (1-g)\varepsilon_{resin} \qquad \text{Eq. 26}$$

$$\varepsilon_z = g\varepsilon_{fiber}^{-1} + (1-g)\varepsilon_{resin}^{-1} \qquad \text{Eq. 27}$$

One layer of G0926 fiber composite from Hexcel[3] Corporation is compared to the analytical model. This 5-Harness Satin Weave has a 0°/90° pattern with an average fiber diameter of 7 µm. The fiber density is 1.77 g/cm^3 and the resistivity is $20\Omega mm^2/m$. A piece of 100 cm^2 presenting a 5.75 g weight was evaluated. According to the datasheet the material presents a thickness of 0.38 mm. According to the fiber density the evaluated piece has 5.31 g of fiber and 0.44 g of resin. The period (P=0.58µm) is the distance between fibers and it is obtained from the amount of resin to fiber present assuming the material is homogeneous.

Knowing electrical conductivity of resin and carbon fibers are: $\sigma_{resin} = 1$ and $\sigma_{fiber} = 5e4$. Then Eq. 24 can be aplied, so the CFRP plate properties can be calculated resuting in a conductivity of $8.74 \cdot 10^{-3}\ S/m$. For the same piece with a meassured thickness of 0.5 mm corresponds a conductivity of $1 \cdot 10^{-4}\ S/m$. Both cases, the analytical and the actiual meassurement from the data sheet were used to estimate the skin depth. These results are presented also in Figure 7.

Thermoset Polymers and Moisture Uptake

Resin Transfer molding (RTM) process with vacuum infusion is the main composite manufacturing method reviewed in this thesis. The principal advantage of this method is the realization of high-quality components without using an autoclave as previously described. However, it is long known that epoxy and epoxy composites easily absorb moisture when exposed to humid environments. This is especially true for thermoset resins, like RTM6; which is an aerospace industry standard for resin transfer molding. This is a mono-component resin system with a high glass transition temperature. The moisture absorption can reduce the mechanical properties of the composite and therefore its lifetime. The rigidity is lowered and deformations and elongation properties can be affected. Moisture increases chain flexibility, resulting in degradation of the strength. Also, absorption of moisture means an undesirable increase of weight.

The focus of this thesis is the Lamb-wave response and how it is affected by the modification of the material properties due to water absorption. It is necessary to evaluate this phenomenon of water diffusion in RTM6 in order to better understand the Lamb-wave and give a basic approach for future designs and compensation algorithms in sensor/-actuator networks. Absorption of moisture and vapor in glassy polymers follows complex water diffusion mechanisms. The behavior could be approximated to Fick's laws of diffusion. According to the producer Hexcel Corporation, RTM6 as neat resin presents a water uptake of more than 2% after 14 days in water at 70°C. The characterization is shown in Figure 8. Sensor

[3] HEXCEL Corporation, „Hexcel Aerospace Selector Guide," [Online]. Available: http://www.hexcel.com/Resources/SelectorGuides/Aerospace_SelectorGuide.pdf. [Accessed on Aug 2013]

integration to measure the water uptake could aid understanding the change in the behavior of Lamb-waves. The evaluation of this principle is introduced in section 7.2.

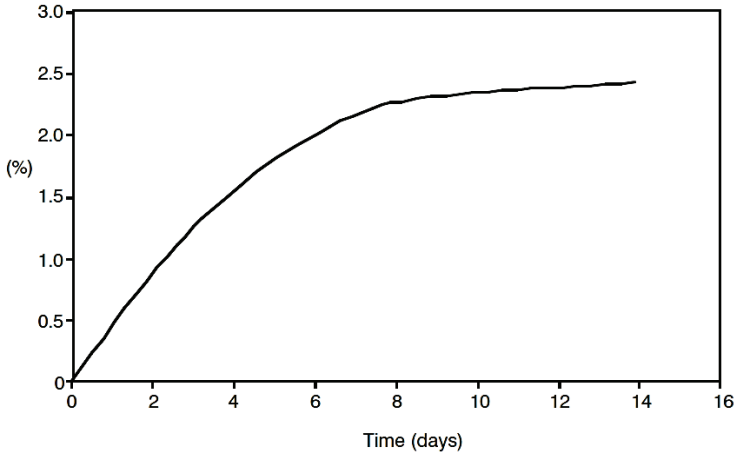

Figure 8: Water uptake of RTM6 (14 Days in Water/70°C) [33]

2.4. Wireless Power Transfer

The term induction comes from inducing, to produce an effect without direct contact. In [34] a promising approach was presented to arrange inductively coupled coils as transformers, thereby driving piezoelectric PZT (lead zirconate titanate) actuators. The magnetic field is modulated to produce the desired signal, which drives the PZT. Then the magnetic field is turned off quickly, and the echo received by a sensor that modulates it and sends it back to the opposite coil. This method demonstrates a very simple way of detecting faults in a given center frequency [4]. With the chosen method, however, difficulties to generate excitation at different center frequencies are significant so that the ability to analyze larger structures remained limited. Also due to the characteristics of such coils the achieved reading distances were of only a few millimeters. Other systems [5] require large embedded computing capabilities and thus the need for batteries and other energy harvesting sources. The system presented in this thesis has been successfully implemented to generate Lamb-waves wirelessly and receive the responses via amplitude modulation. Then later compare with different baselines to determine the presence of damages.

Usually, the coupled coils are used for supplying energy to a microcontroller or a transponder which modulates digital data to the transceiver. In this research, an analog method is proposed for the data transmission. The coil coupling is the decisive measure of the quality of energy and data transmission, which sequentially depends on a higher inductance ratio that is associated with the implementation of a higher number of turns or a higher radius of the secondary coil.

Using state-of-the-art RFID technology sensor nodes can be designed according to specific requirements. Systems can be therefore passive, semi-passive, or active. A passive system will use no additional sources

of energy other than the one provided by the wireless link. Meanwhile, semi-passive and active systems rely on other sources of energy. In a semi-passive system, it is very common to use energy harvesters, while in active systems a battery is implemented. Undeniably, passive and semi-passive systems get usually more attention not only due to their simplicity but also because the absence of batteries allows the system to have a longer life span. Figure 9 shows the operating principle of inductive RFID systems having a reader generating a magnetic field and a transponder (R_L).

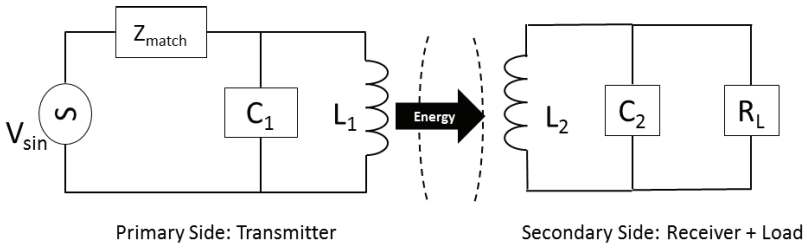

Figure 9: Principle of Wireless Power Transfer

Passive wireless power transfer occurs by implementing the principle of inductively coupled coils. Two Industrial Scientific and Medical (ISM) bands are commonly used in the international community. The first one is High Frequency (HF) working at 13.56 MHz and the second one is Low Frequency (LF) located from 125 kHz to 134.2 kHz [4]. RFID coils that work reliably even when embedded in GFRP parts have been developed recently by Fraunhofer IIS [35]. Such systems need to endure temperatures up to 180°C and high pressures during the manufacturing processes of FRP. An application of these technologies is found in SHM by means of PWAS implementing low-frequency signals with significantly high power consumption.

The magnetic flux, which flows through the primary coil, depends on the coil area. The energy requirement consequently determines the geometry of both inductors. High energy content is linked to high inductance. k is the dimensionless coupling factor in Eq. 3 which describes the mutual inductance M between the two coils and is decisive for the energy content of a wireless coil system [4].

$$k = \frac{\mu_o \mu_r \pi N_1 N_2 r_1^2 r_2^2}{2\sqrt{L_1 L_2}\sqrt{(r_1^2 + z)^3}} = \frac{M}{\sqrt{L_1 L_2}} \qquad \text{Eq. 28}$$

The voltage transferred can be obtained according to Eq. 4 where C_2 is the capacitance in resonance with the receiver coil at a given frequency f_o

$$u_2 = \frac{j\omega k\sqrt{L_1 L_2}\, i_1}{1 + (j\omega L_2 + R_2)\left(\frac{1}{R_L} + j\omega C_2\right)} \qquad \text{Eq. 29}$$

$$f_o = \frac{1}{2\pi\sqrt{LC}} \quad \text{Eq. 30}$$

where R_L is the load on the secondary side and f_o is the resonance frequency with $\omega = 2\pi f_o$.
Under some circumstances, only the efficiency of the system is to be observed, given by the load power to the power sent ratio of Eq. 6. Furthermore, k can be experimentally obtained according to the relation in Eq. 32.

$$\eta = \frac{P_2}{P_1} \times 100 = \frac{\frac{u_2^2}{R_L}}{u_1 \cdot I} \times 100 \quad \text{Eq. 31}$$

$$K = \frac{u_2}{u_1}\sqrt{\frac{L_1}{L_2}} \quad \text{Eq. 32}$$

The desired z_{read} distance between coils goes ideally up to a couple of centimeters for ease of use. Using Eq. 8 the diameter D of the coils can be found.

$$z_{read} = \frac{D}{2\sqrt{2}} \quad \text{Eq. 33}$$

The inductance of a planar coil can be calculated according to Wheeler's formula [36] where N is the number of turns, a is the coil mean radius, and c is the thickness of the winding.

$$L = 31.33\mu_o N^2 \frac{a^2}{8a + 11c} \quad \text{Eq. 34}$$

The inductance of a solenoid is calculated according to Wheeler's formula [36]:

$$L = \frac{D^2 N^2}{h + 0.45D} \quad \text{Eq. 35}$$

The inductance of the coil can also be calculated using the total magnetic energy. The energy is created by the current which goes through the coil with the following formula:

$$W = \frac{1}{2} L I^2 \quad \text{Eq. 36}$$

W is the total magnetic energy in the coil which can be calculated automatically using Finite-Element-Models (FEM) in order to compare to the theoretical and measured results.

For the high-frequency planar coils the self-inductance is calculated using the simple expressions given by the Data Fit Monomial presented on [37] for a square planar coil:

$$L = \beta\, d_{out}^{\alpha 1}\, w^{\alpha 2}\, d_{avg}^{\alpha 3}\, n^{\alpha 4} s^{\alpha 5} \qquad \text{Eq. 37}$$

Where αi and β are layout dependent coefficients already given for a square coil as:

$\alpha 1 = -1.21$
$\alpha 2 = -0.147$
$\alpha 3 = 2.4$
$\alpha 4 = 1.78$
$\alpha 5 = -0.03$
$\beta = 1.62E - 3$

Radio Frequency Identification (RFID)

RFID systems can be classified as seen in Table 1 depending on the physics involved and the Electromagnetic band selected [31]. This work will focus on understanding the application of LF and HF bands for the purpose of actuating and collecting sensing data from the PWAS.

Table 1: RFID Classification

Physics Involved	**Electromagnetic bands**
Inductive coupling	LF (125-134.5 kHz)
	HF (13.56 MHz)
Capacitive coupling	UHF (~900 MHz)
	ISM (2.4 GHz)

Inductive coupling has the advantage of generating energy enough to power a tag without the need of a battery or other energy harvesters. The 125 kHz band is unregulated and typically use for animal identification. The 13.56 MHz band, on the other hand, is considered worldwide as Industrial, Scientific and Medical Band (ISM). There are different existing protocols to communicate at13.56 MHz:

- ISO/IEC 14443-1: Physical characteristics
- ISO/IEC 14443-2: Radio frequency power and signal interface
- ISO/IEC 14443-3: Initialization and anticollision
- ISO/IEC 14443-4: Transmission protocol

The transmission protocol specifies data block exchange and related mechanisms: data block chaining waiting time extension multi-activation. ISO/IEC 14443 uses the following terms: PCD for proximity coupling device (reader) and PICC for proximity integrated circuit card (tag), represented in Figure 10.

Passive systems present limitations of power and data rates. For example, systems based on the use of digital backscatter to communicate sensor data suffer from power and protocol limitations as explained in [38]. ADCs are power voracious components, and sampling at a few Hertz rate can consume more energy than can be harvested if the tag is far from a reader or in a metal environment. Furthermore, the protocol overhead and low bitrate of existing protocols limit the maximum uplink rate to tens of packets per second.

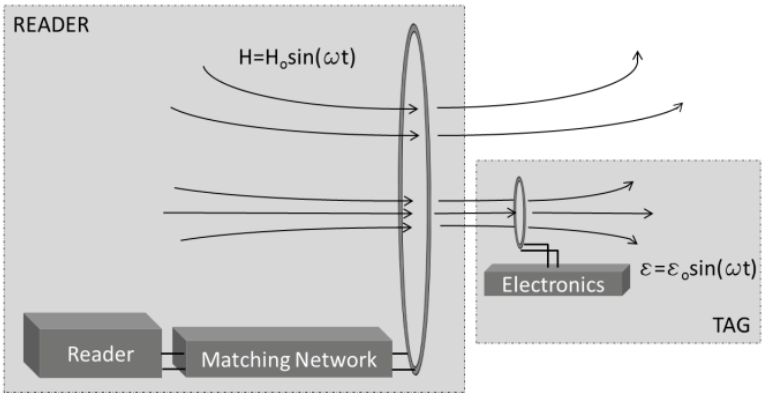

Figure 10: Inductive Coupling RFID Principle

In order to alleviate this problematic, new design of wireless systems that use the RF front end, for example, dipole antennas, have been demonstrated to transmit data from a microphone. This is known as Hybrid Analog-Digital Backscatter Platform for High Data Rate, Battery-Free Sensing [38]. The authors switched a microphone in and out of the backscatter network using an RF switch. The microphone has no additional biasing circuitry and the internal JFET is self-biased in the triode region. The RF switch and the digital RF MOSFET are both controlled by the output ports of the microcontroller. This system used a wireless Internet service provider (WISP) with Gen 2 protocol completely in firmware by modifying the state machine so that it transitions to analog backscatter mode when it receives a "read" command. After a set amount of time, the firmware switches the microphone out of the network and returns to digital mode. Similar to this approach an analog signal from a PWAS can be transmitted by the sensor node to the reading device. Using a MOSFET in the triode region, amplitude modulation of the Lamb-wave signal is done. The communication proceeds by alternating analog and digital information over the same channel. With this switching, there is no need for dual communication as the tag or sensor node is continuously transmitting. This technology allows the implementation of other important information such as an ID number per node. Finally, the possibility to add more sensors to one node can also be considered.

3

Wireless Power Transfer for Structural Health Monitoring

The development of new approaches for wireless SHM has raised interest from the research community as well as from the industry. The major challenge is the integration of such technologies without affecting the low weight of the structure or generating an impact as mentioned in Section 2.1. It is not possible to predict the long-term impact of the foreign body in the CFRP [10, 6]; hence the interest in the use of small and very thin systems. The aim is to create a wireless sensor network for use in SHM by implementing the approach of inductively coupled coils. The contents of this section have been published partially by Salas, Focke, Herrmann and Lang in [39] and [40].

Choice of operating frequency varies according to the needs. However, standard operating frequencies exist, with 125 kHz and 13.56 MHz bands being the most widely used worldwide for radio-frequency identification (RFID). The design of antenna coils for low frequency (LF) and high-frequency bands (HF) for the integration in fiber reinforced composite materials to achieve wireless power and data transfer are evaluated in this section. This section focuses on the experimental evaluation of the possible problems in the realization of such system. The application of SHM in aeronautics is one of the main targets of this work, where composite material most commonly used is Carbon Fiber Reinforced Polymer. These structures are interesting due to their complex geometry, anisotropic properties, as it was briefly explained in the previous section. There are concerns regarding the electrical conductivity of Carbon Fiber Reinforced Polymer which might render it impossible to transmit energy into the material and data out.

Experimental demonstrations of coil coupling for the inductive power transfer in such surrounding are presented here, indicating that it might be feasible to wirelessly transmit enough power to a receiver bonded onto the surface or even covered with one thin layer of CFRP. The quality of such transmission changes depending on layer geometry; frequency and range of transmission desired. CFRP behaves as a conductor, which hinders the use of wireless techniques as it will be explained in section 3.2.

Little literature is found regarding the lower frequency inductive power transfer in CFRP environment. Perhaps the data transmission rates are too slow or the antenna sizes are too large for embedding. Nonetheless, considering that Lamb-waves are excited at low frequencies of 100 kHz to 350 kHz, the direct combination of LF antenna coils with the piezoelectric elements is of high interest.

SHM by means of PWAS implements low-frequency signals with considerable power consumption. When considering material-integrated systems, the necessary power can most easily be provided via induction. Here, the quasi-stationary magnetic field, which is generated from the primary coil, must stimulate the secondary coil and generate enough power to provide the PWAS actuator-sensor array. An example is found in conventional RFID systems, at high frequencies (13.56 MHz), where the transponder is located in the permanent magnetic field. In this case, all activities of the transponder, such as the collection of sensor data, end as soon as the magnetic field is cut off. Alternatively, in low frequency (125 kHz) systems, a consecutive method is used. During the pulsed excitation of the primary coil, the transponder is charged, followed by the switching off of the magnetic field on the primary side, at which point the transponder transmits its data by consuming the stored energy.

In the following work both technologies are taken into consideration to determine which will better fit the needs of SHM environments. The first tests carried out only focused on the antenna system. It should be kept in mind that the desired system is fully passive and inductively powered for easier integration in the fiber composites where no external power sources are required on the secondary side.

The reading distance is between 0.25 cm and up to 5 cm. The coil system can be modeled knowing that a PWAS needs a pulsed excitation voltage of one burst between 50 and 100 V peak-to-peak (V_{PP}) with around 50 mW to 200 mW consumption. For each set-up the transmitter antenna coils were matched according to the 50 Ω from the signal generator, this means 250 mW are transmitted. Next, the design of coils for LF and HF is presented. Furthermore, the evaluation of the coupling was carried out using different geometric combinations of transmitters and receivers.

3.1. Planar Coil Design for the HF (13.56 MHz) Band

The results presented in this section have been shortly introduced in the publication [39]. Since the geometrical limitation is the thickness approximately 0.5 mm and not the area of the antenna, and in order to avoid imperfections that may occur on air core coil design, antenna coils were implemented on printed circuit boards. In this first test the coils were made on the FR4 substrate; however, finally they are brought to flexible PCB (Polyimide 50µm thick) in order to reduce the total thickness of the system.

Software modeling tools that implement generalized minimal residual method (GMRES) algorithm (i.e. COMSOL) were used to validate results. Also, Fasthenry, open source software that solves Maxwell equations and dues extraction of inductances and resistances, was used to evaluate the coils. As shown in

Figure 11 (a) A DC analysis using COMSOL Multiphysics to determine self- inductance and the resistance of the coils are shown, where the streamlines indicate the magnetic flux density and the surface is the electric potential. This example has five windings of 0.6 mm width and 0.3 mm spacing. The outer diameter is 2.5cm. The maximum Magnetic flux density norm of 1.52 mT was obtained. In Figure 11 (b) using Fasthenry the geometries of transmitter and receiver coils were varied and self-inductance as well as mutual inductance was obtained. The figure shows the graphical interface FastModel also available from FastFieldSolvers.

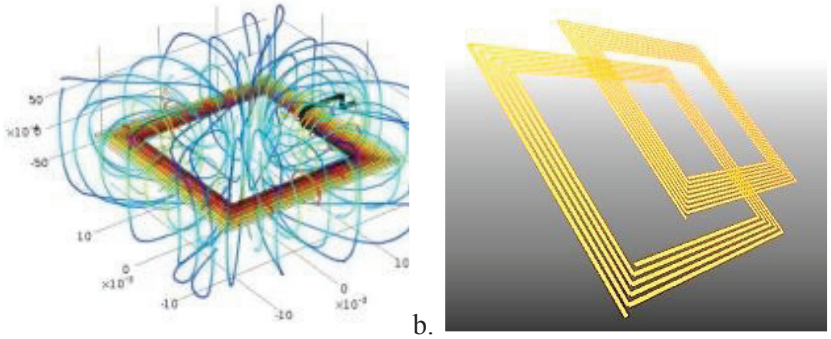

a. b.

Figure 11: (a) COMSOL planar coil DC analysis. (b) Fasthenry model of the coils in the air and mutual inductance evaluation.

Self-inductance can be calculated using theoretical methods as Modified Wheeler, Current Sheet, and Monomial Fit [37]. Recalling the data fit formula in Eq. 37 the inductance can be analytically estimated. Some of the evaluated coils are presented in Table 2. Also, their corresponding number of windings (N) and dimensions: side length (ab_{out}), winding width (w), and spacing between windings (s) are specified. The presence of parasitic components cannot be ignored. Parasitic capacitance (C_{par}) consists of two terms: C_{tt} located between turns, and C_{ox} between turns and substrate [41]. The self-resonance of each coil was measured as shown in Table 2 in order t to validate the calculations.

Table 2: Examples of Planar Coil Characterization

		Dimensions			**Calculated**			**Measured**
Coil Nr.	N	d_{out} [mm]	w [µm]	s [µm]	L [uH]	Cpar [pF]	Fsres [MHz]	Fsres [MHz]
1	5	40	500	500	2.03	31.51	19.91	19.68
2	3	30	150	300	0.77	40.12	28.64	30.45
3	4	30	150	150	1.39	39.47	21.51	22.98
4	5	30	150	150	2.05	39.54	17.70	19.08
5	8	30	300	300	3.34	29.89	15.94	15.34

The first trial used coil Nr.2 as the transmitter and coil Nr.4 as the receiver. The set-up for the coil evaluation is presented in Figure 12. The receiver coil is fixed at z = 0 cm and the transmitter is moved in the vertical direction. At each step, V_{PP} on the receiver is recorded using Labview interface that automatically calculates the coupling coefficient. In this case only up to at 1 cm distance between coils

approximately 10 V_{PP} was measured on the secondary. Since a larger reading range is desired, another test system is selected using a larger coil, Nr.1, as the transmitter, while coil Nr.5 placed at the receiver position. Efficiencies of 47.2% at close contact and 9.1% at 2cm were obtained.

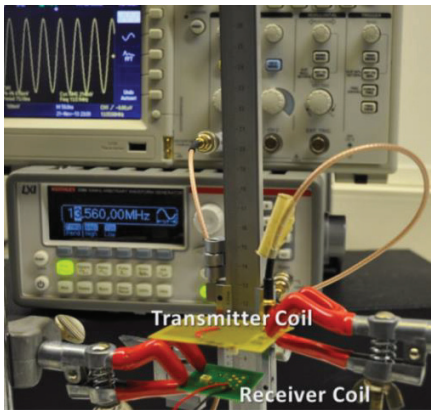

Figure 12: Coupling evaluation set- up

3.2. Antenna design for the LF (125 kHz) Band

The simulation of inductive coils at LF implies long computation times for solvers using Finite-Element-Method (FEM) for instance, COMSOL or Microwave Studio CST, due primarily to the small geometry size of the coils with respect to the large frequency wavelength. In the following design, a theoretical approach is used. The contents of this section have been partially presented on [39, 42].

A low-frequency wireless actuator node is achieved by combining the PWAS with an inductive coil in resonance similar to a Radio-Frequency-Identification System [4]. In this case, the voltage transferred can be obtained according to Eq. 4, where C_2 is the capacitance in resonance with the receiver coil. Substituting the load in the receiver for the piezoelectric, the PWAS is connected in parallel with the coil, while the resonance frequency is adjusted by means of a capacitor, as seen in Figure 13. Additional components may be necessary to keep the PWAS power supply stable and to obtain the pulse from the primary side.

To generate Lamb-waves the necessary voltage at the actuator should be 50 V to 100 V in amplitude with about 200 mW power consumption. For example, an input power of 250 mW is necessary on the primary side if the losses due to the conductive material CFRP are not considered and assuming a non-ideal coupling between coils of 0.8. The limitations on the secondary side are the thickness of the system and the weight it adds to the structure. In this work, an analog method is followed for the Lamb-wave wireless transmission. A low-frequency wireless SHM system is achieved by combining the PWAS with an inductive coil in resonance similar to RFID. In this case, the load in the receiver is replaced by the piezoelectric element. The coil is connected in parallel with the PWAS and the resonance frequency is adjusted by means of a capacitor, as seen in Figure 13. Additional components may be necessary to control

the voltage and to obtain the pulse from the primary side. Piezoelectric elements present large capacitances. A PWAS has about 3.4 nF, having, therefore, an influence on the resonance system when connected in parallel to the receiver coil. Consequently, the resonance must be adjusted.

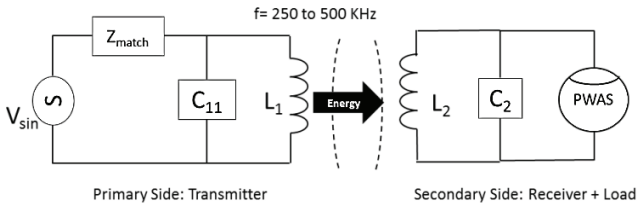

Figure 13: Wireless Power Transfer to a PWAS

The reader unit containing the primary coil should be located within 0.5 to 5 cm away from the CFRP structure in which the secondary coil is surface applied. According to Eq. 33 for a distance of 5 cm between coils the radius of a solenoid coil should be approximately 7 cm. To double the diameter of the coil can increase the read range as long as the quality of the coil is kept. On the other hand, it is also possible to double the power sent to increase the read range, this is done by increasing the current drive into the primary coil. This is the intended approach in the next sections due to the above-given geometry limitations and the presence of electrically conductive materials. Based on the coupling of a coil system the power can be proportionally increased to reach larger ranges.

In order to evaluate this WPT principle transmitter and receiver solenoid coils are made with Litz wire of 25/0.071mm and the calculated inductance follows Eq. 36. In Table 3 the descriptions are shown for the coils used on the first coupling test. The system has a reading distance of almost 3 cm according to Eq. 38. Using a signal generator Keithley 3390, a 500 kHz sine excites the coil system in resonance with 250 mW output on the primary side. The maximum voltage peak-to-peak V_{PP} obtained at the secondary coil is 33.5 V as seen in Figure 14 where the received voltage has been plot versus the distance Z_{READ} between coils. The maximum measured coupling is 0.8.

Table 3: First System - Receiver and Transmitter Characteristics

	Number of Windings	**Diameter [mm]**	**Calculated L[µH]**	**Measured L[µH]**
Receiver	45	80	273	272.2
Transmitter	15	80	36	34.4

The analytical calculation for the received voltage is done implementing Eq. 29, based on the coil system coupling. This approximation method is ideal and does not account for the negative effect given by the proximity effect of the coils that produces a shift in the resonance frequency thus detuning the system. On the other hand, the Spice simulation agrees with the measurement showing that this de-tuning effect ends when the coils are 25 mm away from each other. The Spice simulation is done by adding the calculated coupling from Eq. 28 and running a parametric sweep for k using a transformer model. The results in Figure 14 are close to the values measured.

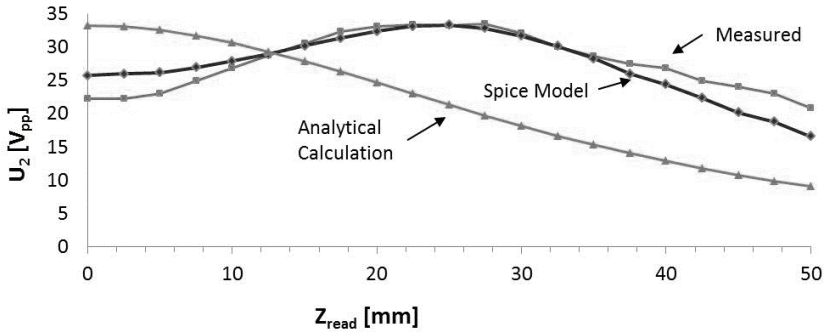

Figure 14: Coupling at 125 kHz – analytical calculation, numerical evaluation, and measurement

One of the main goals is to reduce the area occupied by the secondary coil in the structure. Therefore, the diameter of the receiver is reduced to 4 cm. The objective is to apply the coils to the surface of the CFRP. One way would be by glue or binders and another approach is the use of sewing techniques known as tailoring. For tailored placement, the coils need to be as thin as possible to avoid bulky geometries. In order to produce thinner systems, a planar receiver coil is made with magnetic bifilar wire AWG 32 from MWS Wire Industries[4]. Polyimide wire isolation is selected for up to 200°C thinking of future integration during plate manufacturing which occurs at high temperatures for aerospace resins like RTM6. The transmitter solenoid coil is built with the same diameter as the receiver to obtain the best coupling. Using 15 windings to keep a high ratio from primary to secondary side allows increasing the voltage amplitude received. Values for the coils are presented in Table 4. The inductances are calculated according to Wheeler's formula for the planar coil (Eq. 34) and a solenoid (Eq. 35). With this coil system at a frequency of 125 kHz a maximum of 13.7 V_{PP} is obtained on the secondary side, this corresponds to a measured coupling of 0.98. At a distance z of 5 cm between coils, 1.4 V_{PP} are received. This is equivalent to a coupling of 0.1. At the maximum coupling the response from the PWAS sensor, located 15 cm from the actuator, is of 30 mV_{PP}.

Table 4: Second Test System - Receiver and Transmitter Coil Characteristics

	Number of Windings	**Diameter [mm]**	**Calculated L[µH]**	**Measured L[µH]**
Receiver	30	40	34.5	32.4
Transmitter	15	40	17.1	16.7

Reducing the size of the coils decreases the read distance and the power received. An approach is to reduce the radius but increase the windings of the secondary side. Therefore, it is necessary to evaluate the system using the smaller secondary coil but keeping the quality of WPT. In consequence, the windings on the secondary side are increased to 50 and a thin magnetic sheet is added under it to improve the quality. The diameter of the receiver coil is kept at 40 mm with an inner diameter of 15 mm. The description is presented

[4]MWS Wire Indstries, [Online]. Available: http://www.mwswire.com/multifilar.html. [Accessed on April 2015]

in Table 5. The difference between the measured value and the calculated value is attributed to the use of a high permittivity material. As transmitter, the coil with inductance 9.7 µH available in the market and presented in Table 5 is selected due to its ferrite core and high-quality factor. The final coupling test is done at 125 kHz. The winding ratio of 1:3 offers the advantage of higher voltage gain at the receiver. With this system, the final coupling is shown in Figure 15 with a maximum voltage of $23V_{PP}$ obtained at the receiver coil which corresponds to a k factor of 0.82.

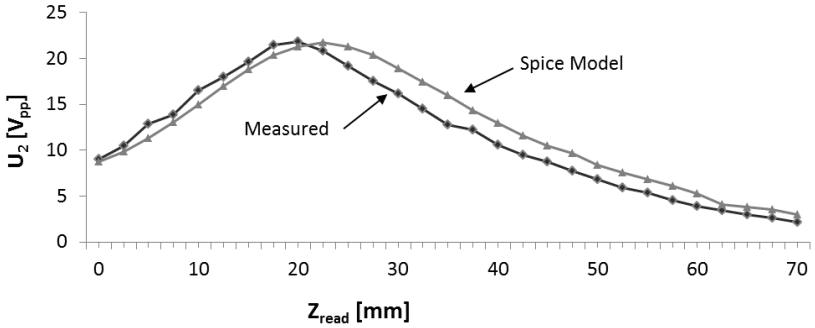

Figure 15: Coupling for the final coil system

Table 5: Final System - Receiver and Transmitter Coil Characteristics

	Number of Windings	Diameter [mm]	Calculated L[µH]	Measured L[µH]
Receiver	50	40	75.2	83.4
Transmitter	15	Vishay Dale (IWAS-4832FF-50)		9.7

3.2.1. Finite Element Method (FEM) Simulation

In COMSOL Multiphysics the AC/DC module is used to estimate the Magnetic field behavior. A five turns coil is designed with the diameter of 2.5 cm. Copper wire cross section diameter is 1 mm with polyimide layer thickness 10 µm. Current flows through the coil which is a stationary surrounding so there is a magnetic field generated according to Maxwell's theory and equation Eq. 34. All parameters of the coil are defined: Winding number, the diameter of the coil, the diameter of the copper wire, the thickness of polyimide, and materials. The coil physics condition is set as a Single-turn coil, suitable to compute the current–carrying conductor models which create magnetic fields. A closed current loop is necessary, so assigning a closed current path was done by setting the ground and the boundary feed to the corresponding surfaces as seen in Figure 13. After dealing with the boundary conditions and the meshing, the stationary study was run. Then the magnetic flux density distribution of the whole model was calculated and based on that and according to Eq. 11 the inductance of the coil is obtained as 0.374µH. The resistance of the coil is obtained in a similar manner. After choosing the resistance expression and evaluating it, the resistance value of the coil is generated as $7.2\times10^{-3}\Omega$.

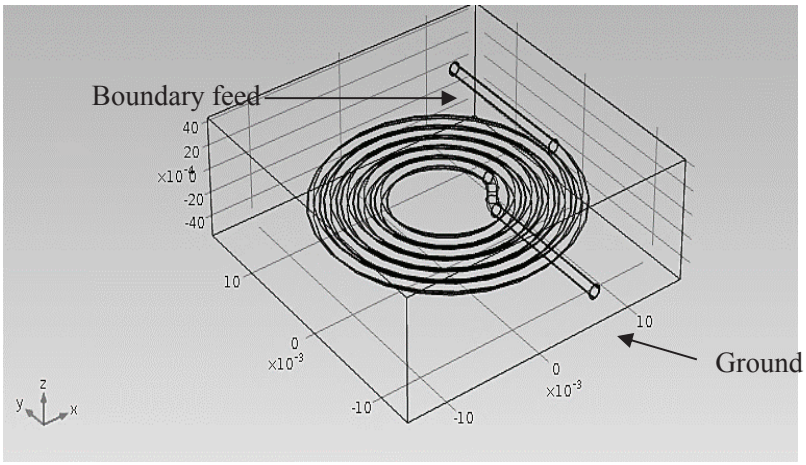

Figure 16: COMSOL Multiphysics Coil geometry

3.2.2. Taylor-Fiber-Placement of LF Coils

The integration of sensor-actuators and coil antennas within the material is achieved using TFP process by sewing onto the textile. Usually, a machine used in the garment textile industry is adapted to stitch fiber roving material onto a base material. This is done by continuous placement of a single roving. The roving material pulled off a spool and it is guided by a pipe which is positioned in front of the stitching needle. This roving and the base material move synchronized as a zigzag stitch. The base material can be a textile such as woven or non-woven fabric or a matrix-compatible foil material. The stitching path can be designed with the help of classical embroidery software or recently by using a 2D computer aided design (CAD).

The infiltration of resins on TFP products can be done with conventional processing techniques such as RTM, vacuum bag molding, pressing and autoclave. The base material can be a thermoplastic foil which consolidates and becomes part of the matrix.

This TFP technology is used by Faserinstitut e.V. An example of how embedding of the coils in FRP is done is shown in Figure 34. Here, a coil is stitched on glass fiber fabric by a modified embroidery machine Tajima TMHL- G 108 which is used for Tailored-Fiber-Placement at Faserinstitut e.V. [43]. Also, the PWAS and the necessary electronics can be placed in the same way on an embroidery ground. The signal integrity should be evaluated and compared to that without embroidery.

a. 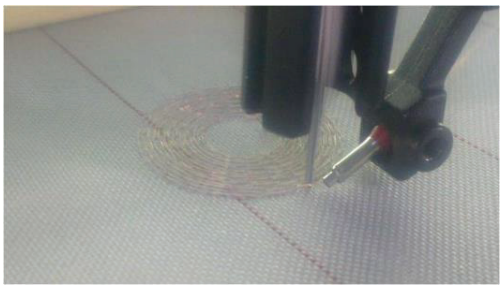 b. 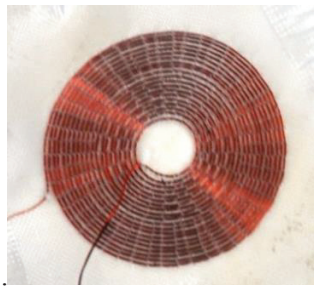

Figure 17: (a) Tailored-Fiber-Placement process (b) Receiver coil produced with 25 windings [42]

Table 6: Low- Frequency Receiver Coils

Method	Number of Windings	Outer Diameter [mm]	Calculated L [µH]	Measured L[µH]
Glued Coil	50	40	75.2	83.4
TFP Coil	25	40	22.86	19.84

3.3. Influence of CFRP on the Wireless Power Transfer

The different effects produced by metals on RFID systems come from the presence of eddy currents. These effects are the distortion of the electromagnetic field, detuning, and shielding. As a result, the readable distance is reduced. The inductive coupling method is based on the resonance of the antenna-tag circuit as explained in Figure 10. A metal produces a drift of the working frequency. This is the so-called detuning effect. A proper design of the system can allow it to work with metals on the surroundings avoiding this effect. Some different techniques and methods have been proposed. They are based on introducing dielectric gaps in between the metal and the tag, or in the use of magnetic materials like ferrite [31]. Considering that a reinforced polymer is a matrix of epoxy or resin with fibers, the conductivity is dependent on fabrication techniques and the frequency of the wireless transmission. Subsequently, it should be possible to see some power transmitted by inductive coils when only one layer of CFRP with low fiber density is placed relatively close behind to the receiver coils or when the receiver is completely covered.

3.3.1. Experimental Evaluation

Different tests to validate the influence of CFRP on the transmission were carried. These results have been presented in IEEE Sensors journal [39]. First, a one layer laminate was cut into small square pieces and placed on top and bottom of the receiver, sealing it in order to observe the effect on the coupling at different distances between coils. At HF the efficiency was reduced to one-third of its original value. In the LF range, the efficiency decreased to half the original value. On the second test, a one layer unidirectional laminate was placed directly under the receiver in order to observe the effect on the reflection coefficient of the antenna coil. The quality of the antenna coil in the LF range decreased, but the effect of CFRP is

stronger in the HF range, where the resonance frequency shifted.

G0926 fiber composite from Hexcel[5] Corporation presented in Section 2.3 was selected for the following evaluation. This 5-Harness Satin Weave pattern has an aerial weight of 370±14 g/m^2, the average fiber diameter of 7 µm and fiber density of 1.77 g/cm^3. Resistivity is known to be$20\ \Omega \cdot mm^2/m$. In order to rule out corruption of the measurement by a parasitic wave path around the CFRP material, the closed pocket of CFRP around the receiver coil was built as seen Figure 18. One layer was placed on the top and another at the bottom of the coil to observe the influence on the coupling. This set-up, from this point on is the "pocket" construction and will be addressed when referring to CFRP surrounding. The same construction was implemented using GFRP with a 90°/+45°/-45° pattern. The data was fitted in Matlab using smoothing spline function.

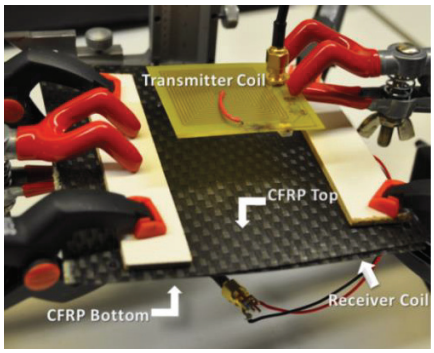

Figure 18: Coupling evaluation set-up: CFRP is placed top and bottom of the receiver coil [39]

Figure 19 shows that the coupling decreases when introducing CFRP and the efficiency is highly attenuated to 14.1%. The values were obtained at a vertical distance between coils going from 0.25 cm to 4 cm. With only one added layer of carbon fiber top and bottom, roughly one-third of the efficiency are obtained in comparison to the reference case without any cover.

Coupling improves with respect to the first LF system. Additionally, a lower effect from CFRP in comparison to the HF system is observed. An efficiency of 4.85% was found at close distance with the receiver inside the CFRP pocket. This corresponds to about half of the power obtained with air surrounding the receiver coil. Coil Nr.9 was also evaluated as a transmitter, showing a lower efficiency due to its low inductance, and was later discarded. In Table 6 a summary of the LF and HF designs is presented. It indicates which coils were used as a receiver (RX) and transmitter (TX), the frequency of the system f_o, the coupling at a distance of 2 cm, the power efficiency without cover and finally the efficiency when RX is inside the CFRP pocket.

[5] HEXCEL Corporation, „Hexcel Aerospace Selector Guide," [Online]. Available: http://www.hexcel.com/Resources/SelectorGuides/Aerospace_SelectorGuide.pdf. [Accessed on Aug 2013]

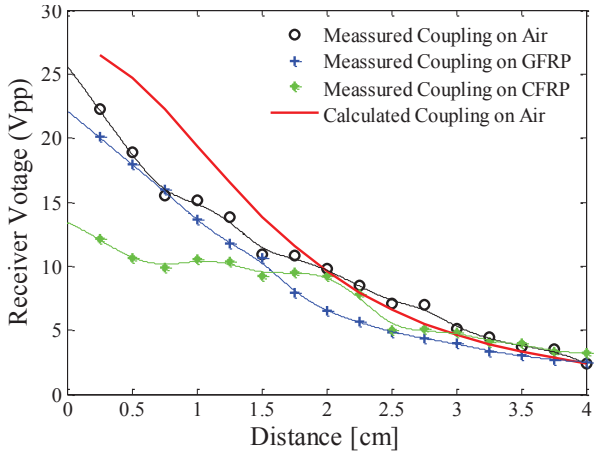

Figure 19: Coupling between planar coils near 13.56MHz [39]

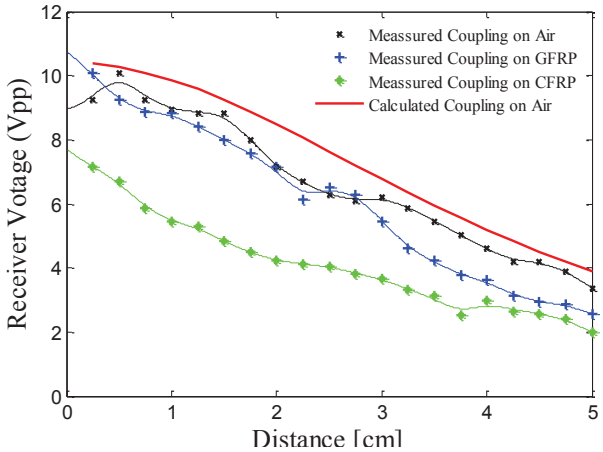

Figure 20: Coupling at Low Frequency near 125 kHz [39]

Table 7: System Comparison: HF versus LF

	Coil Nr.	f_o	K at z=2 cm	η without cover z=0	η inside CFRP Pocket z=0
HF System	Rx1,Tx5	13.56 MHz	0.768	47.2%	14.1%
LF System	Rx8,Tx7	125 kHz	0.494	8.1%	4.85%

Depending on their frequency, radio waves can be shielded by such materials due to eddy currents. These effects constitute a problem for the implementation in real SHM environments. In the high-frequency range, the influence is higher compared to the low-frequency range. At the 13.56 MHz range, the efficiency decreased to one-third of its value once the CFRP was introduced to the antenna system. Meanwhile, at the 125 kHz range, efficiency decreased to half of the reference value.

In order to validate the coupling results, the coil input reflection coefficient (S11) was measured using a Vector Network Analyzer. These results have been previously presented on [39]. This way, the radiation capabilities of the receiver coils specifically can be better observed under the presence of CFRP. In Figure 21 the reflection coefficient S11 of the antenna is attenuated from -50.4 dB to -14.4 dB, implying that the quality of the antenna coil degrades when placed at a distance of 1 cm from the CFRP material.

On the other hand, the effect is worse at the HF range, as can be observed in Figure 22 where the reflection is not only attenuated from -43.9 dB to -9.9 dB, but also the resonance frequency shifted to 14.52 MHz: Thus a better understanding of the earlier coupling results can be inferred. This topic is presented in [30], where the challenges of HF passive system integration were introduced.

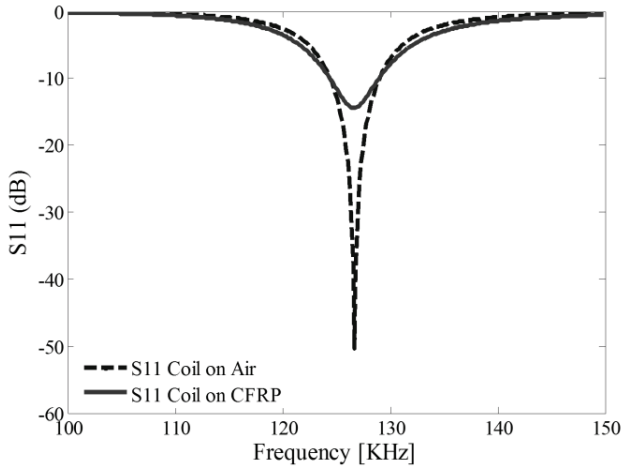

Figure 21: Influence of CFRP to the resonance frequency in the LF band

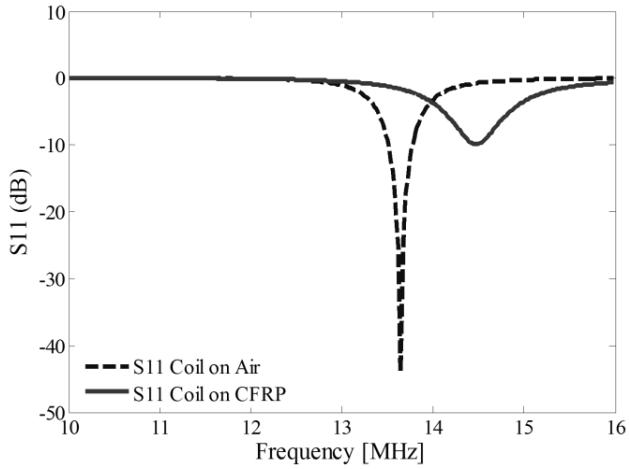

Figure 22: Influence of CFRP to the resonance frequency in the HF band

The location of the antenna coil plays an important role for the performance of the full system. Therefore the effect of the distance from the receiver to CFRP surface was studied, where the receiver coil was placed as approximately 2 cm away to a side fuselage structure, courtesy of Faserinstitut e.V., showing the same results as obtained in the experiments with smaller panels. This leads to believe that the size of the CFRP panel can be approximated as a very large structure, as long as the receiver coil has enough separation to the laminate. The optimum separation distance would then depend on the antenna size, the frequency used and the fabrication techniques of the CFRP.

3.3.2. Finite Element Method (FEM) Electromagnetic Simulation

As explained in section 2.3 when a plate of metal, for example, aluminum, is placed near a copper coil, the induced magnetic field will reduce the original magnetic field because of the eddy currents and Faraday and Lenz Laws. Compared to the anisotropic aluminum plate as explained in the previous section CFRP has anisotropic properties. This characteristic of CFRP leads to the difficulty to define material in COMSOL Multiphysics. As CFRP is considered as a conductor, there will be also eddied current generated inside CFRP. The distance between CFRP and the coil can influence the coil performance, but to which extent is necessary to investigate. When CFRP plate is placed near the coil a decrease of impedance can be expected. The influence of CFRP to the resonance in high frequency and low frequency has been tested in the previous section. When the power is incident to the antenna, a part of it can be reflected. Another part of the energy is absorbed or radiated, which is the lost inside the antenna. The commonly used parameter S11 represents how much energy is reflected from the antenna, which is also known as return loss. The unit is dB. Hence the parameter S11 represents the quality of antenna coil. FEM simulation tools use different algorithms and approaches. When using quasi-static FEM solvers there is a rule of thumb that the size of the maximum distance between two points should be less than one tenth of the wavelength as described in Eq. 38, c_0 is the speed of light. Therefore, in the case of small geometries the use of large wavelength is not possible to solve. In such cases other solvers can be used that evaluate the electromagnetic wave behavior.

$$a > \frac{1}{10}\lambda = \frac{1}{10}\frac{C_0}{f} \qquad \text{Eq. 38}$$

- ***High-Frequency***

In order to confirm the results, the high-frequency behavior of the coefficient S11 was simulated by using CST Microwave Studio, placing a very large plate with thickness 0.5 mm at a distance of 1 cm from the receiver coil. The anisotropic behavior of CFRP material was defined using a model, where conductivity and permittivity are determined by the ratio of carbon fiber to resin content [24, 44]. The results as see in Figure 23 were similar to those found in [30].This simulation tool treats the coil as an antenna and not as an inductance. S11 is here compared under three different situations: Coil on air, coil on aluminum and on CFRP. The receiver coil is 1 cm away from the plate. The reflection coefficient S11 reduces and resonance shifts as expected from the experimental results.

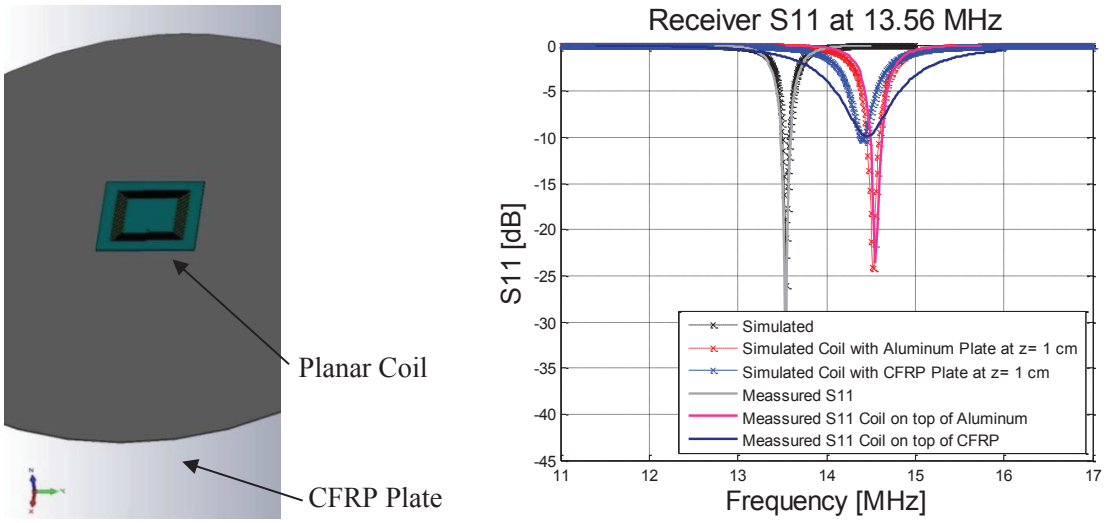

Figure 23: Microwave CST Simulation for HF coils placed near CFRP and Aluminum

With the simulation model, the behavior of the antenna can be predicted and therefore the corresponding matching networks to compensate this effect can be designed. In consequence, the antenna resonance can be tuned to the desired frequency. This has been demonstrated by re-tuning an antenna coil and getting the resonance frequency back to 13.56 MHz. Moreover as seen in Figure 24 the quality of the antenna decreases when introducing a CFRP plate under it. This is effect was partially eradicated by adding high a permeability (μ) sheet[6] between the coil and the plate. The frequency shifts to a lower range, but with the help of a matching network the resonance at 13.56 MHz can be achieved again.

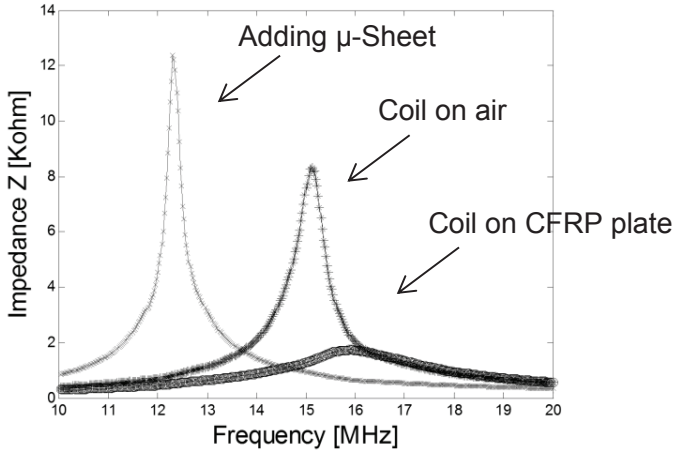

Figure 24: High-frequency (13.56 MHz) receiver antenna tuning

[6] "Noise Suppressing Magnet Sheets" TDK Corporation, [Online]. http://product.tdk.com/en/products/noise-sheet/noise-sheet/catalog/ [Accessed on Jan 2015]

❖ ***Low-Frequency***

As shown in the experimental evaluation at the low-frequency band, the reflection coefficient S11 was observed to attenuate but the resonance did not shift. The following simulations done using COMSOL Multiphysics AC/DC module were partially carried out by Liu J. [Appendix]. First of all, to find out the self-resonance of the coil, a lumped element was added as in the reference model offered by COMSOL. The materials of the whole geometry including air block, copper wire, and isolation layer were defined. Then the 1V potential is added to the lumped port in order to provide the wave excitation. The meshing was chosen for each portion separately and the frequency range for the study was set from 10 MHz to 100 MHz in 10 MHz steps. Figure 25 presents the coil model in an air block.

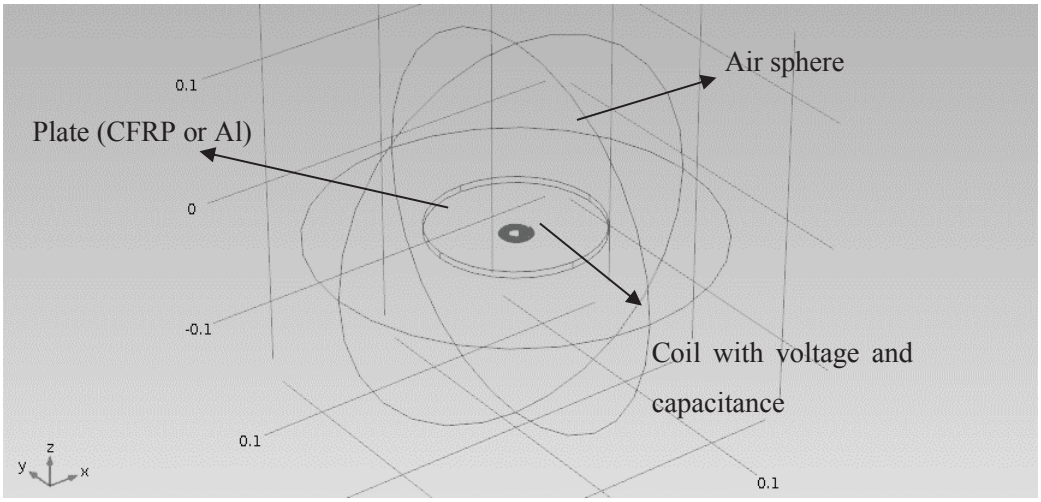

Figure 25: Geometry of low-frequency coil with Al plate and materials distribution

The self-resonance of the coil model can be found at the highest impedance point. In the low-frequency domain, the simulation was carried for 500 kHz. In order to achieve resonance as seen in Figure 26, a capacitance is added as a lumped element, which is 0.292μF. Considering the skin depth of the coil, it is defined as an impedance boundary, which takes into account for the calculation only the surface. The resonance of the system is not located at 500 kHz but at 450 kHz, probably produced by parasitic capacitances on the air gaps between coil windings. The parasitic capacitance is what defines the coil self-resonance and will only be of importance at much higher frequencies where the inductor starts to behave as a capacitor.

Moreover, an aluminum plate of 0.5 cm was added at a distance of 3mm under the coil. The diameter of the aluminum plate is set about five times of the coil diameter. The skin effect of the aluminum plate is considered using a Boundary layer mesh. After adding an aluminum plate, the impedance decreased as expected. In Figure 26 the comparison of a coil without a plate and with aluminum plate are presented.

The resonance of the coil with aluminum plate can be found out, which is 550 kHz. In this simulation due to the eddy current and the induced magnetic field, the total inductance decreases.

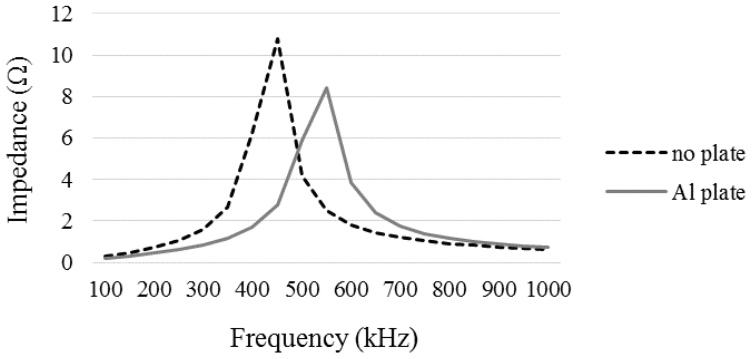

Figure 26: Impedance-frequency comparison Coil without plate and with Al plate

Finally, the CFRP plate influence to the low-frequency coil is investigated. Since CFRP cannot be found in the material library and it is an anisotropic material, a new material is added and defined. A symmetric matrix is chosen for electrical conductivity and relative permittivity as explained in section 2.3. The material electrical conductivity σ and relative permittivity ε are given:

$$\sigma_{resin} = 1 \qquad \varepsilon_{resin} = 4$$
$$\sigma_{fiber} = 5e4 \qquad \varepsilon_{fiber} = 12$$

Then the CFRP plate properties can be calculated:

Electrical conductivity:

$$\sigma = \begin{bmatrix} 2.74 \times 10^4 & 0 & 0 \\ 0 & 2.74 \times 10^4 & 0 \\ 0 & 0 & 0.4509 \end{bmatrix} \text{S/m}$$

Relative permittivity:

$$\varepsilon = \begin{bmatrix} 8.39 & 0 & 0 \\ 0 & 8.39 & 0 \\ 0 & 0 & 0.1584 \end{bmatrix}$$

According to [45], relative permeability μ is a quantity which measures the ratio of the internal magnetization to the applied magnetic field. A quantity X_m, called magnetic susceptibility, the relationship between X_m and relative permeability μ is $X_m = \mu - 1$. If the relative permeability μ=1, it means that the material does not respond to the magnetic field by magnetizing, and then the field in the material will be just the applied field. For CFRP material, the relative permeability μ is equal to the relative permeability of graphite. The magnetic susceptibility X_m of graphite is -1.6× 10^{-5}, so the relative permeability μ can be approximated as 0.99984.

Since "Impedance boundary condition" can be only applied to isotropic materials, the CFRP should be defined as "Magnetic field". The impedance vs frequency is shown in Figure 27.

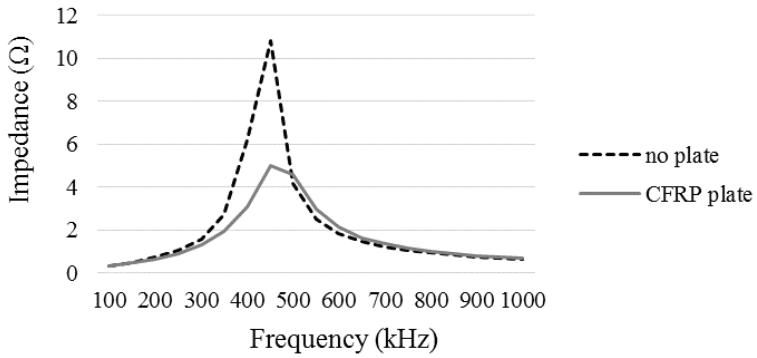

Figure 27: Impedance-frequency comparison

The maximum impedance of coil with CFRP decreases heavily to the half value without a plate. To investigate how the distance between the plate the coil influences the performance of coil, three distances are chosen: 3mm, 5mm, and 10mm. Results are shown in Figure 28 and can be compared to the test results, which was carried taking a coil of 20 windings with 7.6µH inductance and 0.4 Ω resistance with the outer diameter 4cm the inner diameter 1 cm. The test shows how the impedance varies when the CFRP plate is 3mm, 5mm and 10mm from the coil in the frequency band from 100 kHz to 1 MHz.

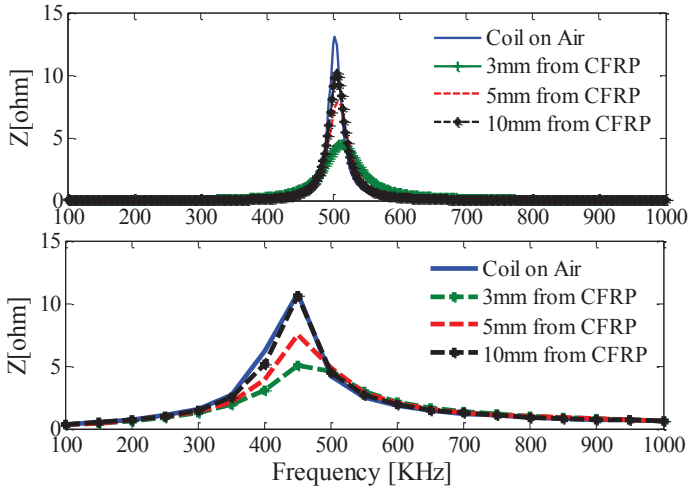

Figure 28: Receiver coil impedance vs. distance to CFRP plate (a) Measurement; (b) Simulation.

At the distance of 3mm, 5mm, and 10mm, the resonance of the coil keeps the same at 450 kHz. When CFRP plate is placed near the coil, the eddy currents inside CFRP plate generated by external magnetic field become stronger, so the induced magnetic field increases. This leads to lower impedance.

A comparison shown in Figure 29 shows what happens when the CFRP plate is at 3mm distance in respect to no plate. Moreover, a µ-sheet is added to the model, placed 3mm from the coil and 3 mm from the plate. The inductance of the coil improves, however, a small shift occurs. In conclusion, it can be deduced that CFRP plate does not affect the resonance frequency but the quality of transmission, so the smaller the

distance is to the plate, the larger the impact CFRP has on the received power. The addition of high permeability materials can be a great aid as well as the use of spacers to the CFRP, both at HF and LF ranges.

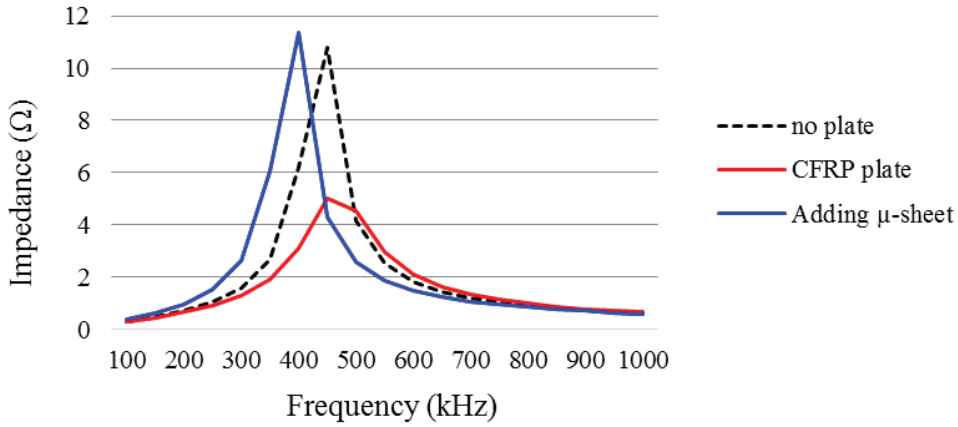

Figure 29: Low-frequency impedance-frequency comparison

4

Piezoelectric Sensors and Actuators

The actuators and sensors operate on the piezoelectric principle and achieve direct transduction of electric energy into elastic energy and vice versa. The piezoelectric equation combines the electrical and mechanical variables in the material in a relation. An alternating voltage applied to the actuator terminals produces an oscillatory contraction and extension of the material. The other way around, an oscillatory contraction and expansion of the material produce an alternating voltage at the sensor terminals. In Lamb-waves applications, the piezo elements couple their in-plane motion, excited through the piezoelectric effect, with the Lamb-wave's particle motion on the material surface. PWAS can be both exciter and detectors of Lamb-waves traveling in the material. PWAS and conventional ultrasonic transducers operate on the piezoelectric effect, their modes of operation are however different [6] [46].

First of all, conventional ultrasonic transducers are weakly coupled with the investigated structure through the gel, water, or air. In contrast, PWAS are strongly coupled with the structure through an adhesive bond. Secondly, conventional ultrasonic transducers are resonant narrowband devices. On the other hand, PWAS are not- resonant broadband devices that can be tuned selectively into certain Lamb modes. Finally, conventional transducers excite and sense the Lamb-waves in the structure indirectly through acoustic waves imposing on the structural surface and the mode conversion phenomenon. Oppositely, PWAS excite and sense the Lamb-waves in the structure directly through in-plane strain coupling. In recent years, several investigators have explored the generation and detection of structural waves with piezoelectric wafer active sensors (PWAS).

Figure 30 shows an array of PWAS mounted CFRP plate with simulated crack and delamination. Most of the methods used in conventional NDE, such as pitch-catch, pulse echo, and phased arrays, have also been demonstrated experimentally with PWAS [2]. These successful experiments have positioned PWAS as an enabling technology for the development and implementation of active SHM systems. PWAS are inexpensive, nonintrusive, and minimally invasive. They can be surface mounted on existing structures, inserted between layers, or placed inside composite materials.

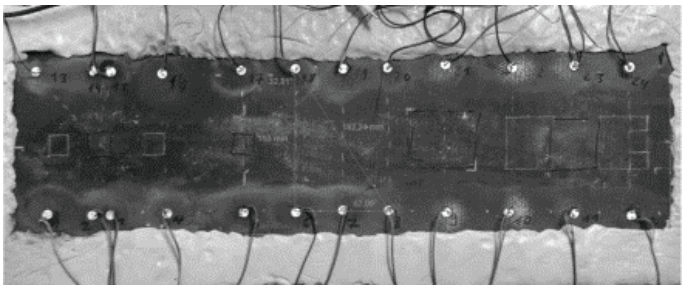

Figure 30: PWAS on a CFRP Plate with introduced defects

4.1. PWAS Characterization

In this study, PIC255 disc of diameter 10 mm and thickness 0.2 mm from Preceramic[7] are used. The PWAS are surface bonded to a Quasi-Isotropic plate. Impedance measurements are made using HP 4194A Impedance Analyzer. Based on five different PWAS an average was found and used as the departing point for an easy model (another form of the Van Dyke Model) approximation for a PZT that uses a parallel RLC tank circuit as seen on Figure 28e. This model is explained on [47]. Results are shown where (a) is the resistance of the PWAS. (b) Is the phase in radians, (c) is the magnitude of the impedance and (d) is the reactance.

The samples are plotted together with the approximation given by the model. The electrical model is a resonance circuit based on the phase and resistance of the PWAS. From the reactance curve and the magnitude curve it can be observed that the PWAS has a series resonance at 250 kHz and a parallel resonance at 275 kHz. It can also be noted from the resistance curve that the base resistance Ro is about 37.5Ω. The calculation of the electrical component values is used in the modeling process. Using the approximation model C_O is about 3.4 nF while the parallel circuit is given by L_P=14.2 µH, C_P=21 nF and R_P is 48.8 Ω. The total load can be calculated for a given frequency f_O =125 kHz as Z=37.5 Ω - j374.5 Ω. With these values, a spice model can be built to optimize the system accordingly. For the remaining of this thesis, it should be also kept in mind that the PWAS acts as a load of 37.5 Ω - j187 Ω at 250 kHz and 37.5 Ω - j93.6 Ω at 500 kHz.

Using a 10 V sine signal at a frequency of 500 kHz a coil system set in resonance using the PWAS actuator as the load has been evaluated. The signal from the PWAS sensor is about 60 mV_{PP}. For this test, the transmitter coil was used as the transmitter and the receiver is from Table 4.

In order to further evaluate the feasibility of generating Lamb-waves a small test was done. The simple class- AB amplifier in Figure 33 is used to evaluate and compare measured signal at the actuator and the behavior using the Spice model. The coil system from Table 4 is used here. On the primary side, L_1 and

[7] Piceramic [Online]. Available: http://www.piceramic.de/piezokeramische_werkstoffe_4.php

C_1 are in resonance. The secondary side is formed by the receiver coil in parallel to the PWAS with a capacitor to adjust the resonance. Both diodes and the resistors R_1, R_2, R_3, R_4, set the biasing for the transistors and regulate the base current to Q1. The current at the load is regulated by R_5 and R_6.

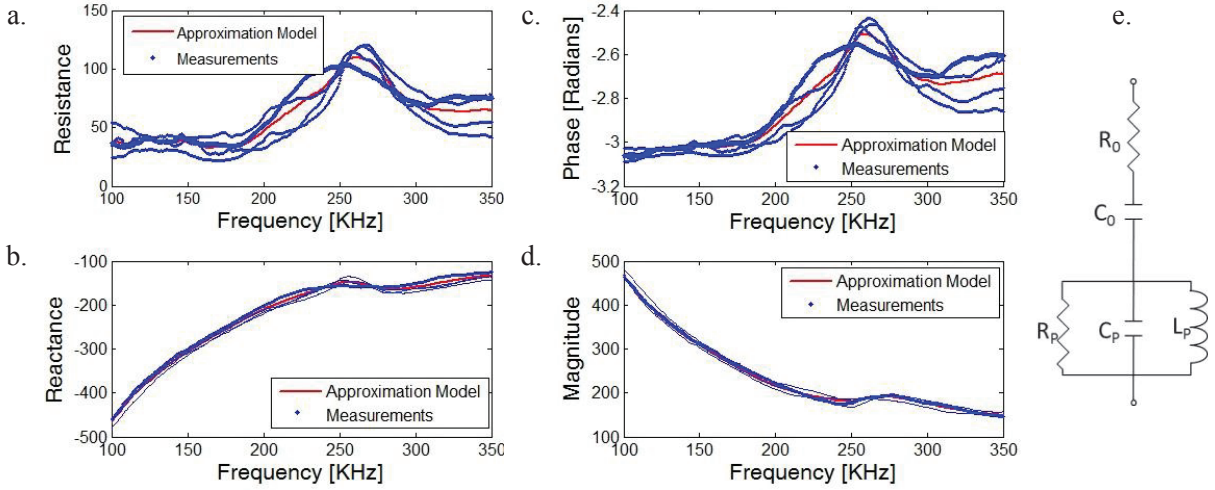

Figure 31: (a-d) Electronic Model based on Impedance Measurements (e) PWAS Electronic Model

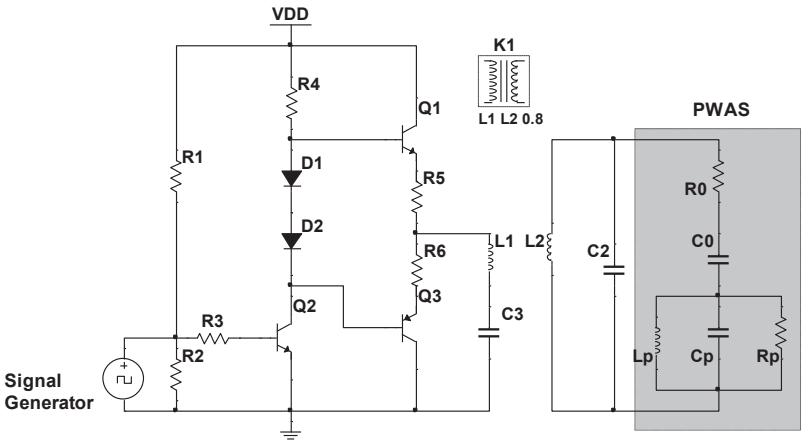

Figure 32: Schematic for Spice simulation of the behavior from a receiver coil with PWAS Actuator.

The signals are the results for the simulations and measurements with a 5-peak signal at a frequency of 250 kHz. The signal at the sensor indicates that the wave travels in one direction without seen any modes. This is given by the nature of the excitation signal being too weak. A stronger current on the primary side would produce the necessary energy on the secondary side as explained in section 2. Therefore a high power amplifier is designed and it is introduced in the next section.

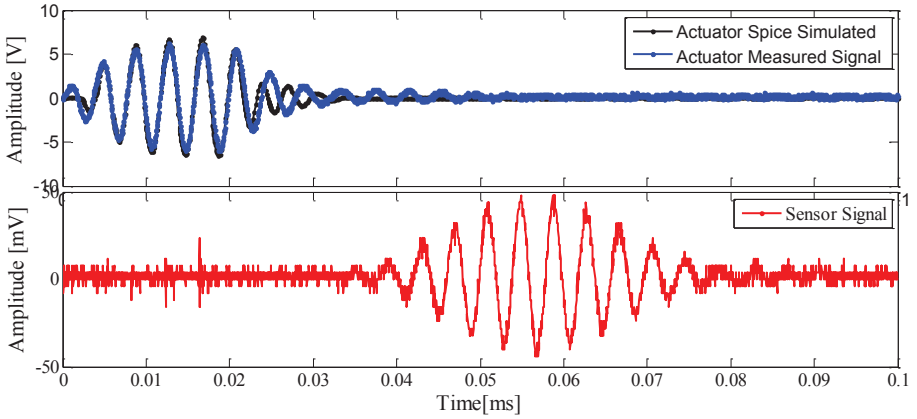

Figure 33: (Top) Simulated results and measurements; (Bottom) Signal measured at the PWAS sensor.

Moreover, it can be seen in that the signal from the actuator is delayed according to the distance it has to the sensor, but also the number of oscillations increased while keeping the center-frequency. This indicated that the Lamb-wave is traveling along and transversally on the plate. Nerveless, the excitation time was not short enough and the energy content is too low due to the amplitude so that to generate the multimode Lamb-wave is not feasible. Even though it is not possible to generate modes, it has been shown that a resonating coil system can excite a PWAS-Actuator according to the selected frequency. The power transmitted will depend on the coil system coupling and efficiency, which in turn is affected by the conductivity of CFRP, with worse results at higher frequencies. The wireless excitation will be further explained in Section 5.1.

4.2. **DuraAct™ Flexible Sensor/Actuators**

Invent DuraAct[8] sensors and actuators can be used in many different ways. They can be used directly as actuators, as sensors or as energy harvesters. They can be also used for structural health monitoring. Their flexibility allows for integration as patches in any surface without disturbing the mechanical characteristics of the structure. They are available in many shapes and thicknesses. During this experiment two formats of 0.2 mm thickness were evaluated; one of diameter 10 mm and a rectangular one (40 mm x 9 mm). Figure 34 presents the measurements from the rectangular piezo patch glued on the CFRP plate (before) compared to the same patch within the resin infusion and measured (after) integration. It can be observed that the impedance characteristics stay after embedding, but change slightly on magnitude due to the better bonding to the surface. This type of piezo-composite materials allows for a better surface conformability.

[8] Invent GmbH, „ACTUATORS AND SENSORS – DURAACT PIEZO PATCHES,“ [Online]. Available: http://www.invent-gmbh.de/. [Accessed on April 2015].

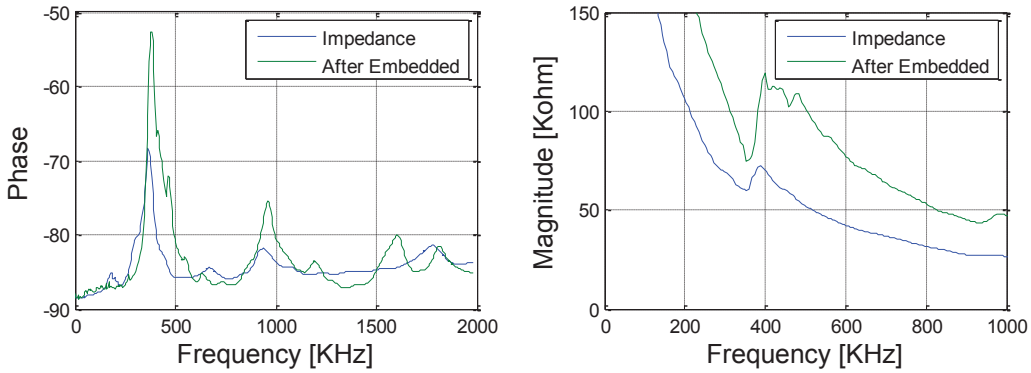

Figure 34: Impedance measurement DuraAct piezo before and after material integration

The advantage of the rectangular format is the generation of signals with a specific orientation for better implementation in specific geometries. On the other hand, the round format allows for generation and detection of signals in a uniform way; the main reason why they are used in this study and in many SHM applications. Based on the impedance model from Section 4.1, the flexible round piezo were characterized out of the average of four different specimens embedded on CFRP. From the reactance curve and the magnitude curve it can be found a series resonance at 307 kHz and a parallel resonance at 338 kHz. From the resistance curve base resistance, Ro is found to be about 101.9Ω. The calculation of the electrical component values is used in the modeling process. Using the approximation model C_O is about 6.9 nF while the parallel circuit is given by L_P=16.4 µH, C_P=4.6 µF and R_P is 28.2 Ω.

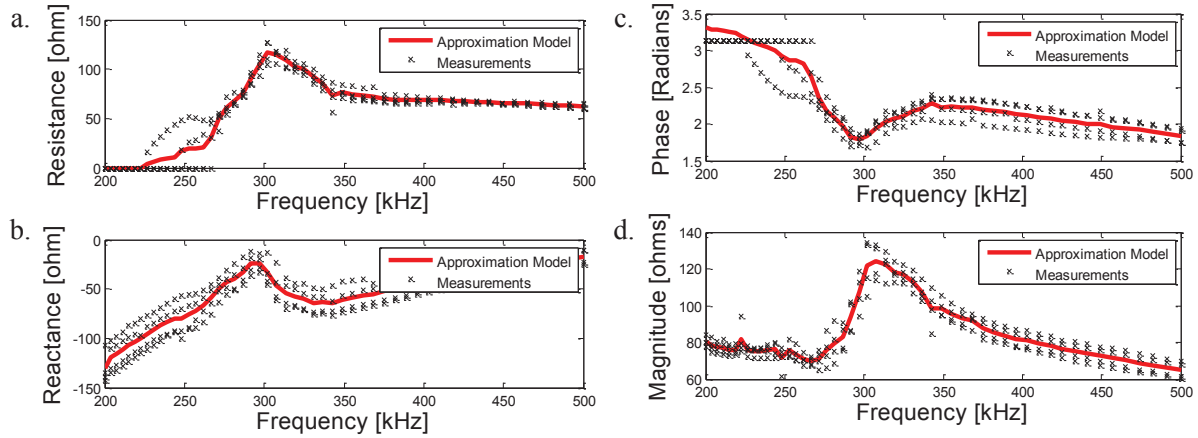

Figure 35: (a-d) Impedance measurements and model of DuraAct round piezo

5

System Design

In most cases a lot of effort is put into creating complex electronics within the wireless node itself, making the system heavy and not embeddable. In this study, we evaluate the possibility of implementing simpler concepts on the nodes and leave all the complexity to the external reading unit. The results here introduced are considered the next stage developing a wireless SHM sensor network using piezo elements and inductive coils. The system has been tested in the presence of drilled holes, damping masses, and environmental changes indicating that these signals can help identify the presence of failure.

PWAS require a high voltage excitation signal, therefore in order to achieve the transmission a low-frequency coil was selected according to [42]. The goal is to surface apply the coils or embed during manufacturing of CFRP and other materials like GFRP. Possible approaches include glue or binders and the use of sewing techniques (tailoring) as explained in the previous section. No matter how coils may be add on the plate it should be always considered that the quality of the receiver antenna will be damped to about half the value given on a free space measurement and depend on the frequency used a shift in resonance might occur [39].

5.1. The Actuator Node

Generally, Lamb-wave generation occurs by excitation of a PWAS actuator via a Hann-windowed-sine signal. In order to try to mimic this behavior, the primary coil is connected to an amplifier that provides the necessary signal and power for the secondary system. This approach was also used in section 4.1; however, the amplifier design could not deliver enough power to the actuator. Figure 36 shows a representation of the test set- up. The entire system can be divided into three sections. The primary side responsible for the signal generation with the necessary amplification connected to a primary coil L_1 that oscillates at the necessary frequency. The primary coil is glued to the bottom of the holder seen in Figure 36. The secondary side is formed by the receiver coil L_2 together with the PWAS actuator, denoted by

number two, and tuning circuit necessary to bring the system to resonate at the selected frequency. Finally, the third section is a PWAS sensor and a digital oscilloscope for detection. The distance between coils is vertical to the plate under test and it is controlled by a servomotor.

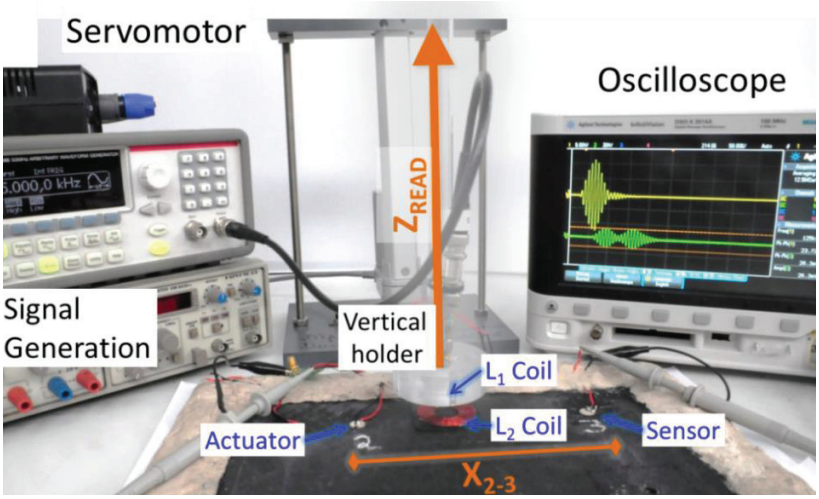

Figure 36: Measurement Set-up.

5.1.1. Wireless Windowed Sine Excitation

The current at the transmitter coil is given by providing five pulses to a full bridge class-D amplifier further explained in Section 5.3.1. The resonance is set to 125 kHz with the bonded PWAS acting as a 376.4 W load. At the secondary side 380, V_{PP} is measured when 40 V_{PP} were applied on the primary side. The received signal at the sensor, located at a distance of 15 cm, is in the order of 600 mV_{PP}. The signals are presented in Figure 37.

It can be observed that instead of the expected 5 oscillations at the actuator, as in the wired system, the signal takes a long time to settle back to zero. Thereby, an unknown mechanical response from the PWAS is generated. Observe that the excitation signal continues to run after the S_O mode has been detected at the sensor node indicated by the dashed arrow. Furthermore, the following mode emulates the oscillations from the excitation signal with some overlapping from the actual A_O. By using only three pulses this effect can be better observed as seen at the top of Figure 38.

The S_O mode appears clear at the beginning of the response, while the A_O mode is overlapped by the unwanted signal. The results of the wireless test can be compared by reference measuring with a traditional wired system on the same plate at the same 125 kHz frequency using a 3-cycles modified Hann-windowed-sine signal of 50 V_{PP}. The results are shown in Figure 38. As expected the responses are different. The wireless excitation as explained previously is too long causing other mechanical responses from the piezo element. This system is analyzed to determine the presence of large damping factors.

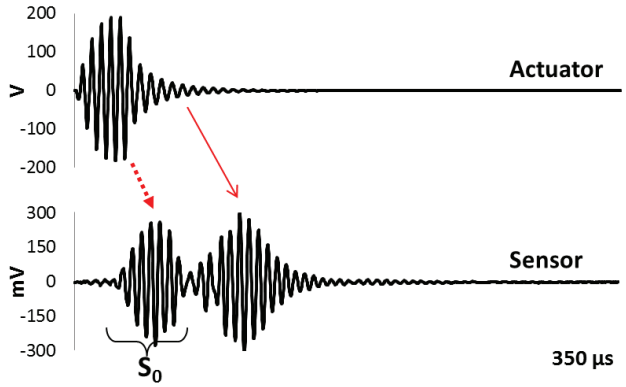

Figure 37: Wireless actuation and sensor response

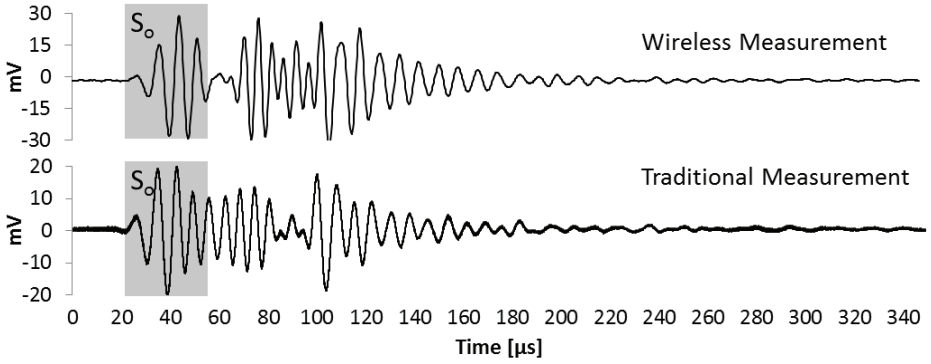

Figure 38: Comparison wireless and wired actuation

5.1.2. Single-Pulse Excitation

A simpler version of the pulse generator is made in order to produce only one high energy peak of up to 50 V with the assumption that a clearer response without mode overlapping from the sensor will be observed. Two Zener diodes of rating 100 V and 51 V are used to charge the wireless transmitting coil with up to 50 V and a pulse width of 2 µs. The secondary side the actuating signal is 30 V due to the influence of CFRP as explained in previous sections. The secondary side has a half rectifying diode in order to eliminate the unwanted oscillations given by the presence of resonance. The response from the sensor is delayed due to the distance to the actuator and the oscillations maintain the center frequency with strong amplitudes between 20 mV_{PP} to 100 mV_{PP}, but no modes were generated. This indicates that the Lamb-wave is traveling longitudinally and transversally on the plate but the excitation frequency of the pulse is too high. The signal response depends on the fiber layup, the orientation of wave propagation and fiber orientation as well as in the distance between the PWAS and their geometry.

Using the class D amplifier from the previous section with a fixed pulse width of more than 4 µs and a long wait time can also offer similar results but more power for excitation. The purpose of a one pulse signal is to quickly excite the PWAS system and wait to see a clear fixed response from the sensor. The

response should be composed of symmetric and/or asymmetric modes. However, the presence of undesired oscillations given by the wireless excitation made it impossible to obtain clear Lamb-waves as in the previous section; therefore the need for a half-rectifying diode observed in Figure 39. One of the biggest challenges in the future is to find out at what frequency it is possible to eliminate the interference from the symmetric and the asymmetric modes as explained in [48].

In order to produce thinner systems, the thin receiver coils explained in Section 3.2 and presented in Figure 39 (a) and (b) were used. The first coil is produced manually by gluing to the CFRP while the second generation has been manufactured using the TFP method explained previously. At the actuator node representation the low frequency receiving coil, denoted as LFRX, obtains a pulse with fixed width from the external device. The half-rectifying diode damps the undesired oscillations. Traditionally Lamb-wave generation occurs when exciting via a Hann-Windowed-Sine, such signal generation requires large computation capabilities, digital-analog conversion, and precision. Since the thickness of such embedded nodes is limited, a one pulse signal should excite the piezo at a narrow frequency, which should be previously known so the desired modes are generated.

With this final system, a more controlled excitation is given at the actuator as well as a more precise response from the sensor. Nonetheless, in the next section, the possibility of a Piezo Driver to be included within the actuator node is addressed.

a. 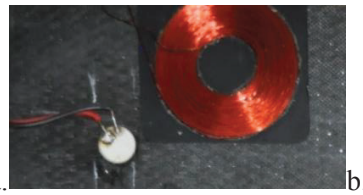 b. 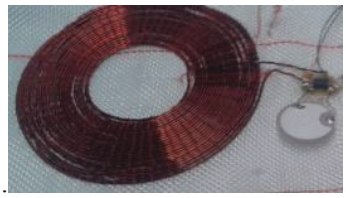 c. 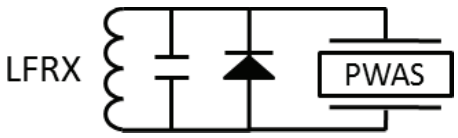

Figure 39: (a) Sensor glued (b) Sensor node with TFP Coil (c) Sensor node Schematic.

5.1.3. Piezo-Driver for Hanning-Windowed-Sine Generation

Ideally, a Hann-windowed-sine is used to actuate the PWAS because such signal contains a narrow band spectrum so it excites coherent single frequency waves with low dispersion. As mentioned in the previous section when using the wireless link to actuate the piezo the excitation signal oscillates too long and therefore more cycles than needed are observed. On the other hand, with one pulse excitation, the response is better controlled but the sharp transition brings in high harmonics which are not desired. The signal received at secondary side depends also on the coupling between primary and secondary coil which changes according to the distance between them. A way to address all these issues is to transfer signal generation circuitry to the secondary side and use primary side only to transmit the necessary power. The following circuit is explained in detail in the work from Patel [See Appendix].

The AC voltage received at secondary side is converted to DC by a full bridge rectifier. The signal generation circuitry can be supplied with this power to generate the required actuation signal. To this end, a PWAS driver is built.

❖ ***Design specifications and limitations***

The PWAS driver will be later on integrated on the surface of the structure and therefore the size and geometry of driver is a major concern. Shape and weight of the circuit should not affect the mechanical behavior of the structure. Therefore the idea is to keep the PWAS driver as small as possible; most importantly it has to be thin. The smaller the size, the lesser the impact produced on the material. For the research purpose, the PWAS driver is prepared as the first step with discrete components on a PCB.

Up to 10 W can be wirelessly delivered to charge a battery using market available RFID modules[9]. Based on this it is assumed that less than this power will be available for the driver. The PWAS needs to be supplied with about 200mW power in order to generate Lamb waves inside the structure. Therefore, with the power available it is important to design high-efficiency driver circuitry taking care to reduce unnecessary power consumption at different stages of circuitry.

The excitation of PWAS should be done with smooth tone burst signal. This approach is very important when dealing with dispersive waves such as Lamb waves. The windowing is applied to reduce the excitation of side frequencies associated with the sharp transition at the start and end of the conventional tone burst. It is intended to minimize dispersion effects and characteristics of the elastic wave propagation. This signal is obtained from a sine tone burst filtered through a Hanning window. This mathematical operation is described as:

$$Signal = A\sin(2\pi ft)\frac{1}{2}\left(1-\cos\frac{2\pi ft}{k}\right)$$

f = frequency [Hz]

n = discrete resolution

k = number of cycles

A = Amplitude [Volts]

t = time factor

$$t = \frac{1}{n}\frac{k}{f} : \frac{1}{n}\frac{k}{f} : \frac{k}{f}$$

[9] Texas Instruments "Wireless Power Solutions" [Online]. Available at: http://www.ti.com/lsds/ti/power-management/wireless-power-receiver-solutions-overview.page [Accessed: Oct 2015]

Compared to a sine windowed with a rectangular formula the windowed tone burst signal does not produce side lobes. Both tone bursts have the same central frequency of 250 kHz, the pure tone burst also excites a considerable number of side lobes, below and above the central frequency.

The frequency is 0 to 500 kHz and the required amplitude across PWAS is between 50 to 100 V_{PP}. The high amplitude is required because of the small amplitudes in the mV range at the receiver side. Low-excitation amplitude results in poor signal-to-noise (SNR) ratio at the sensor side. The target frequency is selected as 250 kHz for the first evaluation.

The purpose of the tone burst is to reduce the side frequencies occur because of sharp transition at the beginning and at the end of the signal. Any voltage ripple, overshoot or interference at the output of the driver results in the introduction of side frequency and deteriorate the performance of SHM system. Therefore, the SNR at the output stage should be kept as minimum as possible. The maximum noise tolerance limit at the output stage is set at the -40dB.

The signal could be generated by implementing a digital-to-analog converter (DAC) and a linear amplifier. However, there are many problems associated with this approach. The quality of output signal depends on the number of samples per cycle. In order to generate a smooth waveform, at least 64 samples per cycles are required. For 250 kHz output signal, the sampling frequency is 16 MHz. In order to execute sampling frequency of 16 MHz, the microcontroller frequency should be at least ten times to avoid loading of 100%. There is no 8/16 bit microcontroller which can run at the frequency of 160 MHz. For the 32-bit microcontroller, the footprint is bigger and power consumption is also higher. Furthermore, the output is not exactly smooth and after amplification, the total harmonic distortion (THD) of sampling frequency becomes more visible which causes interference in the amplified output signal.

Moreover, all linear-stage amplifiers consume a significant amount of power and this reduces the overall efficiency of the system. Consumed power will be converted to heat which would increase the temperature of PWAS driver. This needs to be taken care of if a material integration is to be done.

Switched stage amplifier implementing Pulse-width-modulation (PWM) addresses the problem associated with the linear stage amplifier. Class-D amplifier is the type of switched amplifier generally found in audio amplification; it amplifies not the analog signal itself but a stream of pulses that represents the signal by PWM. The signal is retrieved from the PWM signal by means of a low-pass filter. The output filter is there to smooth the pulse stream to an analog signal, removing the high-frequency spectral components. The frequency of the output pulses is typically ten or more times the highest frequency of the input, thus the output filter can satisfactorily reduce the unwanted harmonics and accurately reproduce the input. This approach can be considered ideal in terms of distortion. An advantage of the class-D amplifier is that it can operate from a digital signal source without requiring a DAC to convert the signal to analog form. If the signal source is in digital form, the binary digital signal can be directly converted to a pulse width modulation signal to be applied, simplifying the circuitry considerably.

Due to its power efficiency, in recent years the interest in class-D amplifiers has increased not only as audio amplifiers but for other applications such as motor control and higher frequency power amplification. The distinguishing feature of class-D amplifiers is a high efficiency that allows for smaller heat-sinks or higher output power before running into thermal limitations. The efficiency of class-D amplifiers is so high because the power transistors in the output stage are either switched off or fully on yielding respectively zero or very low dissipation [49].

The traditional modulation technique (AD) for class-D amplifiers modulates the duty cycle of a rectangular waveform in such a way that its average content corresponds to the input analog signal. The comparator is used to compare the input analog signal to a sawtooth signal which will generate a pulse width modulated output signal. The width is proportional to the difference between analog signal and sawtooth signal. The duty ratio of the PWM signal is proportional to the amplitude of the input Hanning windowed signal. This configuration gives two output inverses of each other to the bridge Class-D amplifier.

- ***Design Approach***

A commercially available microcontroller has the ability to generate such needed pulses. First, the desired times for the PWM have to be found. In order to find the necessary time values for the pulses, the sawtooth wave is compared to the original analog signal in order to generate the PWM signal representing that analog signal. If the amplitude of the sawtooth wave is higher than the compared analog signal then it gives high output for side-A and it gives low output for side-B across the bridge. For this design, the input analog signal is assumed to be always a 5-cycle-Hanning-windowed-sine. The main challenge is to generate the waveform at the hardware level. It requires a source of sine waveform which needs to be multiplied by the window function. This method is really complex and it needs further circuitry to perform this function. Another approach is to simulate modulation with the help of MATLAB and Simulink and derive the PWM signal. Once the PWM modulation is available, the microcontroller can be programmed to generate the pulses and feed the class-D amplifier without any feedback system.

Class-D amplifier is a switching stage amplifier which means at the output stage, voltage swings between full voltage and zero voltage. The MOSFET operates in triode region for high input and in the cut-off region for a low input. Therefore it does not consume any additional power during cutoff operation giving superior performance over the linear amplifier. Furthermore, the gate of the MOSFET consumes current only during the switching; once the gate capacitor is charged it doesn't require any additional current. As the power consumption of the amplifier reduces, the heat generation is also reduced. It gives 100% theoretical efficiency. But the high frequency and high amplitude PWM signal also introduce Electromagnetic Interference (EMI) which will require special care during PCB design.

The choice of MOSFET is a significant factor in whether or not the amplifier will meet this efficiency specification. The most important characteristics in this application are the peak drain-source voltage it

can handle, the resistance in the drain-source (R_{DS}–on), the gate capacitance (C_{GS}), the time it takes to turn on and off, and the voltage required to drive it.

The PWM switching frequency is 2MHz and therefore total time period of one cycle is 500ns. Minimum and maximum duty cycle of PWM signal is around 10% and 90% respectively which means the minimum pulse width is around 50ns and maximum pulse width is 450ns. The dead-time between high and low signal is around 15.6ns. It means the satisfactory turn-on and turn-off time is around 10 to 15ns. The required gate current (IG) is assumed around 2A. Based on this information, the calculation of required gate charge can be calculated according to:

$$Q = I_G t$$
$$Q = 2\ Amp\ \times\ 10\ \times\ 10^{-9}\ sec = 20\ \eta C$$

However, if a device with lower than 20 ηC gate charge is available the required gate current can be reduced for same amount of turn-on time. Gate charge is usually mentioned in the data-sheet of device and therefore it helps to select suitable device for required switching frequency. The required MOSFET parameters are presented in Table 8. In addition the foot-print of MOSFET is also an important parameter because of PCB size requirement. NXP semiconductor device PMV130 n-channel enhancement type MOSFET satisfies all the requirements.

Table 8: MOSFET Parameter Selection

Symbol	Parameter	Value
$V_{(BR)DSS}$	Drain-source Breakdown Voltage	> 30 V
Vth	Threshold Voltage	< 3 V
$R_{DS(ON)}$	Drain-source ON state Resistance	< 0.5 W
$Q_{G(TOT)}$	Total gate charge	$\leq 20\ \eta C$
V_{GS}	Gate-source Voltage	20 V
ID	Drain-current	> 1 A

The PWM output from the microcontroller IC is in the range of 0 to 3.3V which is not sufficient to drive the MOSFET gate directly. A MOSFET driver is a special circuitry which provides necessary voltage and current to turn-on and turn-off both High-side and Low-side of the class-D amplifier. High side MOSFET sources current to the load and Low-side MOSFET sinks current from the load. The turn-on condition of MOSFET in Triode mode is given by:

$$V_{GS} - V_{th} > V_{DS}$$

For the High-side MOSFET, the required gate voltage must be higher than the drain voltage of the device. The gate driver is usually designed to supply required gate voltage with appropriate current to turn on the

device as fast as possible. Gate driver “ISL2111ABZ” from Intersil is used for switching both High and Low side.

- ***Analog low-pass filter***

At the Class-D amplifier outputs a PWM signal of 2 MHz frequency carrying the actual lower frequency modulated signal to be applied across the PWAS. The numerous side frequencies have to be removed by using a low-pass filter. Essentially the filter suppresses the amplitude of all the high-frequency components leaving only that original low-frequency signal. There are different methods of implementation such as an active or passive filter. The quality of the output signal depends on the filter order and filter type.

To design a suitable filter it is necessary to understand the nature of the PWM signal that reveals the information of frequency spectrum required for the design. A low-pass filter with cut-off frequency of 300 kHz at -3db would completely remove all the unwanted high-frequency harmonics and leave the desired values remaining. This allows the PWM duty cycle to be varied at frequencies up to the cut-off frequency and reflect this variation with a corresponding voltage level in the output.

An analog LC low-pass filter can be used to reconstruct the original signal from a PWM. It uses only passive components and doesn’t require any external power supply when compared to active filters. There are different standard approaches to design analog filters like Chebyshev, Bessel, and Butterworth based on frequency response and Time domain response.

All these approaches have different characteristics and therefore the selection is always based on the application requirement. For the PWAS driver, input PWM signal can be considered as the step input and therefore filter’s time response plays a major role in the quality of the output signal. The high-frequency component should also be filtered out, otherwise, it generates a voltage ripple at the output which is not desirable; therefore, the filter should also have a good frequency response. Only Butterworth approach offers good frequency and time response and therefore it is selected.

When designing a filter the load impedance plays an important role to decide the filter’s frequency response and time response. A filter should be designed for a specific load and any variation in load impedance causes an unwanted effect like peaking near cut-off frequency and oscillation in the time response.

A PWAS has an electrical equivalent model that has been described briefly in Section 4 . It is the combination of parallel RLC branch in series with RC. This model exhibits a different value of impedance at different frequencies. This electrical equivalent model can be transformed into resistor with a series capacitor as shown in Figure 40. The resultant impedance of transformed model is equivalent to the original PWAS electrical model and therefore can be used during filter design. The purpose of using this transformed model is to include the response in filter’s transfer function which affects frequency and time response of design.

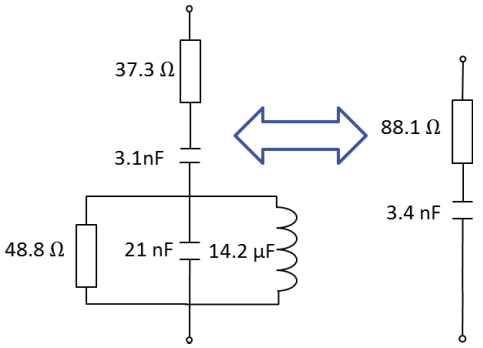

Figure 40: Equivalent circuit of a PWAS

The main goal of the low-pass analog filter is to extract Hanning windowed signal of 250 kHz as mentioned before. The required filter specifications are here mentioned:

- Cut-off frequency (Fc): it should be set above the required output analog frequency in order to get large amplitudes at the output. It is defined as 300 kHz.
- Passband Ripple (Amax): The Pass-band response should be totally flat in order to avoid distortion among various frequency components.
- Stopband attenuation (Amin): It should be reasonable enough to filter out the entire high-frequency component. Amin defines the minimum stopband attenuation at the stop-band frequency. There is no strict requirement on this parameter.
- Filter order (M): it defines the number of poles in the transfer function of the filter. Each pole gives -20db/decade attenuation in the frequency response. It is a trade-off between circuit complexity and desired attenuation. The third order low-pass filter can provide enough attenuation in this case.
- Source impedance (R_S): It is the impedance offered to the input of the filter. According to the MOSFET datasheet, the on resistance is 0.1 Ω. But such low impedance causes the too much transient current through the filter components. Also during the resonance, the output impedance of the filter becomes very high, therefore it is required to make the input impedance high enough to limit the excessive current and limit output impedance during resonance. So adding a 10 Ω series resistance serves this purpose.
- Step Response: the PWM frequency is 2 MHz which means a 250 ns pulse represents 50% of amplitude and 500 ns pulse represents 100% amplitude of the signal. Step response should be fast enough to achieve adequate voltage changes with changing the PWM signal. Overshoot and ringing should be minimal in order to avoid interference.
- Filter approximation: Butterworth approximation seems to fulfill all the necessary specification because it offers the best trade-off between frequency response and transient response required for this application.

Standard filter design always deals with resistive loads and therefore the filter design for a reactive load is not a straight-forward method. Impedance matching technique can also be employed to compensate the capacitive behavior of PWAS but the introduction of new passive component changes the filter's behavior significantly and therefore it is not a suitable technique. The transfer function was derived and later on compared with standard transfer function equation for finding out the required component values of the filter. The T-section and Pi-section are two configurations of filter design based on passive components. T-section filter is more suitable for PWM signal due to its high dv/dt. In a Pi-type filter sudden voltage changes cause peak current in the first shunt capacitor, where the system might not be able to handle such high current. The 3rd Order Butterworth filter with T-section for PWAS load is shown in Figure 41. The presence of capacitor at PWAS load introduces one additional pole and one additional zero in the equation and filter becomes fourth order. Calculating component values from transfer function for the required cut-off frequency and damping ratio becomes really cumbersome because of addition of extra pole-zero pair. A different approach is to derive the component values for an equivalent resistive load. The designed filter is analyzed with bode-plot and step response for transformed PWAS load, so filter component values can be tuned to achieve the desired frequency response and step response. At 250 kHz the impedance of PWAS is around 200 Ω this is taken as the load for the filter design. Once the filter component values were found, MATLAB/Simulink can be used to analyze the bode-plot and time response of a designed filter with PWAS load instead of resistive load. The bode-plot and step response for proposed filter with PWAS load instead is shown in Figure 42.

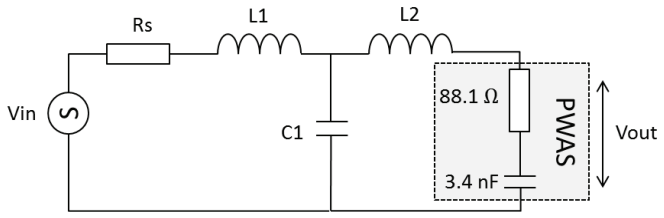

Figure 41: Butterworth 3rd order low-pass filter

The step response shows a significant amount of overshoot in time domain. Such filter produces overshoot across the load. This overshoot is the result of complex conjugate pole-pairs. As shown in pole-zero diagram the dominant complex conjugate pole pairs have overshoot of around 60% and with damping ratio 0.16. The second complex conjugate pole pairs also have overshoot of 50%. The bode-plot has two peaks in frequency response due to the resonance effect between filter component and PWAS capacitor. The first peak occurs around 150 kHz and the second peak occurs around 500 kHz. The amplitude attenuation at 250 kHz is -3.43dB which means the output amplitude will be half of the input amplitude. This filter design exhibits poor time response as well as poor frequency response for given component values and would fail to reconstruct the Hanning windowed signal.

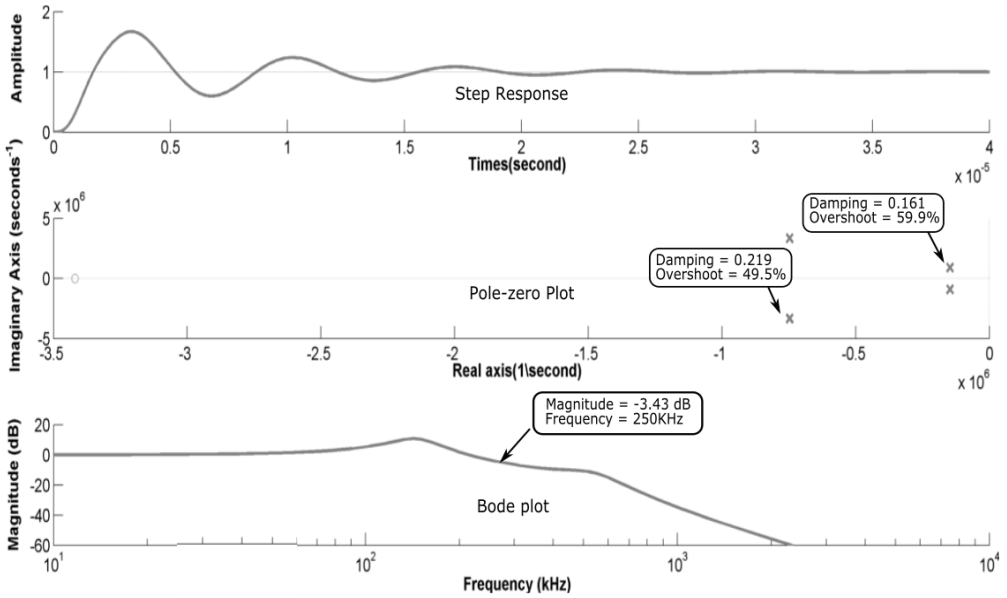

Figure 42: Frequency and time response analysis with PWAS as resistive load

The time and frequency response can be improved by tuning the component values. The filter's component value should be chosen in such way that the complex conjugate poles move towards the left side of the imaginary axis. This will reduce overshoot in time-domain and increase system stability. However, this change will also shift resonance frequency towards higher values in the bode-plot resulting in higher cut-off frequency. Repetitive experiments were done by changing filter's component values and analysis of time and frequency response was done in order to achieve desirable filter performance. The new filter design time response and frequency response is shown in Figure 43.

The time response of the tuned filter has increased significantly compared to the previous filter design. The settling time of step response is almost half compared to the previous design. The dominant complex conjugate pole pair has moved towards the left. The overshoot associated with dominant complex conjugate pole pair is 38.1% and less dominant pole pair has 21.9% which is almost half compared to the previous design. This improvement in time response gives better stability at the output of the filter. The peak amplitude has also reduced and the passband is almost flat. This peak also amplifies the input signal and therefore the output signal has higher amplitude compare to the input signal. This results in more than 50 V_{PP} at the output across the PWAS with only 25 V input voltage. The cut-off frequency has shifted to the 450 kHz and therefore the total amplitude attenuation at 2 MHz is around 42 dB with respect to the amplitude at 250 kHz. This low-pass filter design was the best possible trade-off achieved after repetitive experiments by tuning filter components.

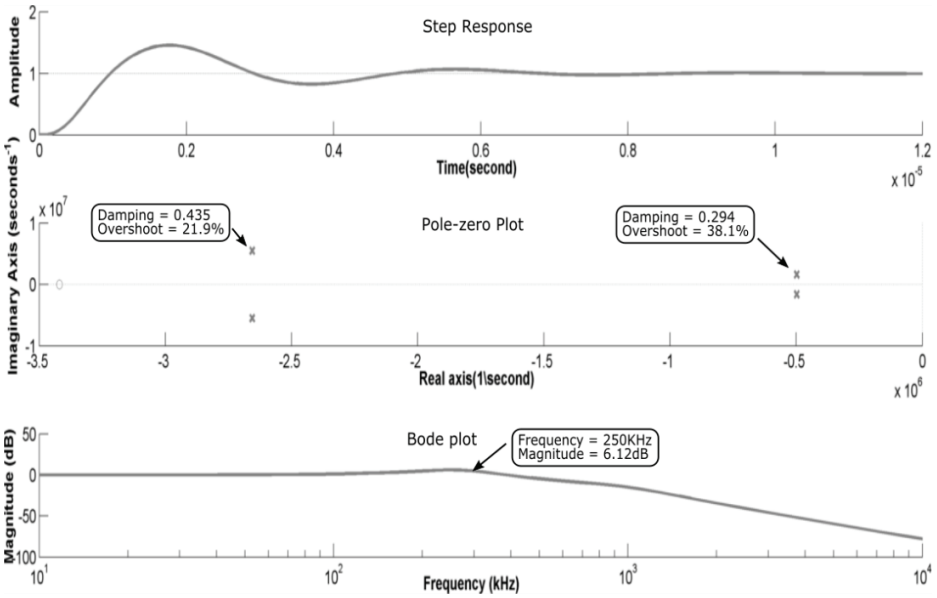

Figure 43: Improvement of complex conjugate pole pairs after tunning

❖ ***Wireless Power***

The power provided by the wireless link can be limited. The wireless link power is rectified and regulated to a certain maximum. Based on the measurements made the circuit has a power consumption of 2.6 Watts at 20 Volts which is equivalent to a load of 154 ohms. In the same way at 15 V 100 mA are supplied. To obtain a Hanning-windowed-sine of more than 50 V_{PP} 25 V are needed. Therefore, about 4.1 Watts need to be received wirelessly. The piezo driver requires different voltages to operate. In the first prototype in order to regulate the voltages, linear regulators are used (LDOs) this design can be improved by using switching mode modules with higher efficiency. If the regulators are changed less power would be lost in heat, providing a better efficiency.

5.2. The Sensor Node

While placed above the carbon fibers the geometrical limitation is the thickness and not the area of the node. Therefore, in order to avoid generating imperfections antenna coils were implemented on flexible printed circuit boards of Polyimide 50 μm thick, reducing then the total thickness of the system. Figure 33 shows that the quality of the antenna decreases when introducing a CFRP plate under it. This effect is partially eradicated by adding high a permeability sheet between the coil and the plate. Once the antenna has been tuned the components are added. This includes a full-bridge rectifier and an NMOS for modulating the analog signal. The circuit is shown in Figure 32 where the voltage divider biases the MOSFET to the necessary level with the aim of transmitting the signal, also known as amplitude modulation. The MOSFET stays in the triode region when the PWAS signal is transmitted; in this case,

the voltage divider is on. The configuration can be partly compared to that of radio frequency identification (RFID) receiver; however, the signal transmission is more similar to AM radio.

In Figure 44(a) the sensor node is prepared for embedding. It is necessary to isolate the piezo from the carbon fibers. Here a layer of polyimide is added, however, there are other solutions including pre-curing locally the resin or the use of special glues. For the last test mentioned in the next sections, the piezo elements used are fully isolated by a polymer to allow for a better adhesion to the structure. The mechanical characteristics of the piezo are altered after the autoclave process takes place because they become fully in contact or part of the surface. Properties of the piezo, like damping and resonance frequency change; consequently, their Lamb-wave response has to be further studied individually.

a. 

b. 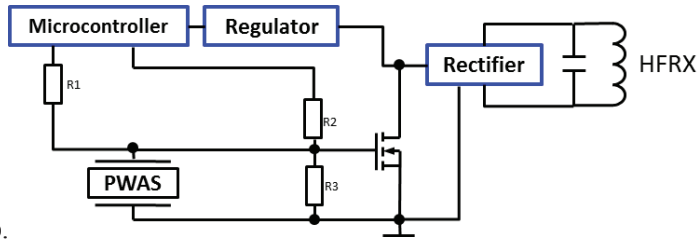

Figure 44: (a) Sensor Node, (b) Sensor Node Schematic

5.2.1. Hybrid Analog- Digital Data Transfer

Integration of passive RFID tags and the sensor is a common practice nowadays. It allows a fully implantable everlasting application in which sensing is necessary only at specific times. Sensing is performed when the tag is in the reading range of the reader, and the reading and sensing is triggered by the reader. This principal does do not require batteries, therefore, the nodes are mostly maintenance-free. Lamb-waves manifest themselves usually at ranges between 100 kHz and 500 kHz for the type of CFRP plate used in this study.

Adding an ADC within the tag would increase the power requirements and the area needed since the rate required to sample should be at least 10 times faster as that of the signal. In consequence, transmitting the analog data eliminates the need for vast computations within the tag by performing entirely outside at the reader device. The reader sends the actuating signal also considered the trigger. Then the analog signal is sampled and stored. The digital signal is continuously sent by the tag at a lower frequency and switched off by setting the microcontroller port as input to allow sending the analog signal during this time. The triggering starts only when the ID number of the sensor has been checked; here a simple parity method for detecting errors in transmission was used by using “XOR” of all the digital signals as see in Figure 45. Protocols could be added in order follow ISO standards.

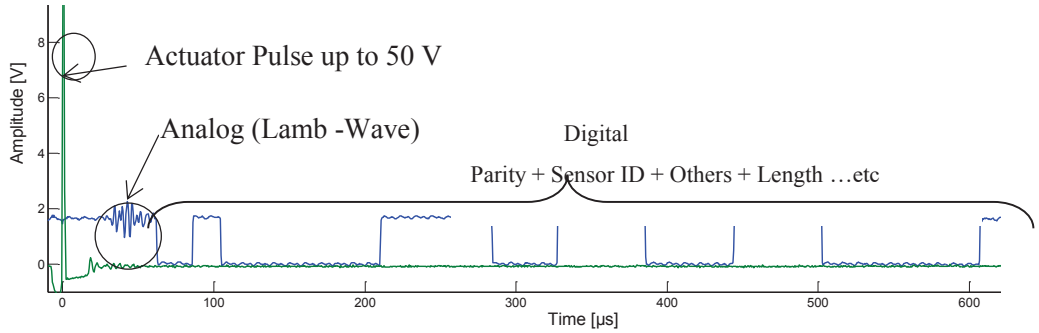

Figure 45: Hybrid Analog- Digital Signal Transmission [50]

5.3. The Mobile Reader

The transmitter coil (LFTX) [51] that generates the actuating signal is that from Table 5. A train of pulses is generated by the microcontroller and amplified by the configuration presented on the right-hand side of Figure 46. This is the final configuration for the transmitter both with the Piezo-driver as a receiver or with the analog receiver. On the other hand, on a first trial, two Zener diodes were placed such that the coil would charge up to approximately 50 V. The transfer occurred by discharging the coil to the secondary side. This excitation proved not to be enough to generate the necessary modes as explained in 5.1.2 on the single-pulse excitation.

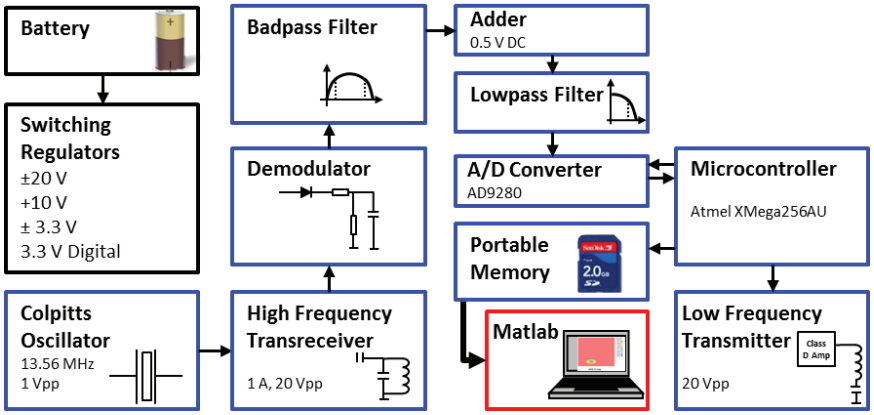

Figure 46: Mobile Reader

On the final prototype, the LF module implements a half bridge class-D Amplifier or full-bridge architecture when more power is required. This amplifier is presented in 5.3.1. The reader, on the other hand, provides a stable carrier frequency by implementing a crystal oscillator. The transmitter coil for the power transfer (HFTX) was implanted on a PCB with the geometry of 4x4 cm and 5 windings as seen in Table 2. The first measurements were taken at the demodulator pin with an oscilloscope and signals were further analyzed using Matlab filtering capabilities in order to have a proof-of-concept. Later on filtering

and storing was added to the device as it will be explained in the following sections; where each building block of the reader is explained in detail.

5.3.1. Low-Frequency Band Module

A 5V, 50% duty-cycle signal of five pulses is used as the input to the H-bridge class-D amplifier presented in the schematic in Figure 47. This configuration provides twice the supply voltage over the load. The load, in this case, is composed of the transmitter coil and capacitor set in resonance. Intersil ISL2111 half bridge drivers create the gate voltage necessary for the four NDT3055 n-channel MOSFETs. An anti-shoot-through circuit prevents both the upper and lower transistors to turn on at the same time and generates the complementary signal for the drivers. The anti-shoot is only necessary for higher frequency ranges, thus at 125 kHz it will not be used.

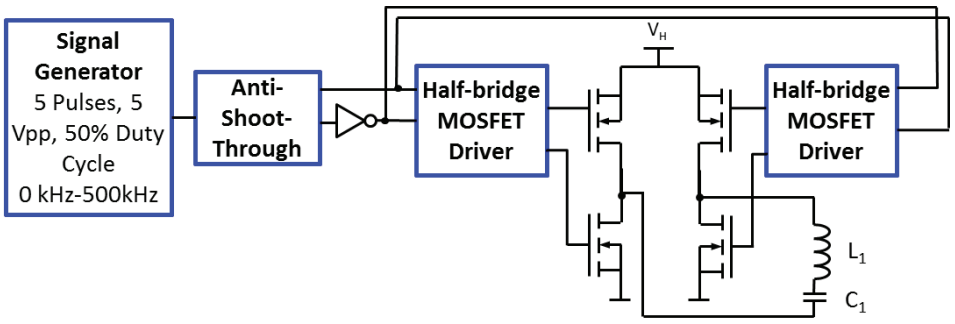

Figure 47: Reader LF Module

The secondary side is formed by the receiver coil together with the PWAS actuator and matching capacitor necessary to bring the system into resonance. The matching capacitor can be calculated for a given frequency according to Eq. 30. This configuration can be used with only half of the bridge depending on how much power needs to be transmitted. When V_H is 10 V, 10 V_{PP} will be transmitted by the half bridge, as double will be achieved by the full configuration.

5.3.2. High-Frequency Band Module

A quartz crystal of 13.56 MHz resonance is powered by a single transistor construction that uses capacitors to match the oscillator load. This Pierce oscillator is a derivative of the Colpitts oscillator with the quartz placed on the feedback loop. It presents high stability and precision. The output is fairly sinusoidal of 1 V peak to peak. This signal is then amplified twice by two different inverting operational amplifiers. The second one from Analog Devices can handle currents of up to 1 Amp. The signal to power the Antenna is then 15 V_{PP}. Depending on the matching network, the power delivered to the antenna can be regulated. The amplifier can additionally be turned on and off when necessary to save battery life. Using a Network analyzer the impedance of the antenna is obtained and the discrete components to match the network are

found with the help of a smith chart. The matching network is slowly adjusted by trim capacitors as seen in Figure 48.

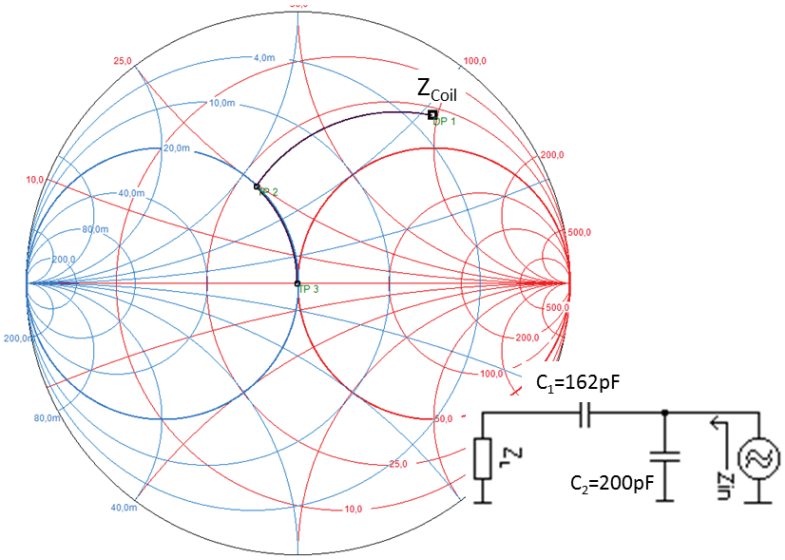

Figure 48: High-frequency antenna matching

In the following sections the transmitter used for testing the system is coil number one from Table 2, with a self-inductance of 2 µH, The matching capacitors are 29 pF and 95 pF to tune to 50 ohms as seen from the load, this is done when using a signal generator with an equal input impedance because to get the maximum power transfer from a source to a load, the source impedance must equal the complex conjugate of the load impedance. However, the driving circuit is an operational amplifier with large output impedance. In this case, only one capacitor is necessary to set the resonance.

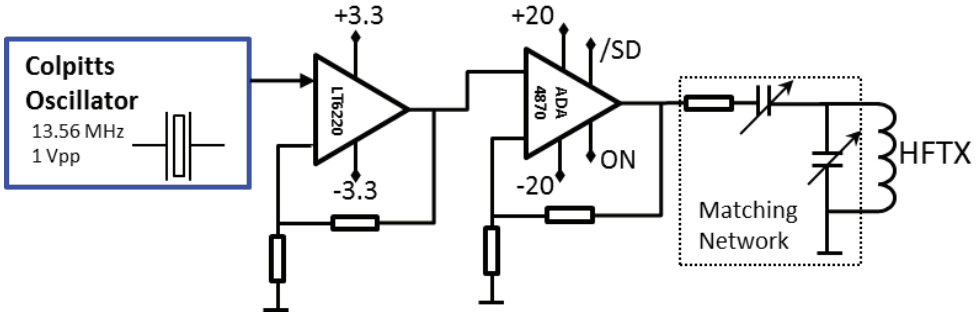

Figure 49: HF Module

5.3.3. Demodulation and Signal Conditioning

The demodulation of the signal is done using a diode detector, which entails a diode to rectify the signal and a voltage divider to re-size the signal as seen in Figure 50. A first order low pass filter is built by adding capacitor C1 (Figure 50) to obtain the desired frequencies and remove the carrier. A buffer inputs

the signal to a 2nd order active low pass filter with a -3dB Cutoff frequency of 915 kHz according to the spice simulation.

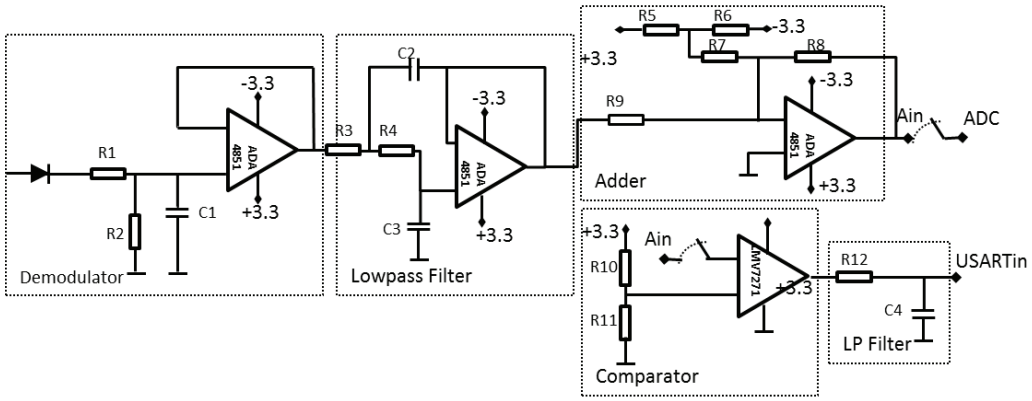

Figure 50: Reader demodulation and signal conditioning

The filtered signal is adjusted to fit the range of the external A/D Converter. This signal conditioning is made with the high-speed rail-to-rail operational amplifiers ADA4851. By means of a switch, the signal can be also compared using a voltage reference and comparator LMV7271MF to be sent to the USART input of the microcontroller.

5.3.4. Communication Protocol

The following serial protocol is a simple interface here presented to demodulate and store both the digital as well as the analog data. This Simple Serial Wireless Communication will be further referred as SSWC. To obtain the digital signal the protocol follows a serial asynchronous communication based on the USART and SPI protocols. It depends on the frequency at which the microcontrollers are working. In this case, the bit length is given by the sensor node.

The line is always high waiting on a low signal to start collecting the serial information. Therefore the first bit is zero and it is ignored. From bit 2 to 9 the sensor number contents are stored into the USART register. Here the last bit is either a 1 or a 0 for even or odd parity. The last bit is always a one for stop. This allows for up to 255 sensors. The purpose of the start bit is to enable the reception of the data package by marking the beginning of the actual data package and to synchronize. The length of the start bit must enable a distinction to be made easily between the pulses of the training sequence and the pulse of the start bit. In the current version, the pulse width was set to 80 µs for a bit rate of 12.5 kbps.

Once the reader is initialized and configured, it operates in the receive mode waiting for a sequence. The wireless receive protocol has the stages of waiting, start bit recognition, data bits recognition, and stop.

The communication is achieved by implementing an analog switcher, which alternates the channel between “digital” and “analog” receiver. Using the USART receiver pin on the reader device the Sensor

ID is captured. Once parity has been checked the external ADC is activated and the Lamb-waves are collected and stored into an external NAND Flash memory. The raw data is retrieved with a USB cable.

Table 9: Wireless UART Receiver Protocol

1	2	3	4	5	6	7	8	9	10	11
Start	B0	B1	B2	B3	B4	B5	B6	B7	Parity	Stop
0	Sensor ID Number								1 or 0	1

5.3.5. Battery and Power regulation

Different voltage levels are required by each analog module in the final prototype of the hand-held reader device. The power requirements are identified in Figure 30. First of all the Low-frequency module requires 10 V for the gate drivers and the MOSFET half-bridge to generate enough power to be transmitted. The high-frequency module requires also 10 V for the oscillator to function, while ±20V are required for power amplification to the planar coil antenna. Moreover, ±3.3 V are necessary to power the pre-amplifier, the filtering, and the ADC.

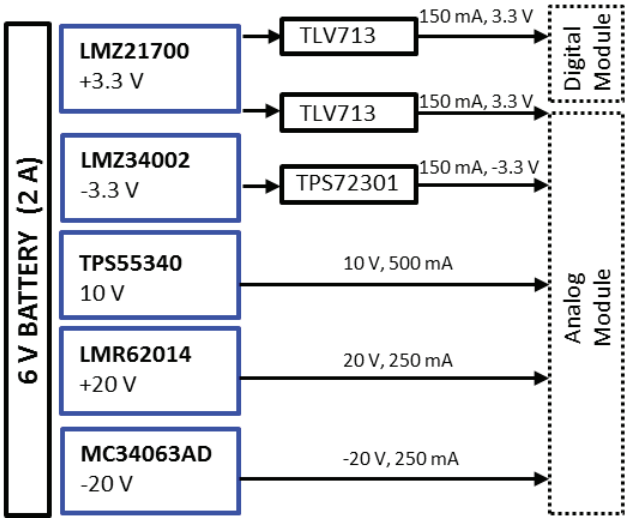

Figure 51: Power requirements

The system is powered using a battery of 6 V in order to reduce weight and size for the ease of use. For best efficiency switching regulators with high performance have been selected. In order to eliminate noise analog and digital separation of grounds and power are done at the PCB level. The digital module corresponding to the microcontroller and memory works at 3.3V. The simple switch module LMZ21700 provides an efficiency of up to 95%. By implementing a low dropout linear regulator (LDO) TLV713 the voltage is stabilized and the digital and analog voltage supplies, as well as the grounds, are separated in order to reduce noise. The LMZ34002 negative output power module from Texas Instruments was selected because of its ease of use. The analog voltage is passed to the negative output LDO TPS72301 in order to create a stable source. The efficiency achieved is 91%.

Most of the power required by this design is consumed by the low-frequency module responsible for power transfer to the actuator node. This amplifier, as described in section 5.3.1, is powered by 10 V and 250 mA approximately. Therefore, the DC/DC Output Boost Converter TPS55340 was selected, to which end the evaluation board from Texas Instruments fulfilled all the requirements. The efficiency of this module is 94%.The simple switcher LMR62014 with 20 V output was selected because of its high current capability of up to 500 mA. This step-up voltage regulator has an efficiency of 90%
The MC34063ADG switching regulator is used with an external P-channel MOSFET NTD20P06LT4G. It is built as a voltage inverter with up to 250 mA output for an efficiency of 71%.

5.3.6 Reader Prototype

Final design is done on different FR-4 boards. The top-side layer of the PCBs is laid out in a typical manner. The top and bottom layers are 2-oz. copper. The top layer contains the main power traces. Also on the top layer are most of the connections for the signals. The top-side ground traces connect to the bottom and internal ground planes with multiple vertical interconnect accesses (VIA) placed around the board. VIAs directly under certain ICs device provide a thermal path from the ground plane to the bottom ground plane. The output decoupling capacitors are as close to the ICs as possible. The copper area of critical signals is kept small, minimizing noise.
On the power modules, some important resistors and capacitors are close to the IC. For the TPS55340, an additional input bulk capacitor is necessary. Other components such as the voltage set point dividers, frequency set resistors, slow start capacitor, and compensation components terminate to the ground using a separate ground trace connected power ground but discharged only at one point directly by the IC.
This design presents still a lot of noise due to the implementation of different PCBs but shows improvement compared to the first generation. The microcontroller has been substituted by an SAM4S ARM-based processor, keeping the same system architecture as explained in section 5.3. The development board Xplained Pro from Atmel is selected because it has an external Flash memory that with a File Allocation Table (FAT) system accessible with a USB connection. The speed of the A/D converter improves to 12 Mega samples per second; almost double the speed from the previous design with XMEGA described in section 5.3.
For this prototype, the wireless UART communication was left out and only the analog transmission of the Lamb-wave is considered. The goal is to have a proof-of-concept to predict the damage detectability and to compare to the traditional wired system.

5.3.7 Measurement

The Lamb-waves are measured with a non-wireless measurement process. The frequency of the Hanning-windowed-sine is variated in a sweep that goes from 50 kHz to 350 kHz in steps of 25 KHz. The

measurement indicates that between 200 kHz and 250 kHz, the stronger responses are obtained from the sensors. Also, at this frequency, it is possible to separate the modes even visually. Some reflections from the edge of the plate are observed in Figure 52. Here can be also perceived that the sensors S2 and S4 have shorter travel distances and larger amplitudes due to the geometry of the plate. Sensor S3 has clearly smaller amplitude and its modes travel a larger path of 1.41 times the travel distance of the other two sensors. The similarity of the paths is likewise seen from the shape of the responses.

The signal for the wireless actuation has a larger number of peaks and therefore more energy is associated with it compared to the 3-peak actuation used in the traditional system. However, this method is more suitable for long travel paths. Increasing the number of peaks increases consecutively the interference and reflections from edges and damages. As a consequence, the anti-symmetric and symmetric modes are more challenging to distinguish. For this plate, it is a better solution to have a larger energy content as it can be observed when the responses from Figure 52 and Figure 53 are compared. The distance between nodes is relatively large at 40 mm; previously evaluated plates had half of that. Moreover, the wireless system's energy for the actuator should be utilized efficiently; a longer pulse allows a steadier response.

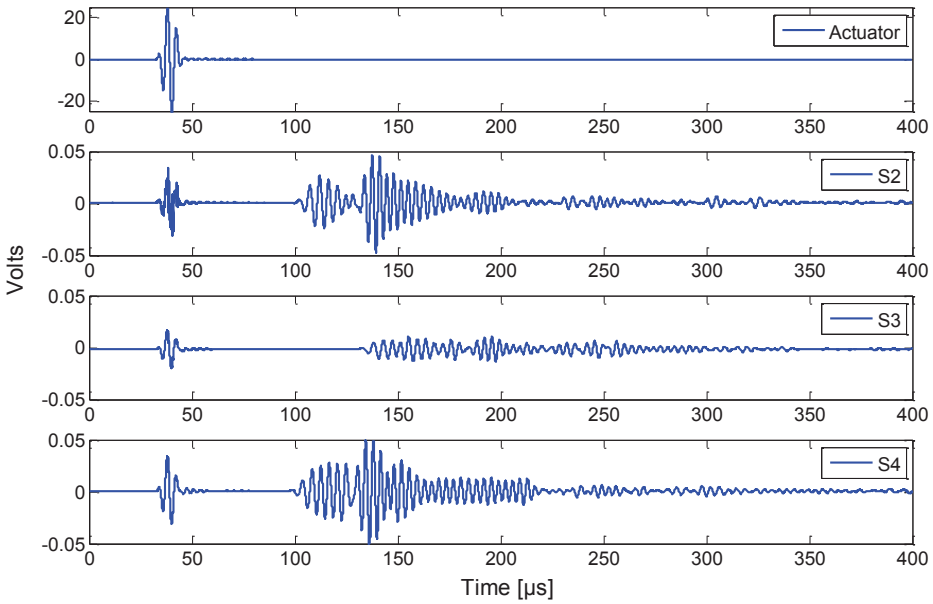

Figure 52: Measurement of the plate with the standard set-up

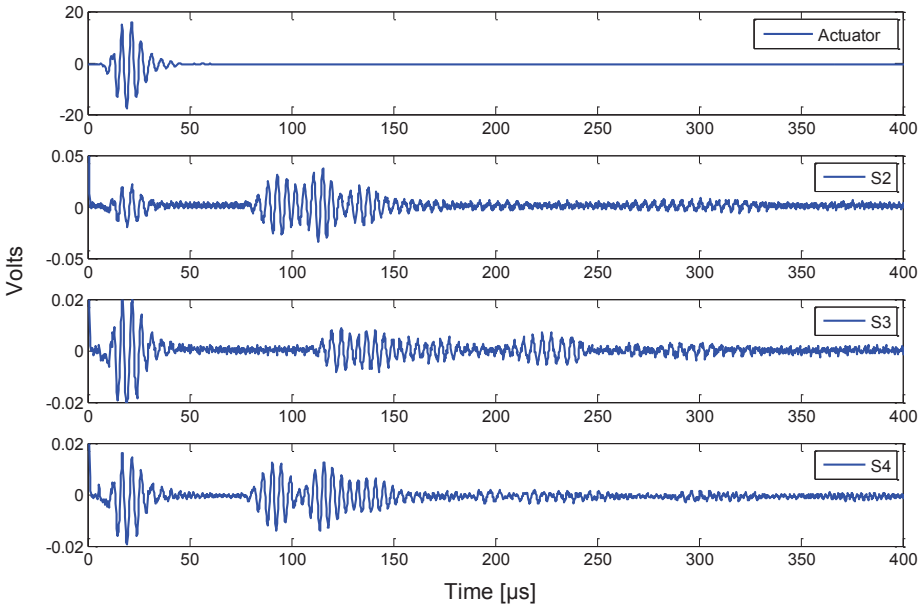

Figure 53: Measurement of the plate with wireless piezo driver

6

Software for Damage Detection

The last step is detection and localization of damages. This follows once the in-situ measurements have been done and having the reference measurement of the healthy structure. The software presented in this Section has been partly developed during the master thesis work of Gow (Appendix C). The methods used by the software were inspired by past and actual work at the Faserinstitute Bremen e.V. Particular attention was paid by the author to ensure that the recorded data is quickly processed in order to be able to make larger measurements. This is why evaluation using a wavelet with a single scaling was used. Furthermore, the frequency range was limited to 200 kHz, because preliminary work has shown that it is possible to find imperfections the best. To ensure reproducibility, all defects were made temporary without causing residue after removal. For example, an opening at the plate's edge damping mass, an area with water on the plate, and magnets on both sides of the plate. The revision and adaptation of the here described software has been done to match the limitations of the available hardware.

The analysis of the recorded signals is done by Continuous Wavelet Transformation (CWT) and not by Fast Fourier Transform (FFT). The main difference is that the Fourier Transform decomposes the entire signal into its frequency component. It uses sine and cosine oscillations as the base. The wavelet transform uses a Mother-wavelet function to display the signal resemblance. This Mother-wavelet can be stretched and compressed so that different scales are covered. If these scales can be selected as desired, then we refer to CWT. The choice of the mother wavelets represents an important step in the analysis based on Giurgiutiu [2]. The software here presented uses a Morlet Mother-wavelet. The Morlet Mother-wavelet consists of a Gauss modulated cosine:

$$f(x) = e^{-\frac{X^2}{2}} \cos(5x)$$

The Matlab function scal2frq from the wavelet Toolbox calculates the corresponding pseudo frequencies from the respective scaling and center frequency of Mother Wavelets, as well as the period of the sampling points of the input signal. Thus, the scales for the desired frequency or desired range are required. The

wavelet analysis is a time-consuming process, but can be reduced by a pre-selection of the scaling analysis time.

The input signal used in the software has a frequency of 200.1 kHz. A Scaling of Morlet Mother-wavelets by a factor of 203 corresponds to a pseudo frequency of 200.123 kHz. It was demonstrated that the scaling 203 at an input frequency of 200.1 kHz is better suited for evaluation than the scaling 204, which represents a pseudo frequency of 199.142 kHz.

- ***WaveFormRevealer (WFR)***

This software is offered by the Laboratory for Active Materials and Smart Structures (LAMSS) at University of South Carolina [52]. Figure 54 shows the predicted dispersion curves for a 5 mm thick quasi-isotropic CFRP plate. Exciting is done with a 5 peak-Hanning-windowed-sine of 250 kHz. PWAS are 10 mm in diameter and 200 mm away with from each other. Using this tool the damages can be simulated and compared to measurement.

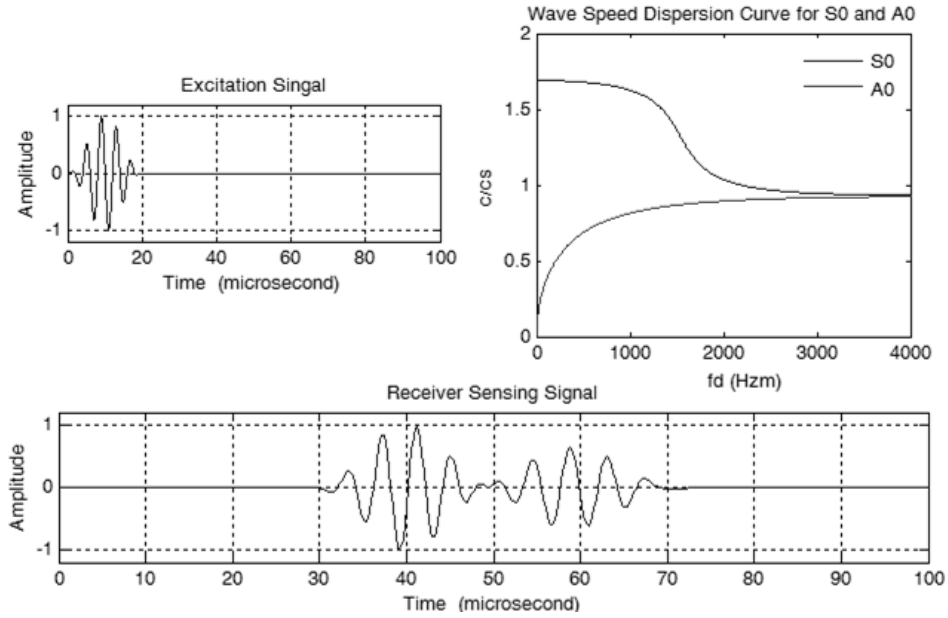

Figure 54: Predicted dispersion curves for a 5 mm thick Quasi-isotropic plate

- ***WaveReader***

This program was a further development of an already existing program, which was used for reading and storing the data from the oscilloscope. The original program provides a way to adjust the frequency of the input signal and a changing among several frequencies. Since in this work only one excitation frequency is needed, the signal generation can be skipped. The frequency generator needs in the current version of the program to be manually adjusted; however, it requires no connection to the measuring computer. This reduces the number of interfaces and thus the likelihood of System error. To be able to draw on the oscilloscope a Matlab toolbox called Instrument Control Toolbox is required. This toolbox controls and

simplified communication with external devices. Wave Reader was used during the first evaluations using a non-wireless system, which was the traditional method. Later evaluations take place using only WaveEval.

- ***WaveEval***

This program is used to analyze the recorded readings. The software is capable of analyzing the captured Lamb-waves obtained from the traditional measurement using WaveReader. In the same way, it is also possible to evaluate the stored signals from the Wireless Reader by previously converting the data to .mat files. Reference measurement and in-situ measurement to be evaluated can be directly loaded. The user interface is shown in .The uploaded data per channel is shown in small on the channel displays. In the middle, all signals are shown together. On the right side of the user interface, the individual signals can be selected as well as different functions to be performed can be called. Those functions are:

- Denoise: It is a function to reduce noise. The waved function finds a wavelet decomposition of the measured data instead. Finally, the function ddencamp gives the initial settings and wdencmp perform the actual filtering.
- Fast Fourier: It is a function used to represent the frequency spectrum of the recorded measurement data by performing a Fourier analysis. For this purpose, initially, the average value of all measured values is subtracted from the measured values to minimize the DC component. CWT-filter performs the CWT using the Morlet Mother-wavelet with a scaling of 203.
- Hilbert: It is a function used after the CWT to generate the envelope. So Maxima and waveforms can be seen better identified. The envelope is calculated from the absolute value of the signal and the Hilbert transform of that signal formed.
- Locate: This feature leads to the algorithm explained in Section 6.2 that describes the localization of the flaw. The actuator is here at the origin of the coordinate system. The three sliders on the far right side can be used to define the maxima of the respective channels by turn. This checks the Algorithm since not necessarily the first maximum can determine the error.
- Print function: opens two new windows. In the first window the Wavelet transformation of reference and the signal, as well as the accompanying envelope are shown. The second window shows this difference from the beginning of the calculation period to the end. The upper limit is the last measurement. This is an indicator of the probability of detection at each sensor.

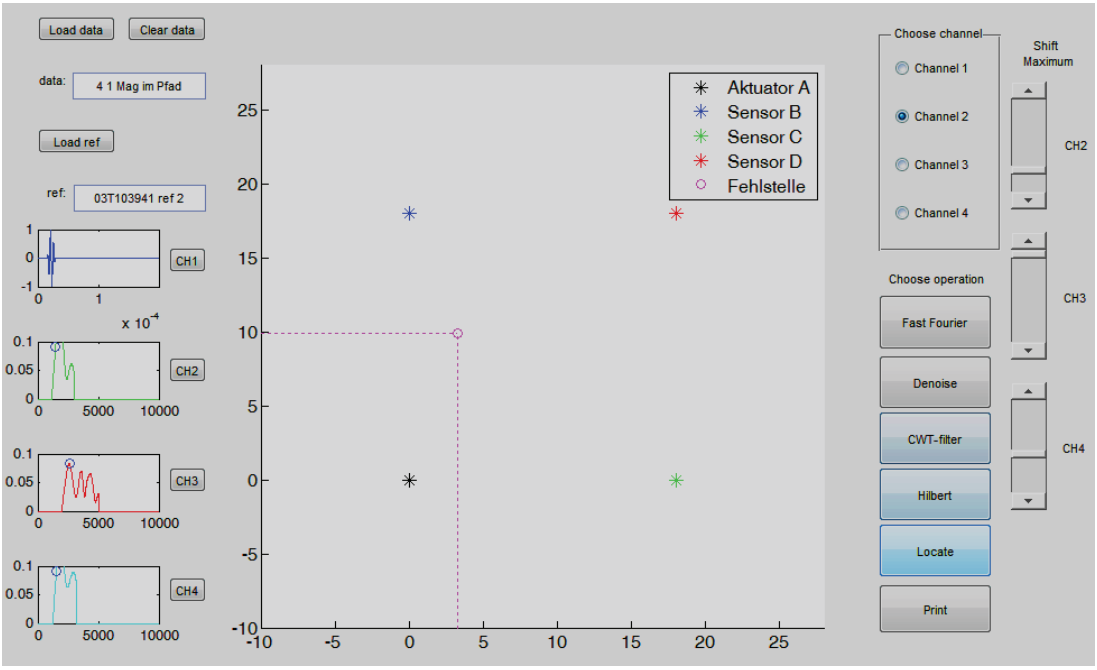

Figure 55: WaveReader GUI

The measurement of a topology shows the detectability of a defect depending on its position on the plate. First of all, as a measure of the detectability is the difference between the reference signal that in this case is the envelope signal of an already CWT- filtered signal. The larger the sum of the differences is, the more probable it would be to localize a defect. Therefore, defects outside the measuring path are more difficult to detect as defect “F” in Figure 56(a); where “A” is the actuator.

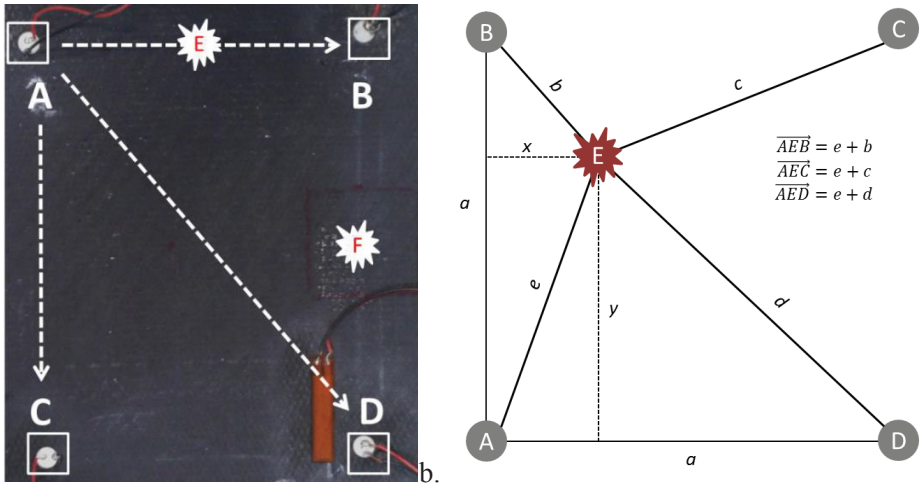

b.

Figure 56: (a) Measurement Set-up, (b) Sketch of the paths for triangulation.

6.1. Principles of path and traveled time determination

The first possibility for defect detection is the path determination. This should show whether a defect is in a measurement path, directly between the actuator and sensor or not. There is in the topology measurement, as explained before, a difference between signal and reference. The sums of the differences per sensor are compared with each other. The highest sum indicates the path, which takes the most change in the signal. On the other hand, a different possibility uses the fact that a defect in the carbon fiber composite plate also represents a change in the medium. With the change in the elastic moduli, there is a reflection and scattering of the incoming Lamb wave, as well as to changes in the attenuation of the wave at the defect site. Because the direct route actuator – sensor is always equal to or less than the way actuator - defect - sensor, the altered wave comes at the same time or delayed to the sensor.

Due to the two-mode characteristic of the Lamb wave and the reflections on the edge of the plate, the identification of the detected wave is not trivial. The superposition of the detected S_0 mode with the reflected S_0 mode or A_0 mode is very common since the A_0-mode is approximately 1.5 times slower than the S_0 mode. Therefore, it was assumed that the defect is not located within the square area surrounding the PWAS on the Plate.

As a measurement path, the AB path is selected and the incoming S_0-mode is reflected at the defect E changing into an S_0-mode reflection. The minimum duration is obtained if the defect is in the measurement path AB itself like represented by E in Figure 56(a). The maximum duration is $(1 + \sqrt{2})$ times bigger when the defect is located directly by a different sensor. Thus, the reflected wave comes at a time between the direct S_0-mode and 1.4 times this time, when the timing of the input signal is considered as the start. After the identification of the direct wave and the reflected wave, the propagation time difference can be determined. Using three sensor responses with the corresponding travel times, an algorithm to triangulate the position of the defect can be found.

6.2. Fault Evaluation Algorithm

After the traveled times are determined a defect can be localized as shown in Figure 56(b). Here $x^2 = e^2 - y^2$ and $y^2 = d^2 - (a - x)^2$. The solution yields:

$$x = \frac{e^2 - d^2 + a^2}{2a}$$

Knowing $\overrightarrow{AED} = e + d$, the values for x and y are:

$$x = \frac{\overrightarrow{AED}}{a}\left(-\frac{\overrightarrow{AED}}{2} + e\right) + \frac{a}{2} \quad \text{Eq. 39}$$

$$y = \frac{\overrightarrow{AEB}}{a}\left(-\frac{\overrightarrow{AEB}}{2} + e\right) + \frac{a}{2} \quad \text{Eq. 40}$$

All variables are known because they can be directly measured except for e. It can be calculated:

$$(a-x)^2 = d^2 - y^2$$
$$(a-y)^2 = b^2 - x^2$$
$$c^2 = (a-x)^2 + (a-y)^2 \quad \text{Then} \quad \Rightarrow \; c^2 = d^2 + b^2 - x^2 - y^2$$
$$\Rightarrow \; (\overrightarrow{AEC} - e)^2 = \left(\overrightarrow{AED} - e\right)^2 + \left(\overrightarrow{AEB} - e\right)^2 - x^2 - y^2$$

$$\overrightarrow{AEC}^2 - 2\overrightarrow{AEC}e + e^2 = \overrightarrow{AED}^2 - 2\overrightarrow{AED} + e^2 + \overrightarrow{AEB}^2 - 2\overrightarrow{AEB}e + e^2 - e^2$$

$$e = \frac{\overrightarrow{AED}^2 + \overrightarrow{AEB}^2 - \overrightarrow{AEC}^2}{2(\overrightarrow{AED} + \overrightarrow{AEB} - \overrightarrow{AEC})} \quad \text{Eq. 41}$$

This algorithm is implemented in the Matlab code that defines the functions of the WaveEval interface.

6.3. Software Evaluation

In order to predict the CFRP plate response, the WRF Software is implemented to simulate the conditions for the Lamb-wave propagation and later compare with a measurement. A measurement was made of the plate presented in Figure 56(a) from actuator ***A*** to sensor ***B.*** The PWAS receiver is located 150 mm away. The Lamb-waves are generated using the wireless piezo driver at a frequency of 211 kHz with a 5-Peak-Hanning-windowed-sine excitation. The QI CFRP plate has a thickness of 4 mm and the PWAS implemented have a 10 mm diameter. The material properties used are from the material library of the WFR Software. It can be seen that the predicted response corresponds closely to the measured Lamb-wave. The presence of side reflections is due to the imperfections on the plate (holes and faulty damping mass) caused by previous experiments. Nonetheless, the software is useful in the estimation of the response and thus an aid for selecting the parameters of the excitation signal as peak count and frequency.

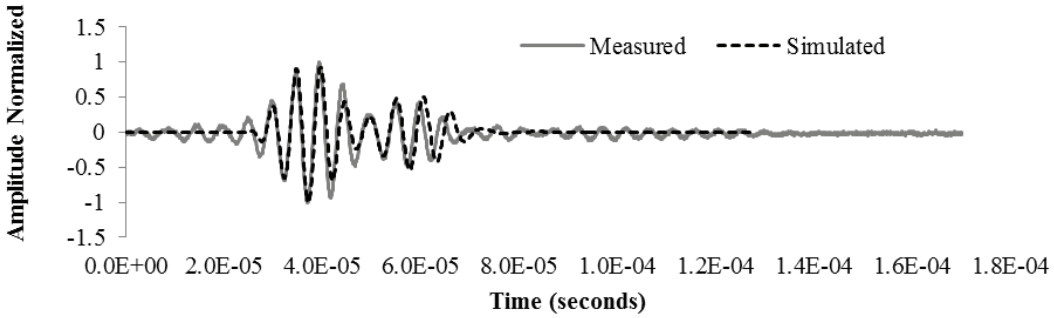

Figure 57: WaveFormRevealer simulation vs. measurement

The WaveEval software has been tested repeatedly by Faserinstitut e.V. using a 4 PWAS system wired to and oscilloscope that collects the signals using WaveReader. Measurements were made both on aluminum as well as on CFRP plates. The results showed that the software is able to successfully determine in which path the changes of the signal are larger. However, the detection is possible only for relative large damages and does not specify at which exact location the damage is to be found. By means of the same algorithm, the wireless signals are evaluated using de-noising and the CWT filter. The Hilbert envelope is shown in Figure 58. The signals are pre-filtered using a Butterworth low-pass to remove the 13.56 MHz wireless carrier that might still be present in the signal. The envelope helps to locate the minima and maxima to find the time of arrival of the modes.

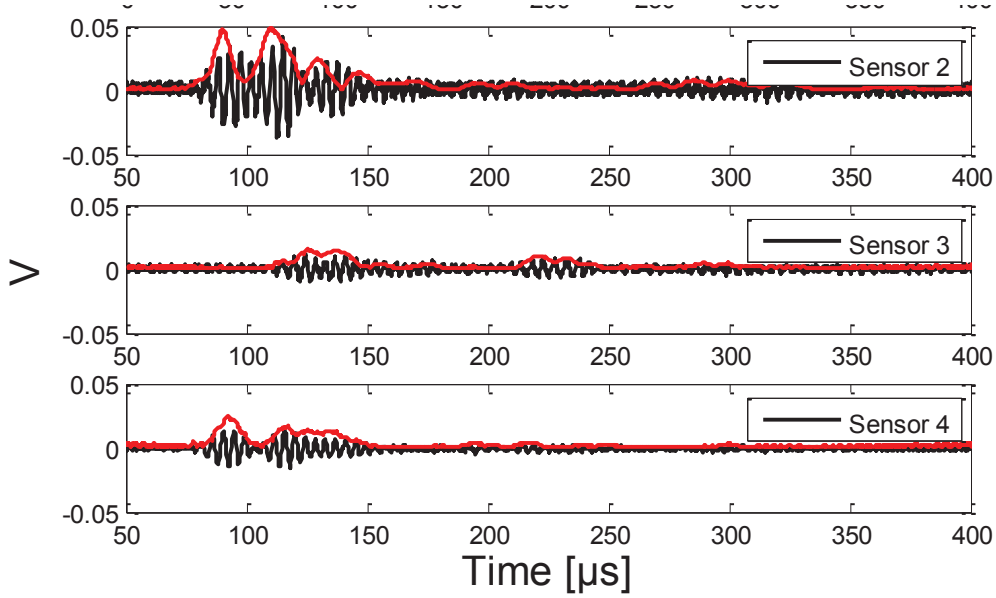

Figure 58: Wireless signal evaluation by CWT filtering and enveloping

7

Material Integration

Embedding electronics in composites is of major interest in future products like smart structures. Some already embedded devices are strain and acoustic wave sensors, however, there is a need to add computing power to such systems. Adding electronics will produce more material discontinuity around the insertions. This, in turn, produces stress concentrations. The influence of piezoelectric and optical sensors on the structure has been estimated by many authors who have simulated the influence of embedded sensors as well as performed mechanical tests [53]. Moreover, during the embedding process, the electronics have to withstand thermal and mechanical stress. When considering thermal stress, it makes a great difference if the electronic circuit is operated or not. In the former case, leakage currents can cause latch-up effects in CMOS and operate points in analog circuits shift. In the latter case, all materials and connections have to withstand the temperature [54]. A good solution is additional thermal shielding and technology options for temperatures above 175 °C.

Before a structure with embedded control might be achieved a temporary step involving the embedding of a single sensor or actuator along with simple circuitry with signal conditioning or amplification needs to happen. Incorporating antenna coils into FRP provides the opportunity to couple enough energy for such simple analog systems. Therefore, on the first tests, only the coils are embedded and tested. Later on, the full integration of a sensor or actuator node is done. Finally, the full functionality has to be tested on a full-scale composite plate.

The following preliminary tests were made in IMSAS using the materials kindly provided by FIBRE. In the same way, humidity sensor evaluation was done in small tests. The final material integration in large CFRP plates, explained later, was fully done at the technical center of FIBRE.

The first trial is the realization of coils embedded in the fiber composite. On an experimental test receiver, HF coils were embedded in the CFRP in order to determine the changes in impedance and quality factor. Here unidirectional woven carbon fiber was chosen with a design of 0°/90°, which was processed with resin RTM6 at 180 °C for two hours. Two versions of a coil were produced. First, the geometry was

evaluated by producing the coil on an FR4 substrate with a self-resonance at 32 MHz. The same coil was made of Pyralux flexible material to reduce the thickness and was insulated with DuPont™ Kapton that withstands high temperatures. The flexible coil was embedded in between four unidirectional CFRP layers as shown in Figure 59. Resonance shifted to 15.5 MHz due, while the quality factor diminished as predicted due to the explained factors in Section 3.3.

Another trial consists in the integration of fully functional nodes on the surface of the plate. The process carried for preparing the composite and embedding the nodes consisted of placing 8 layers of carbon fibers in a quasi-isotropic (0°/90°/-45°/45°) orientation. Three sensor nodes and one actuator node were positioned on each corner 50 cm away from each other. Insulating films can be used to isolate individual sensors from the electrically conductive fibers; however, the process would be tedious for a network involving a large number of sensors.

a.

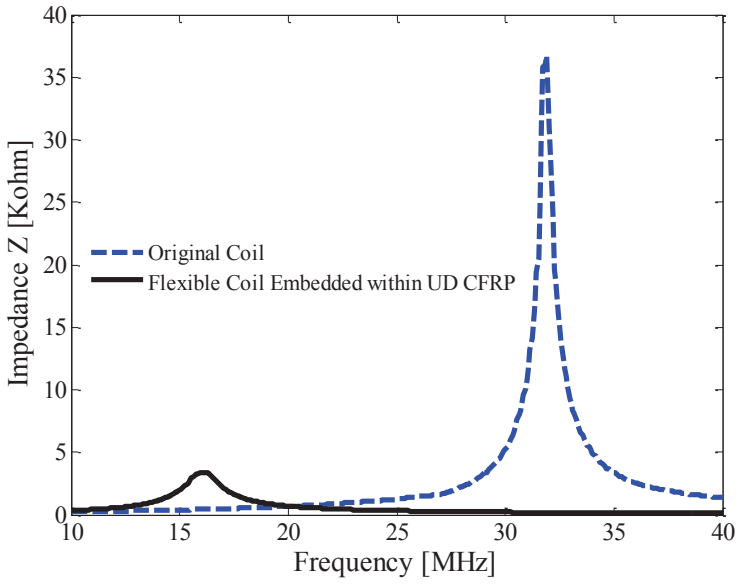

b.

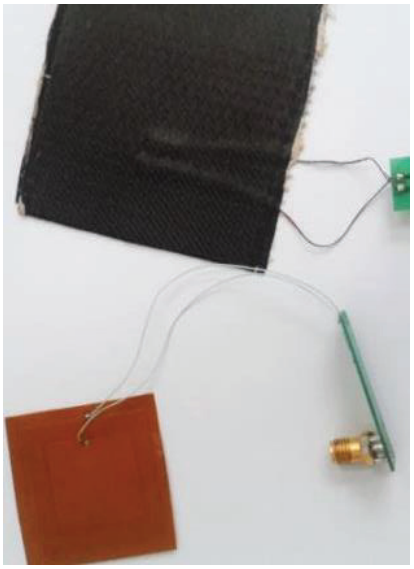

Figure 59: (a) Impedance of coil in CFRP; (b) Flexible coil with isolation and coil embedded between 4 layers CFRP

For this test, the piezo elements were insulated by using Kapton tape. It is important to keep in mind that the isolation layer will affect the properties of the piezo as well as mechanical properties of the composite by itself. Additionally, a high permeability material was placed between the coil and the surface to improve the field and coupling between the two coils. The disadvantage is that the resonance of the receiver shifted to lower frequencies. This process and the results are explained in Section 7.2.

On the final sensor integration, the piezo elements selected are flexible and pre-embedded in epoxy. This prevents the contact of the piezo with carbon fibers while in the infusion process. During the final embedding, other sensors were added as it is explained in the next sections.

7.1. Embedding the Nodes

❖ *Preliminary Tests*

The first test to embed the nodes was carried using 4 layers of carbon and RTM6 resin at 120°C for 8 hours. One sensor and one actuator node were prepared for this process. When removing the peel-ply the PZT broke and the ferrite underneath the coils did not remain on the plate. Due to these results, it was decided to isolate the ferrite and the piezo within two layers of Polyimide tape. The prepared sensors are shown in Figure 60. On the second test at Faserinstitut Bremen e.V. three receivers and one sender were prepared. Each receiver has a couple of resistors, one NMOS for the modulation and antenna with self-resonance at 13.56 MHz as explained in Section 5 . In Figure 60(a) it can be seen the nodes on top of the carbon fibers before placing the vacuum foil. In the upper left the HF antenna with the actuator and the three detection units which can be better seen in the center picture. On Figure 60(c-d) the finalized vacuum resin infusion process with resin supply pipe and vacuum pipe are shown. For the process, the polymer is typically cured in a temperature range of 120°C to 180°C. The plate is an 8 layer quasi-isotropic (0°/90°/-45°/45°) construction prepared with RTM6 and following the descriptions from Section 2.3. The peel-ply, a synthetic cloth, is placed over the plate surface to create smoother surfaces, is removed after the curing process is finished; leaving behind the integrated sensors as a perfectly even surface.

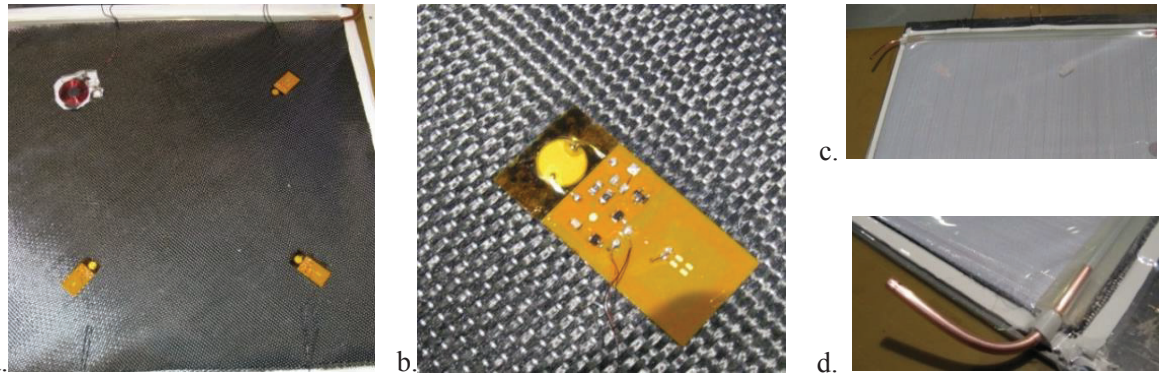

Figure 60: Plate fabrication with embedded sensors/actuators.

The resonance of the high-frequency coils shifted due to the presence of the resin sensor and above and below the sensor node. A higher permittivity (ε_o) from the resin clarifies this outcome if compared to the earlier systems “glued on” the plate. It could also be observed that the quality of the antennas was affected by the distribution of the resin. Where there is less resin the quality factor is less. The resonances are located at around 11.5 MHz; therefore it was necessary to tune to the system frequency in order to test the Lamb-wave signals.

Moreover, the results demonstrate as expected that since CFRP is a conductive material the resonance of the transmitter coil shifts towards higher frequencies causing the power transmission to decrease as

explained in [30] and [39]; however by re-tuning the transmitter coils the power transfer is restored. Finally, the sender and the receiver are tuned to a common frequency below 11.5 MHz. In order to do this, the reader's oscillator was replaced by an 11.29 MHz crystal, observing 77% of the total power being transmitted. This is an improvement compared to the 13% power transfer on a worst case scenario with the detuned system.

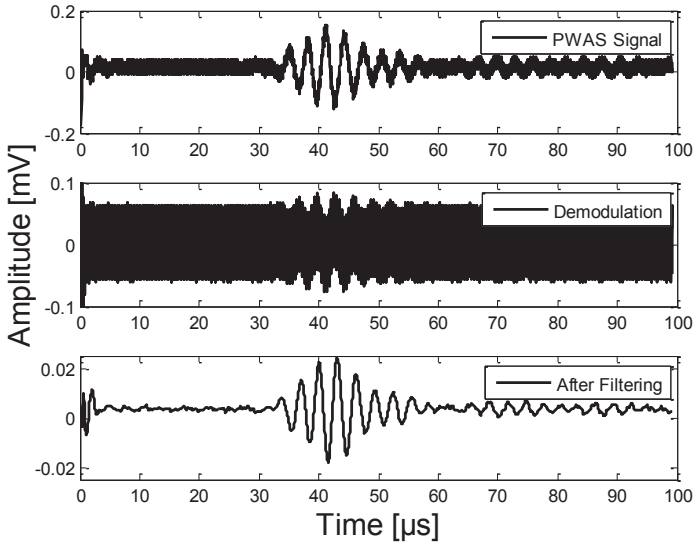

Figure 61: Demodulation at the mobile reader using a plate with embedded sensor nodes.

The voltage at the receiver node after rectifier is between 15 and 30 V going from zero to about 2 cm distances. The signal to noise ratio from the Lamb-wave inhibits the reader from receiving a clear signal. The signal wirelessly obtained as seen in Figure 61 has a maximum of 84 m V_{PP} after filtering, while the signal with surface glued piezo elements had 184 mV_{PP}. The PWAS Signal is noisy and it is possibly damped by the polyimide tape. The properties of the piezo are assumed to be negatively altered.

❖ *Final Embedding*

The embedding of PWAS is done using the DuraAct piezo discs located 40 cm apart from each other with no electronics added. The electronics for the different nodes are glued on the surface of the CFRP plate in order to allow for design adjustments. Among those needed modifications is the tuning of the high-frequency antennas and re-programming of the microcontrollers. For this construction, ten layers of carbon fabric G0926 were placed in the following order [(0/90) /±45/ (0/90)/±45/ (0/90)]. The resin RTM6 is pre-heated at 80°C and the fabrics are placed in a press at 120°C. Infusion is done at 120°C and curing is carried at 150°C for a total of 8 hours.

The selected round piezo sensor/actuators were integrated during manufacturing. Their characteristics were measured with an impedance analyzer as explained in section 4 . The node boards are developed on the very thin FR4 substrate and applied on the surface of the plate by gluing.

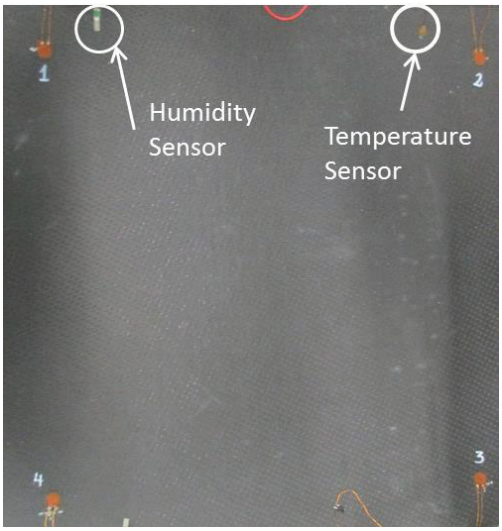

Figure 62: Sensor Integration on the final CFRP (prototype)

Moreover, during resin infusion and curing, two of these PWAS are used to generate and receive Lamb-waves. The goal is to determine to which extend the embedding process is successful, wherein the amplitudes and characteristics of the signals are recorded. This is done using a traditional non-wireless measurement set-up. The resin curing can be therefore monitored by correlating to the signal amplitude and characteristics. This research is not concerned with this information, but future implementations of this process could include manufacture monitoring and quality control.

7.2. Temperature and Humidity Influences

Damage is a change to be detected by the SHM system because it negatively affects the structure's current or future performance. However, structures are usually subject to changing and uncontrolled environmental conditions such as temperature, humidity, and loading. Therefore, anything that changes the system without affecting the performance of the structure should not be considered as damage and should be compensated to avoid a false output [55]. Some influences can be accounted for by performing SHM in a known state; however, there are environmental factors which can both alter the Lamb-wave behavior and the state of the structure despite unchanged conditions. Such factors become more significant when, after compensation, the remaining signal change is indistinguishable from the influence of a possible damage.

In a specimen subjected to various influences, the resulting changes are not only to the material itself but also to the sensors/actuators and the adhesive layer joining between the piezoelectric elements to the structure. Therefore, a compensation approach includes changes to the signal resulting from changes in the SHM system itself. A set of properties which are influenced and have to be compensated are Mechanical and electrical properties of actuator and sensor and the waveguide characteristics itself.

Many possible ways to account for these factors have been researched in [56]. Approaches include the use of a database of known acceptable responses at all possible states (optimal baseline selection – OBS) or the correct compensation of changes to a single baseline (baseline signal stretch BSS, local temporal coherence). Many of these approaches have to be adapted to deal with some of the composite-specific changes. For example, on a reinforced composite structure changes are mode and direction dependent because the material damping of composite materials is far higher than that of commonly used metals such as aluminum and steel. As the influence of the stiffness on wave propagation, this damping is mode-dependent and direction-dependent, making it more complicated to account for than in isotropic cases [55]. There are non-damage related changes in composite materials that happen slowly like aging, absorption processes and fatigue cracks in the matrix.

As mentioned before these changes to the Lamb-waves in composite materials depend on mode and orientation and might vary locally or depending on the structure. Composites are sensitive to moisture and temperature; however, their relevance for real compensation methods depends on the magnitude of change they bring in the signal. The following Section evaluates the system for two factors, temperature, and humidity, which influence typical signal characteristics. To this end, Temperature and humidity are evaluated using integrated sensors on the surface of the CFRP plate.

- ***Temperature Influences***

Most of the structures experience temperature differences and this has a huge impact on guided wave signals. The primary effect of temperature change is the time shift of guided wave signals while the secondary effect is the distortion of the shape of the signal. The temperature effects on Lamb- waves can be due to a change in the phase of the time signal, happening due to the modification of the characteristic wave propagation coefficient (wave speed). Moreover, a change in amplitude of the propagating waves with temperature can be observed as a result of the modifications of the specific acoustical absorption coefficient (wave attenuation).

An analog sensor from Texas instruments (LMT70) was selected because of its high precision and small footprint. The sensor has an area of 0.835 mm^2 with a Ball Grid Array (BGA) package. The sensor was placed on a 0.2 mm thickness PCB by Flip-Chip. Moreover, glue was added to improve stability and avoid shorts that might occur with the carbon fibers. Software from Texas Instruments is offered with the development kit which is used to carry all measurements presented here.

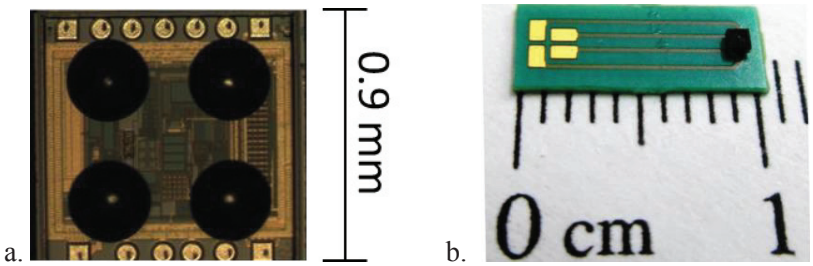

(a) Zoomed bottom view of the CMOS temperature sensor with contact pads . (b) Sensor bonded on PCB

Figure 63: LMT70 Temperature Sensor

❖ *Humidity Influences*

Due to diffusion FRP structures absorb moisture from a humid environment, which causes adverse effects on the material properties. It can be assumed that most moisture is absorbed on the laminate faces (through thickness) than at thin edges. In [18] the authors showed that humidity distribution over the thickness of a CFRP structure is uneven and material damping can both grow and shrink depending on the wave propagation direction and mode; however, the elastic part of the examined materials properties drops in every direction, resulting in a lower velocity for all modes.

As moisture is absorbed into the composite it brings a plasticizing effect. In general, this implies a change in the mechanical properties of a material in which the rigidity is lowered; having an effect on deformations and elongation. This happens because moisture increases chain flexibility. The result is a degradation of the strength. The amount of moisture absorbed is inversely proportional to the strength. Absorption of moisture also means increased weight. While weight gain may not be evident in a very small structure it is quite obvious in large structures. Compared to thermosetting resins, thermoplastic resins have better moisture resistance. Through this work, however, the main resin system used has been RTM6, which is a thermoset. This is the first reason why humidity has to be evaluated.

Another influence of moisture is on adhesives used to mount the sensors on the structures. The typical thickness of the adhesive is about 100µm [57]. The adhesive should not influence the transmitted acoustic waves and has to be mechanically robust to ensure a long-term reliable operation. The influence of moisture on the adhesive layer is not addressed in this study because the sensor is embedded and insulated in a flexible polymer and it is integrated during resin infusion without adding any glue.

Innovative Sensor Technology MK33[10] Sensor was selected to monitor the humidity due to its suitability for extreme environments shown in [58]; where SHM of concrete is evaluated under moisture and temperature influences.

[10] Innovative Sensor Technology "Humidity Elements" [Online]. Available at: http://www.ist-ag.com/eh/ist-ag/en/home.nsf/contentview/~humidity

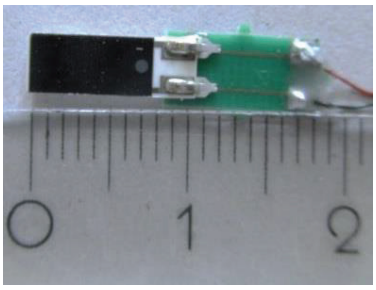

Figure 64: MK33 Humidity Sensor

The MK33 is a capacitive sensor with the properties shown in Table 10. It shows high solvent resistance and withstands high temperatures, thus could be directly embedded or glued on the composite. The sensors are soldered to a small thin PCB to provide more stability and add wire connection to the outside of the plate (See Figure 64). This sensor can detect low humidity levels of less than 3%; especially important if embedded in the composite. The polymers used in RTM process can uptake water only up to 2.5% as indicated by the producer (see section 2.3); therefore the need for high precision at low humidity.

Table 10: MK33 Sensor Properties

Operating humidity range	0 % RH to 100 % RH
Operating temperature range	-40 °C to +190 °C
Capacitance	300 pF ±40 pF (at 30 % RH and +23 °C)
Sensitivity (at C= 300 pF)	0.45 pF/% RH (15 % RH to 90 % RH)
Measurement frequency	1 kHz to 100 kHz (10 kHz recommended)

7.2.1. Experimental Set-up and Calibration

The sensor characteristics given by the manufacturer for the MK33 are at 1 mbar pressure; therefore it is necessary to use a pressure chamber to evaluate the changes that might occur during CFRP plate manufacturing, as observed in Figure 65. The change is 10 pF for a pressure of 1 bar, thus the sensor is thought suitable for embedding in the composite.

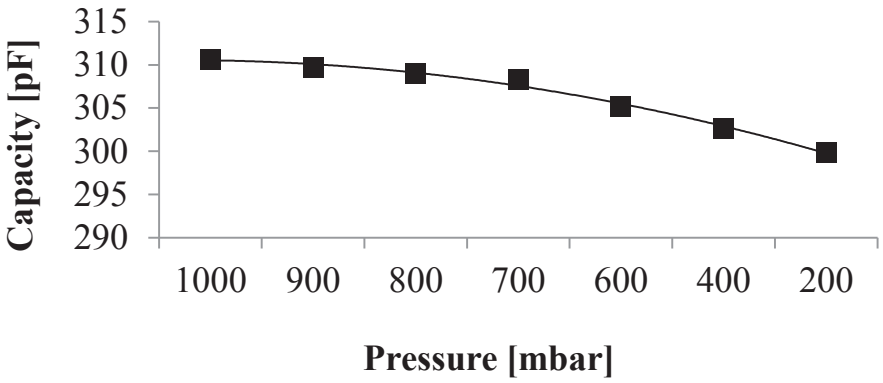

Figure 65: MK33 Sensor Capacitance vs. Pressure

The humidity sensor has a polymer dielectric material. The characteristics of this material are disturbed by the long time high temperatures. According to the datasheet, the temperature influence can be however compensated. On the other hand, the manufacturer evaluates the sensor in air. It is necessary to evaluate the sensor behavior embedded in the material to calibrate as needed for each application. The surrounding material affects the electric field of the capacitor. The next test involved embedding the humidity sensor in only RTM6 at 150°C for 8 hours. The resulting test object is named ***MK33-RTM***. The results from four measurements are presented in Figure 66.

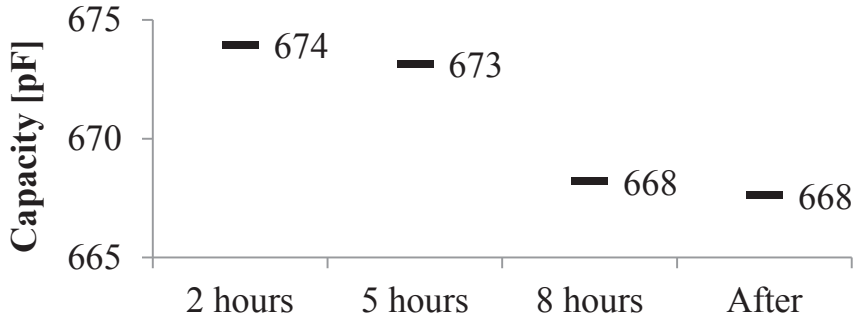

Figure 66: Behavior of the humidity sensor during the integration in RTM6

Two measurements were made during resin curing to make sure the sensor is still hale. One measurement is done after curing, but still at 150°C. Afterward, the piece is cool down and a measurement is made to characterize the new sensor response at room temperature. The sensor presents a capacity of 663 pF at 10 kHz.

The same CFRP plate that was prepared in Section 7.1 with four flexible piezo discs is used to embed the temperature and humidity monitoring sensors. Two MK33 sensors and two LMT70 are integrated at the outer border in order to limit their influence on the Lamb-wave path. All sensors are embedded during manufacture to achieve better adhesion to the structure.

7.2.2. Measurements and Conclusions

The goal of a temperature and humidity compensation is to correct the affected information obtained from the in-situ measurement. In-situ measurements under complex environmental conditions require baselines to be recorded regularly. Instead of a standard fixed Lamb-wave response, a set of responses should be gathered.

❖ ***Humidity Evaluation***

Using the ***MK33-RTM*** test structure, both temperature and humidity are increased simultaneously. To simulate the influences of temperature and humidity and in order to demonstrate the importance of its consideration, a hot and wet conditioning at 70°C and 80% atmospheric moisture are applied for 90 days. The sensor response was recorded until the RTM6 polymer reached saturation as seen in Figure 67. Assuming that 2.5% water is diffused in the material, as given by the manufacturer, then a linear response of the sensor can be obtained. In a similar way, the sensor can be calibrated for each application and material.

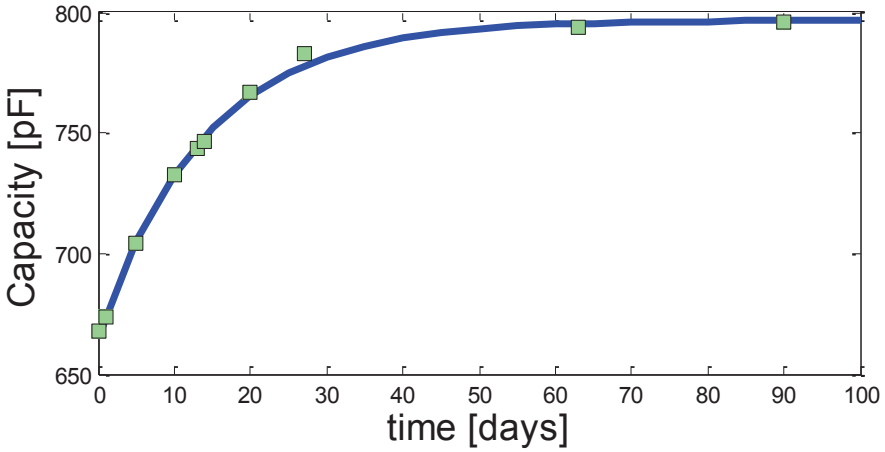

Figure 67: Moisture uptake by MK33 in RTM6 (70°C / 80% RH)

In order to be able to evaluate the moisture uptake of RTM6 with carbon fibers as reinforcement, it would be necessary to evaluate its dielectric response over time when exposed to the humid environment. In this way, the absorption and desorption coefficients for the material can found.

The next test was carried at Faserinstitut e.V.; it consists of embedding the temperature and humidity sensors inside a CFRP plate. Right after the infusion takes place the MK33 sensor is measured to check its characteristics. The vacuum is on and the temperature at the time is 150°C. The capacity of the sensor is observed here 420pF at 10 kHz. The capacity increased as expected from the test carried with only RTM6, the change is less because less resin is surrounding the sensor and the carbon fibers influence the electrical field of the sensor.

After 8 hours, curing has finalized and the plate is removed from the vacuum bag. The humidity sensors are tested, giving a short circuit of 59 to 80-ohm resistance. The capacitive sensor is not suitable for embedding at high temperatures if the process is long and involves vacuum. The possibility of short circuit arises from the electrical conductivity of the carbon fibers. Therefore, in this form, it can only be added to the surface of the plate for further testing. The temperature sensors, on the other hand, are fully functional during and after infusion and curing.

❖ ***Temperature Evaluation***

The plate is placed on a climate camera and the temperature is variated while the Lamb waves are recorded and compared to the reference signal. Measurements over large temperature range show that the time of arrival change with temperature is linear, especially for the second mode; which becomes faster at higher temperatures. The amplitude of the responses also increases proportionally to the temperature. In that way, it is shown that temperature will affect the measurement greatly. Figure 68 shows the obtained responses from the piezo sensor.

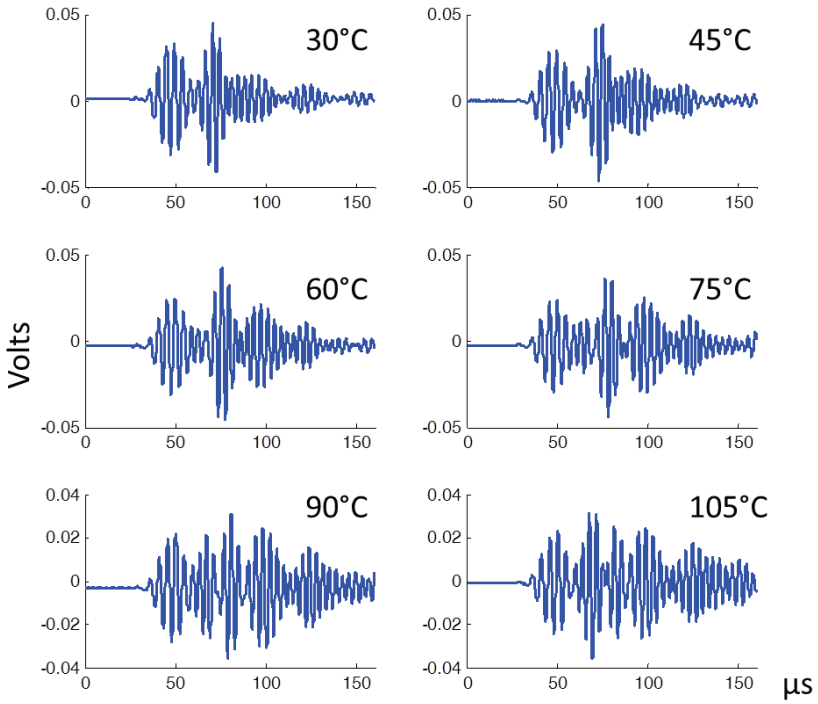

Figure 68: Evaluation of the Lamb-wave vs. temperature [59]

Measurements over a large temperature range show that the time of arrival changes with temperature linearly, especially for the antisymmetric mode (A_O); which becomes faster at higher temperatures. However, above 90° it becomes much faster and overlapping of reflections are observed. The amplitude of the responses also increases proportionally to the temperature.

Conclusions and Outlook

This thesis shows that it is possible to produce enough power by means of inductive coils for a piezo sensor/-actuator system to be used in the structural health monitoring of fiber composite materials. The principle works even if the sensor system is integrated during manufacturing of the composite instead of being glued or bonded after production. In fact, the integration of flexible sensor-/actuators during manufacturing shows better responses in amplitude than those PWAS glued on the plate.

It is shown that even though there is an influence of CFRP on the power transmission, it is possible to achieve power and data transmission using lower frequency ranges. There are available solutions for small transmission distances; in the evaluated system, a required range of 5 cm was successfully achieved. The following steps are to be considered for the implementation of wireless SHM sensor networks in electrically conductive materials like CFRP.

First of all, the antenna design and positioning should account for the negative coupling from the conductive materials. Therefore, the adequate selection of the transmission range is necessary. Overall, the transmission at the low-frequency range was confirmed to give better results than higher frequencies, favoring the kHz range for large power transmission requirements. However, the HF range is needed for faster data transmission rates.

Secondly, in the case of the MHz range, a retuning is necessary since the resonance of the receiver and transmitter is affected by the resin-to-carbon ratio present in the composite. The more conductive the material is the more shielding will occur. In this step, additionally, there is the possibility to use high permeability materials as spacers between the structure and the antenna to improve the coupling.

Finally, the antenna coils can be fully embedded on the surface of the composite. The Taylor-fiber-placement was successfully employed in this work to develop customized low-frequency antennas. It is important to investigate the possible effects of temperature and physical deformations that may occur during the manufacturing process. Bending, for example, can affect the self-resonance of the coils. Also, the substrate material or wire isolation should stand the high temperatures of the process. It was also observed that in the case of GFRP, the coupling is stronger especially at close distances, most likely due to the highly dielectric nature of the material. When possible such high dielectric materials might be used as spacers between the antenna and CFRP to improve the transmission.

The electronics essential for each application will vary according to the data being processed. For example, higher frequencies or low signal amplitudes can reduce the possibility to implement direct analog-to-

digital converters. For instance, the direct connection of the PWAS actuator as a load to the receiver coil was investigated and optimized; in this case, no further signal generation by a microcontroller is needed. On the other hand, it is of interest to actuate the PWAS in a controlled manner; in this case, it is necessary to regulate the power output to optimally supply a microcontroller; which is needed to generate the signal burst to the actuator, amplified to the necessary 50 V_{PP}. In this work both systems with and without digital electronics were evaluated. Better results are obtained from the piezo-driver solution with digital elements because the frequency spectrum of the excitation signal allows less noise at the output stage.

In the presence of a drilled hole on the plate surface between sensor and actuator, a damping of the sensor signal is observed, indicating that these signals can help identify the presence of failure. The system here presented can be used to receive Lamb-waves wirelessly and detect large defects like drilled holes or damping mass; which acts like or mimics a delamination. In future work the detecting limits have to be determined. As it was briefly introduced, the presence of moisture and changing temperatures, modify the properties of the composite material. It is necessary to deeply investigate the long term effects of aging and Lamb-wave behavior.

Another future task is to locate defects with the network system which are outside of the direct path between actuator and detecting sensor by using the triangulation algorithm. A sensor network based on this system for further work needs to be done regarding the mechanical properties of the material once the nodes are embedded. Similarly, the interference of different frequencies has to be lessened; while a solution for the coupling variations due to antenna distance have to be taken into account.

Smaller sizes are desired in order to have the least influence on the mechanical behavior of the structure. For applications such as aerospace and wind energy, it is highly required to maintain the light weight of the structure, so dense wiring presence is unwanted. Moreover, interconnections between the node and piezo are to be tested. Piezoceramic materials embedded in a ductile polymer have shown to be more versatile than standard PWAS because they are not brittle. The composite actuator and sensor offer higher performance with larger responses and sensitivity.

Still, the current electronics and antennas for wireless transfer are much larger than sensors; thus new technologies such as flexible electronics are attractive when embedding within the FRP material. Future research should be directed towards such technologies as flexible integrated circuits, foil technology, and screen printing technologies.

References

[1] G. a. Dillingham, „Status of FAA's Actions to Oversee the Safety of Composite Airplanes," 2011.

[2] V. Giurgiutiu, Structural Health Monitoring With Piezoelectric Wafer Active Sensors, Burlington: Academic Press, 2008.

[3] Cool Silicon, [Online]. Available: http://www.cool-silicon.de/Startseite/Presse/News/Detailseite/id/235.

[4] K. Finkenzeller and D. Müller, RFID Handbook, 3 ed., Chichester: Wiley, 2010.

[5] J. P. Lynch und J. L. Kenneth, „A summary Review of Wireless Sensors and Sensor Networks for Structural Healt Monitoring," *The Shock and Vibration Digest,* pp. 38, 91, 2006.

[6] W. Lang, F. Jakobs, E. Tolstosheeva, H. Sturm, A. Ibragimov, A. Kesel, D. Lehmhus und U. Dicke, „From embedded sensors to sensorial materials—The road to function scale," *Sensors and Actuators A: Physical,* Bd. 171, Nr. 1, pp. 3-11, November 2011.

[7] Y. Guo, C. Aquino, D. Zhang und B. Murmann, „A Four-Channel ±36V Piezo Driver Chip for a Densily Integrated SHM System," in *Structural Health Monitoring 2013: A Roadmap to Intelligent Structures*, Stanford, CA, Department of Aeronautics and Astronautics, Stanford University, 2013, pp. 1551-1558.

[8] H. Janocha, Adaptronics and Smart Structures, Berlin, Heidelberg: Springer, 2007.

[9] M. Shahinpoor und H. J. Schneider, Intelligent Materials, The Royal Society of Chemistry, 2008, p. 21.

[10] W. Lang, D. Boll und T. Schotzko, „Function Scale Integration- Embedding Sensors in Materiasl for Structural Health Monitoring," *6th European Workshop on Structural Health Monitoring ,* 2012.

[11] D. R. Shukla und A. J. Vizzini, „Interlacing for improved performance of laminates with embedded devices," *Smart Materials and Structures,* Bd. 5, pp. 225-229, 1996.

[12] M. Kehlenbach, „Integrierte Sensorik zur Schädigungserkennung in Faserverbundstrukturen für die Luftfahrt," Aachen, Germany, 2003.

[13] I. A. Viktorov, Rayleigh and Lamb waves physical theory and applications, New York: Plenum Press, 1967.

[14] M. Calomfirescu, „Lamb Waves for Structural Health Monitoring in Viscoelastic Composite Materials,“ PhD, University of Bremen : Logos Verlag, 2008.

[15] K. J. Schubert und A. S. Herrmann, „On attenuation and measurement of Lamb waves in viscoelastic composites,“ *Composite Structures,* Nr. 94, p. 177–185, 2011.

[16] A. S. Herrmann und M. Calomfirescu, „Theoretical and experimental studies of Lamb wave propagation in attenuative composites,“ *Sensors and Smart Structures Technologies for Civil, Mechanical, and Aerospace Systems,* 2007.

[17] M. Rheinfurth, N. Kosmann, D. Sauer und G. Busse, „Lamb waves for non-contact fatigue state evaluation of composites under various mechanical loading conditions,“ *Composites: Part A,* Bd. 43, pp. 1203-1211, 2012.

[18] A. S. Herrmann und K. J. Schubert, „On the influence of moisture absorption on Lamb wave propagation and measurements in viscoelastic CFRP using surface applied piezoelectric sensors,“ *Composite Structures,* pp. 3635-3643, 2012.

[19] M. Castaings, B. Hosten und T. Kundu, „Inversion of ultrasonic, plane-wave transmission data in composite plates to infer viscoelastic material properties,“ *NDT & E International,* Bd. 33, Nr. 6, pp. 377- 392, 2000.

[20] A. S. Herrmann and K. J. Schubert, "A Compensation Method for Environmental Influences on Passive Lamb Wave Based Impact Evaluation for CFRP," *Key Engineering Materials,* pp. 1265-1272, 2013.

[21] D. Balageas, C.-P. Fritzen and A. Güemes, Structural Health Monitoring, London: ISTE, 2006.

[22] K. J. Schubert, T. B. Block und A. S. Herrmann, „Untersuchung des Ausbreitungsverhaltens von Lamb-Wellen in viskoelastischen Faserverbundwerkstoffen,“ *DGZfP-Jahrestagung,* 2011.

[23] „ Chapter 1: Introduction, In 3D Fibre Reinforced Polymer Composites,“ in *3D Fibre Reinforced Polymer Composites*, Oxford, Elsevier Science, 2002, pp. 1-12.

[24] A. Galehadar, K. Nicholson, K. S. T. Rowe und K. Ghorbani, „The Conductivity of Unidirectional and Quasi Isotropic Carbon Fiber Composites,“ in *Preceedings of the 40th European Microwave Conference*, Paris, France, September 2010.

[25] C. Soutis, „Carbon fiber reinforced plastics in aircraft construction,“ *Materials Science and Engineering: A,* Bd. Volume 412, Nr. Issues 1–2, pp. 171-176, December 2005.

[26] D. G. Fink und D. Christiansen, in *Electronics Engineer’s Handbook*, 3rd Hrsg., McGraw-Hill, 1989, pp. 115-117.

[27] P. R. P. Hoole, K. Pirapaharan und S. R. H. Hoole, „Electromagnetics Engineering Handbook : Analysis and Design of Electrical and Electronic Devices and Systems.," WIT Press, 2013.

[28] A. Mehdipour, C. W. Trueman, A. R. Saebak und S. V. Hoa, „Carbon-Fiber Composite T-Match Folded Bow-Tie Antenna for RFID Applications," *Antennas and Propagation Society International Symposium,* 2009.

[29] R. R. de Assis and I. Bianchi, "Analysis of Microstrip Antennas on Carbon Fiber Composite Material," *Journal of Microwaves, Optoelectronics and Electromagnetic Applications,* vol. 11, pp. 154-161, 2012.

[30] I. Mayordomo, T. Dräger and J. Bernhard, "Technical Challenges for the Integration of passive HF RFID," *IEEE International Conference on RFID-Technologies and Applications,* 2011.

[31] D. Ciudad, P. C. Arribas, P. S. Aroca und C. Aroca, „RFID in Metal Environments: An Overview on Low (LF) and Ultra-Low (ULF) Frequency Systemsled," in *Radio Frequency Identification Fundamentals and Applications Design Methods and Solutions*, C. Turcu, Hrsg., Intech, 2010, pp. 181-196.

[32] C. L. Holloway, S. Sarto und M. Johansson, „Analyzing Carbon-Fiber Composite Materials With Equivalent-Layer Models," *IEEE Transactions on Electromagnetic Compability,* Bd. Bd. 47, Nr. Nr. 4, pp. 833-844, 2005.

[33] H. Corporation, „HexFlow® Infusion Resins for Aerospace," Hexcel Corporation, July 2016. [Online]. Available: http://www.hexcel.com/products/aerospace/ainfusion-resins.

[34] D. W. Greve, H. Sohn, P. Yue und I. J. Oppenheim, „An Inductively Coupled Lamb Wave Transducer," *IEEE Senors Journal,* Bd. 7, Nr. 2, pp. 395-301, February 2007.

[35] J. Bernhard, T. Dräger, C. Grabowski, I. Sotriffer and T. Philipp, "Integrating RFID in Fibre-Reinforced Plastics," in *ITG-Fachbericht 229*, Dresden, Germany, 2011.

[36] H. A. Wheeler, "Simple Inductance Formulas for Radio Coils," *Proceedings of the I.R.E,* vol. 16, no. 10, October 1928.

[37] Mohan, Hershenson, Boyd und Lee, „Simple Accurate Expressions for Planar Spiral Inductances," *IEEE Journal of Solid-State Circuits,* pp. 1419-1424, Oct 1999.

[38] V. Talla, M. Buettner, D. Wetherall und J. R. Smith, „Hybrid Analog-Digital Backscatter Platform for High Data Rate, Battery- Free Sensing," in *Proceedings of IEEE RFID*, Orlando, Florida, 2013.

[39] M. Salas, O. Focke, W. Lang and A. Herrmann, "Wireless Power Transmission for Structural Health Monitoring of Fiber-Reinforced-Composite Materials," *IEEE Sensors Journal Special Issue on Material-integrated Sensing,* vol. 14, no. 7, pp. 2171-2176, 2014.

[40] M. Salas, O. Focke, A. S. Hermann und W. Lang, „Wireless Actuation of Piezo-elements for the Structural Health Monitoring of Carbon-Fiber- Reinforced-Polymers," *Mechatronics Journal Special Issue on System-Integrated Intelligenc,* Bd. 34, pp. 128-136, 2015.

[41] C. Neagu, H. Jansen , A. Smith, J. Gardeniers und M. Elwenspoek, „Characterization of A Planar Microcoil for Implantable Microsystems," *Sensors and Actuators A: Physical,* pp. 599-611, 1997.

[42] M. Salas, O. Focke, W. Lang and A. Hermann, "Low-Frequency Inductive Power Transmission for Piezo-Wafer-Active-Sensors in the Structural Health Monitoring of Carbon-Fiber-Reinforced-Polymer," in *Procedia technology: 2nd International Conference on System-integrated Intelligence*, Bremen, Germany, 2014.

[43] P. Schiebel und A. Herrmann, „Analyse des verformungsverhaltens von kohlenstoff-rovings im textilen fertigungsprozess fuer belastungsgerechte cfk-strukturen," in *S13. Chemnitzer Textiltechnik Tagung*, 2012.

[44] S. E. Lee, K. S. Oh und C. G. Kim, „Electromagnetic Characteristics of Frequency Slective Fabric Composites," *IEEE Electronic Letters,* Bd. 42, Nr. 8, pp. 439-441, April 2006.

[45] H. D. Young und F. W. Sears, University physics, Reading, Mass: Addison-Wesley Pub. Co, 1992.

[46] V. Giurgiutiu, „Tuned Lamb Wave Excitation and Detection with Piezoelectric Wafer Active Sensors for Structural Health Monitoring," *Journal of Intelligent Materials and Structures,* Bd. 16, pp. 291-305, April 2005.

[47] J. Kim, B. L. Grisso, J. K. Kim, D. S. Ha and D. J. Inman, "Electrical Modeling of Piezoelectric Ceramics for Analysis and Evaluation of Sensory Systems," in *IEEE Sensors Applications Symposium*, Atlanta, GA, 2008.

[48] Y. L. Su Z, „Identification of Damage Using Lamb Waves- From Fundamentals to Applications. Lecture Notes in Applied and Computational Mechanics," *Proceedings of the Institution of Mechanical Engineers, Part L: Journal of Materials Design and Applications 2004,* Bd. 48, Berlin.

[49] P. Wessels, M. Swanenberg, H. v. Z. Benno, K. Henk Boezen, M. Berkhout und A. Grakist, „Advanced BCD technology for automotive, audio and power applications,," *Solid-State Electronics,* Bd. 51, Nr. 2, pp. 195-21, February 2007.

[50] M. Salas, O. Focke, G. Stoltenberg, A. S. Herrmann und W. Lang, „Wireless Sensor Network For Structural Health Monitoring By Means of Lamb-waves," in *Proc. 10th International Workshop on Structural Health Monitoring*, Stanford University, 2015.

[51] Vishay Dale, "IWAS-4832FF-50 product information," 3 July 2013. [Online]. Available: http://www.vishay.com/docs/34311/iwas4832.pdf.

[52] Y. Shen und V. Giurgiutiu, „WaveFormRevealer: An analytical framework and predictive tool for the simulation of multi-modal guided wave propagation and interaction with damage," *Structural Health Monitoring – An International Journal,* Bd. 13, Nr. 5, pp. 491-511, 2014.

[53] M. Prabhugoud and K. Peters, "Finite element model for embedded fiber Bragg grating sensor," *Smart Materials and Structures,* vol. 15, no. 2, pp. 550-562, 2006.

[54] G. Dumstorff, S. Paul und W. Lang, „Integration Without Disruption: The Basic Challenge of Sensor Integration," *IEEE Sensors,* Bd. 14, Nr. 7, pp. 2102-2111, 2014.

[55] K. J. Schubert, O. Focke und A. S. Herrmann, „Relevance of Environmental Influeces for Lamb Wave based SHM with Piezoelectric Elements," in *19th International Conference on Composite Materials (ICCM19)*, Montreal, Canada, 2003.

[56] R. L. Chaney, H. R. Douglas und W. G. Dale, „Physically Flexible High Performance Single Crystal CMOS," in *IEEE Workshop on Microelectronics And Electron Devices (WMED)*, Boise, ID, 2014.

[57] B. Boehme, M. Roellig und K. J. Wolter, „Moisture induced change of the viscoelastic material properties of adhesives for SHM sensor applications," in *Proceedings 60th Electronic Components and Technology Conference*, Las Vegas, NV, USA, 2010.

[58] E. Van Every, A. Deyhim und F. Faridazar, „Embedded Sensors for Life-Time Monitoring of Concrete," in *4th International Conference on Structural Health Monitoring on Intelligent Infrastructure (SHMII-4)*, Zurich, Switzerland, July 2009,.

[59] M. Salas, M. Koerdt, M. Hübner, M. Kahali und W. Lang, „Material integrated sensors for an optimal baseline selection on a wireless SHM network," in *2016 IEEE SENSORS*, Orlando, FL, 2016.

[60] O. Focke, M. Salas, A. S. Herrmann und W. Lang, „Inductive wireless sensor-actuator node for structural health monitoring of fiber reinforced polymers by means of Lamb-waves," in *SPIE Smart Structures and Materials+ Nondestructive Evaluation and Health Monitoring*, San Diego, 2015.

Appendix

A. Publications and Conference Proceedings

- M. Salas, O. Focke, W. Lang and A. Herrmann, "Wireless Power Transmission for Structural Health Monitoring of Fiber-Reinforced-Composite Materials," *IEEE Sensors Journal Special Issue on Material-integrated Sensing,* vol. 14, no. 7, pp. 2171-2176, 2014.
- M. Salas, O. Focke, W. Lang and A. Hermann, "Low-Frequency Inductive Power Transmission for Piezo-Wafer-Active-Sensors in the Structural Health Monitoring of Carbon-Fiber-Reinforced-Polymer," in *Procedia technology: 2nd International Conference on System-integrated Intelligence*, Bremen, Germany, 2014.
- M. Salas, O. Focke, G. Stoltenberg, A.S. Herrmann, W. Lang "Inductive Wireless Sensor-Actuator System for Structural Health Monitoring of Fiber Composite Materials" in *36th Colloquium of Automation*. Steinfeld, Germany 2014.
- M. Salas, O. Focke, A. S. Hermann und W. Lang, „Wireless Actuation of Piezo-elements for the Structural Health Monitoring of Carbon-Fiber- Reinforced-Polymers," *Mechatronics Journal Special Issue on System-Integrated Intelligenc,* Bd. 34, pp. 128-136, 2015.
- O. Focke, M. Salas, A. S. Herrmann und W. Lang, „Inductive wireless sensor-actuator node for structural health monitoring of fiber reinforced polymers by means of Lamb-waves," in *SPIE Smart Structures and Materials+ Nondestructive Evaluation and Health Monitoring*, San Diego, 2015.
- M. Salas, O. Focke, G. Stoltenberg, A. S. Herrmann und W. Lang, „Wireless Sensor Network For Structural Health Monitoring By Means of Lamb-waves," in *Proc. 10th International Workshop on Structural Health Monitoring*, Stanford University, 2015.
- M. Salas, M. Koerdt, M. Hübner, M. Kahali and W. Lang, "Material integrated sensors for an optimal baseline selection on a wireless SHM network," *2016 IEEE SENSORS*, Orlando, FL, 2016, pp. 1-3.

B. Other Publications

- L. Brandhoff, H. Zirath, M. Salas, A. Haller, J. Peham, H. Wiesinger-Mayr, A. Spittler, G. Schnetz, W. Lang and M. J. Vellekoop,"A multi-purpose ultrasonic streaming mixer for integrated magnetic bead ELISAs." *Journal of Micromechanics and Microengineering,* vol. 25, no. 10, 2015
- M. Hübner, M. K. Moghaddam, M. Salas, G. Dumstorff and W. Lang, Materialintegrierte Sensorik für Fahrzeug-Leichtbautechnik. In *Automobil-Sensorik* (pp. 191-216). Springer Berlin Heidelberg, 2016
- Schlussbericht IGF-Vorhaben 17649 N *„Drahtlose Sensoren / Sensornetzwerke zur Strukturzustandsüberwachung (SHM) von Bauteilen aus Faserverbundwerkstoffen mittels Lamb-Wellen. (Drahtloses SHM)"* June 2016.

C. Supervised Work

- Liu, J. “Low-Frequency Model of the Electromagnetic behavior from Carbon-Fiber-Reinforced Polymers during the Implementation of Inductive Wireless Power Transfer.” *Master Thesis at IMSAS, University of Bremen FB1.* October 2014.
- Patel, Chandresh. “Piezo-Driver for Lamb-wave Generation on a Wireless SHM Sensor/Actuator Node.” *Master Thesis at IMSAS, University of Bremen FB1.* November 2015

D. Other Works

- Gow, Marvin-John „Entwicklung und Verizierung von Prüfstrategien zur Detektion von Fehlstellen in Faserverbundplatten mittels Lamb-Wellen“ *Mater Thesis at FIBRE, University of Bremen FB4.* December 2015.

Acknowledgments

Thanks to my supervisor, Prof. Walter Lang, for allowing me to work closely to IMSAS and also for the support and invaluable advice.

Special thanks to the support obtained by "Arbeitsgemeinschaft industrieller Forschungsvereinigungen" (AiF) and the research association "Deutsche Forschungsvereinigung für Mess-, Regelungs- und Systemtechnik (DFMRS)" for the funding by the scheme "Industrielle Gemeinschaftsforschung (IGF)" under IGF- project Nr. 17649N and project Nr. 18651N. To the industry committee for their continuous enthusiasm though the project as well for all the advice and long discussions during meetings.

Thanks to Oliver Focke and the Faserinstitut Bremen e.V. for their relentless collaboration during plate manufacturing and sensor integration. Thanks to Fred Becker and Simon Karau at the Department of RF & Microwave Engineering at the Institute for Telecommunications and High-Frequency Techniques for consenting the use of their lab and for the helpful advice.

Recognition must be given to all my colleagues from FWBI and IMSAS for the amazing work atmosphere. I am especially grateful to Roland Blank, Mykhaylo Borisov, Lukas Brandhoff, Stefan Clara for brainstorming with me during the electronic designs. Thanks to Günter Stoltenberg for his great assistance with the sensor nodes during the second year of this research. It would not have been possible to have completed the project without the support and shared interests from Maryam Kahali and all the Sensor integration AG.

Thanks to master students Liu Ji for the long tedious simulations and Patel Chandresh for his amazing job with the piezo driver.

Last but not least thanks to my family and to my husband Mark for the emotional support during this journey.